

**SEISMIC INDUCED FLOW DEFORMATION AND
REMEDICATION STUDY OF SARDIS DAM**

by

Guoxi WU

B.Eng. Nanjing Institute of Architectural Engineering, 1984

M.A.Sc. Tongji University, Shanghai, PRC, 1987

A THESIS SUBMITTED IN PARTIAL FULFILLMENT OF
THE REQUIREMENTS FOR THE DEGREE OF
MASTER OF APPLIED SCIENCE

in

THE FACULTY OF GRADUATE STUDIES
CIVIL ENGINEERING

We accept this thesis as conforming
to the required standard

THE UNIVERSITY OF BRITISH COLUMBIA

April 1992

© Guoxi WU, 1992

In presenting this thesis in partial fulfilment of the requirements for an advanced degree at the University of British Columbia, I agree that the Library shall make it freely available for reference and study. I further agree that permission for extensive copying of this thesis for scholarly purposes may be granted by the head of my department or by his or her representatives. It is understood that copying or publication of this thesis for financial gain shall not be allowed without my written permission.

CIVIL ENGINEERING

The University of British Columbia

2324 Main Mall

Vancouver, Canada

V6T 1Z4

Date:

April 30, 1992

ABSTRACT

Previous investigations of the seismic stability of Sardis Dam indicated that the entire central silt core and a weak clayey silt layer in the dam foundation are susceptible to liquefaction which could result in large losses of shear strengths in these liquefied soils. The post-liquefaction behaviour of Sardis Dam was evaluated using new flow deformation analysis technique which was developed by Finn and Yogendrakumar(1989). The analysis showed the potential for large displacements including a great loss of freeboard during the design earthquake. A strategy of designing remedial measures to limit deformations to a tolerable amount was adopted over the conventional factor of safety approach. Various levels of remediations were investigated using TARA-3FL. The remediation procedure adopted for field trials was anchoring the upstream slope to the foundation using rows of rectangular prestressed reinforced concrete piles. Estimating post-liquefaction deformations for this remediation scheme posed challenging problems in analysis.

Table of Contents

ABSTRACT	ii
List of Tables	iv
List of Figures	v
Acknowledgement	vi
1 INTRODUCTION	1
2 DESCRIPTION OF SARDIS DAM	6
3 PREVIOUS SEISMIC STUDIES	9
3.1 Previous Investigation	9
3.2 Potential for Liquefaction in Fine Grained Soils	11
3.3 Conclusions Drawn from Previous Seismic Study	14
4 THEORY OF POST LIQUEFACTION ANALYSIS	18
4.1 Conventional Static Equilibrium Method	18
4.2 The Deformation Analysis Theory	18
5 RESIDUAL SHEAR STRENGTH	24
5.1 Introduction	24
5.2 Determination of Residual Strengths	26
5.2.1 Steady state concept	26

5.2.2	A correction between residual strengths and SPT blowcounts	32
5.3	Evaluation of Residual Strength on Sardis Dam	33
6	LIQUEFACTION DEFORMATION ANALYSIS	36
6.1	Initial Stress Conditions in Dam and Foundation	36
6.1.1	Finite element mesh	36
6.1.2	Soil material properties	39
6.1.3	Pool water level and water force	42
6.2	Description of Liquefaction Analysis	42
6.2.1	Liquefiable materials	42
6.2.2	Soil properties after liquefaction	43
6.2.3	Results of liquefaction analyses	46
7	GENERAL REMEDIATION STUDY OF SARDIS DAM	53
7.1	General Remediation Schemes	53
7.2	Effect of the Pore Water Pressure of the Non-Liquefiable Sand Shell	57
7.2.1	Loss of freeboard	58
7.2.2	Horizontal pressures against the plug	58
7.2.3	Ratio of shear stress to strength of the plug	61
7.2.4	Horizontal displacement of the plug	61
7.3	Effect of Plug Width	63
7.3.1	Loss of freeboard	63
7.3.2	Horizontal pressures against the plug	66
7.3.3	Ratio of shear stress to strength of the plug	66
7.3.4	Horizontal displacement of the plug	69
7.4	Effect of Plug Strength	71
7.4.1	Loss of freeboard	71

7.4.2	Horizontal pressures against the plug	71
7.4.3	Ratio of shear stress to strength of the plug	74
7.4.4	Horizontal displacement of the plug	76
7.5	Summary on General Remediation Studies	76
8	REMEDICATION STUDY OF PILE-REINFORCED SECTION	84
8.1	Equivalent Composite Material Properties of the Pile Reinforced Section	84
8.2	Comparison of Results Between the Pile-Reinforced Section And the Plug	99
8.2.1	Loss of freeboard	99
8.2.2	Horizontal pressures against the remediated zone	100
8.2.3	Ratio of shear stress to strength of the remediated zone	100
8.2.4	Horizontal movement of the remediated zone	103
9	SUMMARY AND CONCLUSIONS	105
	Bibliography	108

List of Tables

6.1	Parameters of Strength and Stiffness Used in the Construction Analysis .	41
6.2	Variations of Residual Strengths in the Weak Clayey Silt (psf)	44
6.3	Parameters of Strength and Stiffness after Liquefaction	45
6.4	Summary Results of Liquefaction Analysis (WT277 model)	50
7.1	Different Plug Remediation Schemes	56
7.2	Summary Results of Plug Remediation Studies	78
8.1	Composite Strengths and Moduli of the Pile-Reinforced Section	99

List of Figures

2.1	Typical Section of Sardis Dam (Finn et al., 1990a)	7
3.1	Longitudinal Section Showing Liquefiable Zones in Shell and Foundation Sands 139 m(450 ft) Upstream from Centerline (Finn et al., 1990a) . . .	10
3.2	Plan View of Liquefiable Weak Clayey Silt Zones (Finn et al., 1990a) . .	15
3.3	Longitudinal Section Showing Liquefiable Weak Clayey Silt Zones 139 m(450 ft) Upstream from Centerline (Finn et al., 1990a)	16
4.1	Adjusting Stress-Strain State to Post-Liquefaction Conditions (after Finn et al., 1990b)	21
5.1	Types of Stress Strain Curve for Consolidated Undrained Triaxial Tests on Clean Sand	25
5.2	Changes in Driving Stresses and Undrained Shear Strength During an Earthquake	25
5.3	Steady State Line (void ratio vs effective confining pressure) (after Poulos et al, 1985)	28
5.4	Steady State Line (void ratio vs steady state strength) (after Poulos et al , 1985)	28
5.5	Poulos Procedure for Determining Steady State Strength (after Poulos et al., 1985)	31
5.6	Cross Section of Lower San Fernando Dam Showing Liquefaction Zone (Seed et al., 1988)	31

5.7	Tentative Relationship Between Residual Strength and SPT N Values for Sands (after Seed et al., 1988)	34
5.8	Residual Strength in Topstratum Clay – Sardis Dam (Finn et al., 1990a)	34
6.1	Finite Element Mesh Showing Element Distribution	37
6.2	Finite Element Mesh Showing Node Distribution	38
6.3	Distribution of Soil Material Zones	40
6.4	Variation of Post Liquefaction Configurations with Minimum Residual Strength – WT277 model	47
6.5	Variation of Loss of Freeboard with Minimum Residual Strength	48
6.6	Variation of Horizontal Displacement with Minimum Residual Strength .	51
6.7	Maximum Ratio of Shear Stress to Strength in the Weak Clayey Silt Versus Minimum Residual Strength	52
7.1	Finite Element Mesh Showing Location of Remedial Pile Plug	54
7.2	Detailed Distribution of Remedial Elements	54
7.3	Variation of Loss of Freeboard with Residual Strength (PWP effect) . . .	59
7.4	Pressure Distribution on Downstream Face of Remediated Section (PWP effect)	60
7.5	Pressure Distribution on Upstream Face of Remediated Section (PWP effect)	60
7.6	Distribution of Ratio of Shear Stress to Strength at Downstream Face of Remediated Section (PWP effect)	62
7.7	Maximum Ratio of Shear Stress to Strength in Remediated Section versus Residual Strength (PWP effect)	62
7.8	Distribution of Downstream Horizontal Movement of Remediated Section (PWP effect)	64

7.9	Horizontal Displacement at Downstream Edge with Residual Strength (PWP effect)	64
7.10	Variation of Loss of Freeboard with Residual Strength (Plug width effect)	65
7.11	Pressure Distribution on Downstream Face of Remediated Section (Plug width effect)	67
7.12	Pressure Distribution on Upstream Face of Remediated Section (Plug width effect)	67
7.13	Distribution of Ratio of Shear Stress to Strength at Downstream Face of Remediated Section (Plug width effect)	68
7.14	Maximum Ratio of Shear Stress to Strength in Remediated Section versus Residual Strength (Plug width effect)	68
7.15	Distribution of Downstream Horizontal Movement of Remediated Section (Plug width effect)	70
7.16	Horizontal Displacement at Downstream Edge with Residual Strength (Plug width effect)	70
7.17	Variation of Loss of Freeboard with Residual Strength (Plug strength effect)	72
7.18	Pressure Distribution on Downstream Face of Remediated Section (Plug strength effect)	73
7.19	Pressure Distribution on Upstream Face of Remediated Section (Plug strength effect)	73
7.20	Distribution of Ratio of Shear Stress to Strength at Downstream Face of Remediated Section (Plug strength effect)	75
7.21	Maximum Ratio of Shear Stress to Strength in Remediated Section versus Residual Strength (Plug strength effect)	75
7.22	Distribution of Downstream Horizontal Movement of Remediated Section (Plug strength effect)	77

7.23	Horizontal Displacement at Downstream Edge with Residual Strength (Plug strength effect)	77
7.24	Loss of Freeboard versus Plug Strength	79
7.25	Maximum Ratio of Shear Stress to Strength in Plug versus Plug Strength	80
7.26	Maximum Horizontal Displacement in Plug Versus Plug Strength	81
7.27	Variation of Typical Post liquefaction Configurations after Remediation – Plug Strength 3000 psf, Plug Width 120 ft)	83
8.1	Cross Section of Sardis Dam Showing Remediation Piles	85
8.2	Plane View of Layout of Remediation Piles	85
8.3	Finite Element Model of Single Pile-Soil System	87
8.4	Boundary Conditions and Loading Distribution of Single Pile-Soil System	88
8.5	Shear Stress - Strain Relationship for the Pile-Reinforced Section, Eleva- tion 173 to 185 ft	89
8.6	Shear Stress - Strain Relationship for the Pile-Reinforced Section, Eleva- tion 185 to 191 ft	90
8.7	Shear Stress - Strain Relationship for the Pile-Reinforced Section, Eleva- tion 191 to 200 ft	91
8.8	Shear Stress - Strain Relationship for the Pile-Reinforced Section, Eleva- tion 200 to 205 ft	92
8.9	Shear Stress - Strain Relationship for the Pile-Reinforced Section, Eleva- tion 205 to 215 ft	93
8.10	Shear Stress - Strain Relationship for the Pile-Reinforced Section, Eleva- tion 215 to 220 ft	94
8.11	Shear Stress - Strain Relationship for the Pile-Reinforced Section, Eleva- tion 220 to 230 ft	95

8.12 Shear Stress - Strain Relationship for the Pile-Reinforced Section, Elevation 230 to 240 ft	96
8.13 Shear Stress - Strain Relationship for the Pile-Reinforced Section, Elevation 240 to 250 ft	97
8.14 Variation of Shear Strength in Pile - Reinforced Section Versus Elevation	98
8.15 Pressure Distribution on Downstream Face of Pile - Reinforced Section .	101
8.16 Distribution of Ratio of Shear Stress to Strength at Downstream Face of Pile - Reinforced Section	102
8.17 Distribution of Downstream Horizontal Movement of Pile - Reinforced Section	104

Acknowledgement

I would like to thank my research supervisor, Professor W.D. Liam Finn, for his helpful guidance, suggestions and encouragement throughout my research.

Chapter 1

INTRODUCTION

Sardis Dam is a hydraulic fill, flood control structure located in Northwestern Mississippi. It has a length of 4600 m (15,000 ft) and a maximum height of 36 m (117 ft). From previous seismic investigations, it has been determined that the central silt core of the dam and a weak clayey silt layer in the dam foundation are susceptible to liquefaction under the design earthquake. Liquefaction could result in large movements of the upstream slope and a substantial loss of freeboard. The crucial problem of Sardis dam is how to evaluate the post-liquefaction behaviour of the dam and how to select effective remediation measures.

In general, there are two major problems confronting the soil engineers dealing with a situation where soil liquefaction may occur. The first problem is determining the conditions required to trigger soil liquefaction. This process is usually termed soil liquefaction potential assessment. For sands, soil liquefaction potential may be evaluated by using Seed's liquefaction assessment chart based on the in-situ Standard Penetration Tests (SPT). For soils with plastic fines, soil liquefaction potential can be assessed by using the criteria which was developed by Wang (1979). Evaluation of soil liquefaction potential has been described by Finn (1985), which is based on the level of the dynamic or excess pore water pressure generated during an earthquake loading. The assessment of soil liquefaction potential made during the previous seismic studies of Sardis Dam will be presented in chapter 3.

The second problem dealing with soil liquefaction is determining the performance of the soil structures after soil liquefaction. This process includes the determination of the residual strengths of the liquefied soils and the assessment of overall stability of the soil structures and the level of permanent deformations.

The residual strength of the liquefied soil plays a key role in the assessment of the post-liquefaction behaviour (Seed,1987). Generally, two methods are used to evaluate the residual strengths of liquefied soils. Poulos (1985) proposed that the residual strength be determined from undrained triaxial tests on undisturbed samples with appropriate corrections for differences between field and test void ratios. Seed (1988) recommended that the residual strength be determined using a correlation between the residual strengths and SPT blowcounts developed by analysis of case histories. The determination of residual strengths by the two methods is discussed in detail in Chapter 5.

The stability assessment of soil structures includes two approaches, static equilibrium analysis and the estimation of permanent deformations. The static equilibrium approach is based on the concept of an acceptable factor of safety. The deformation approach is based on the concept of acceptable deformations.

The conventional method in assessing the stability of an earth structure involving soil liquefaction is the static equilibrium method. In this method, the factor of safety against a shear failure along a specified potential failure surface is determined by using residual strengths in the liquefied soils as the mobilized shear strengths. The minimum value of the factors of safety for all possible potential failure surfaces is used to define the stability

of the soil structures under the earthquake loading. The purpose of the static equilibrium method is determining whether a shear failure will occur after soil liquefaction. In earth structures zones of liquefied soils or zones of degraded strengths may lead to acceptable deformations although the factor of safety based on the original geometry of the structure is less than what is normally considered acceptable and in some cases less than unity. The use of deformation criteria can lead to substantial savings in remediation costs.

Therefore, for these reasons and in keeping with the concept of designing dams for acceptable deformations proposed by Newmark (1965), there is a tendency to move away from the factor of safety concept and to evaluate the extent of necessary remedial measures on the basis of a tolerable amount of deformation for the low probability event specified by the design earthquake. This deformation approach requires a reliable method of estimating post-liquefaction deformations.

A nonlinear finite element method for analyzing the post liquefaction response for soil structures has been developed by Finn and Yogendrakumar (1989) which is incorporated in the computer program TARA-3FL. The program has the capability of computing potential flow deformations. The basic methodology of this flow analysis method is to simulate the sequence of shear strengths in liquefied soils. In the proposed flow analysis, the soil structure is analyzed by using initial or pre-earthquake soil strengths and moduli before applying a seismic loading. The stress-strain field prior to the seismic loading is determined. When the seismic loading is applied, rises of dynamic porewater pressures lead to reductions in shear strengths and shear moduli of saturated soils which cause unbalanced shear stresses in the soil structure. As the unbalanced shear stresses are redistributed throughout the soil structure, a new stress-strain field is established and flow deformations are obtained for this level of shear strengths. The process continues until

all strengths reach either residual or minimum values for the level of shaking. For design purposes it is more convenient to evaluate flow deformations using static analysis under gravitational loads. If deformations under gravitational loading are acceptable then the effects of seismic loading are evaluated.

The deformation analysis method described above is used for the post-earthquake deformation analysis of Sardis Dam. The analysis showed that large deformations in the upstream slope of the dam could occur under an earthquake loading for the normal pool elevation. Remediation measures are proposed and their effectiveness in controlling deformations and the loss of freeboard are evaluated by using TARA-3FL.

OUTLINE OF THESIS

Chapter 2 provides a brief description on Sardis dam .

Chapter 3 presents the previous seismic investigations on Sardis dam. Potential liquefaction zones and critical zones are illustrated.

Chapter 4 presents the basic theory of static post-liquefaction deformation analysis. A brief review of the development of earthquake induced deformation analysis and its applications are described.

Chapter 5 describes the procedures for determining residual strengths based on laboratory undrained triaxial tests or in-situ Standard Penetration Tests. The advantages and disadvantages of these procedures are discussed.

Chapter 6 presents post-liquefaction deformation analyses of Sardis dam. Finite element modelling, determination of strength and stiffness parameters and the results of post liquefaction deformation analysis are given in the chapter.

Chapter 7 presents the results of remediation studies. The performances of Sardis dam after soil liquefaction for different levels of remediation are compared.

The preferred remedial method for Sardis dam is anchoring the dam to the foundation by driving large piles through the upstream slope. This procedure is discussed in chapter 8. A preliminary assessment of the effectiveness of this procedure is evaluated by using TARA-3FL analysis.

Chapter 9 presents conclusions drawn from the studies in previous chapters and makes some suggestions for further studies.

Chapter 2

DESCRIPTION OF SARDIS DAM

Sardis Dam, a hydraulic fill , flood control structure, is located in northwestern Mississippi, approximately ten miles southeast of the town of Sardis on the little Tallahatchie River, a tributary of the Yazoo River. Sardis along with three other dams (Arkabutla, Enid and Grend) are the principal features of the Yazoo Basin Headwater project. The purpose of the associated reservoirs is flood control, however, they also provide opportunities for recreation and enhance local navigation on the Yazoo River.

The total length of Sardis Dam is approximately 4600 m (15,000 ft), with a maximum height of 36m (117 ft). The central portion of the dam, located in the floodplain of the Little Tallahatchie River, ranges in height from 28 m (90 ft) to 36 m (117 ft), and is approximately 2620 m (8500 ft) long. This central portion of the dam was constructed by hydraulic filling, and consists of a predominantly silt core surrounded by a sand shell, shown in Fig. 2.1.

The dam foundation consists of a 3 m (10ft) to 6 m (20 ft) thick zone of natural silty clay, designated as the topstratum clay, Fig. 2.1, which extends approximately 370 m (1200 ft) upstream of the dam centerline. In the areas of the original streambed, the top stratum clay was missing and a 3 m (10 ft) thick silty clay rolled fill was placed in those areas. The topstratum clay is underlain by pervious alluvial sands (substratum sands) which are approximately 12 m (40ft) thick and are underlain by Tertiary silts and

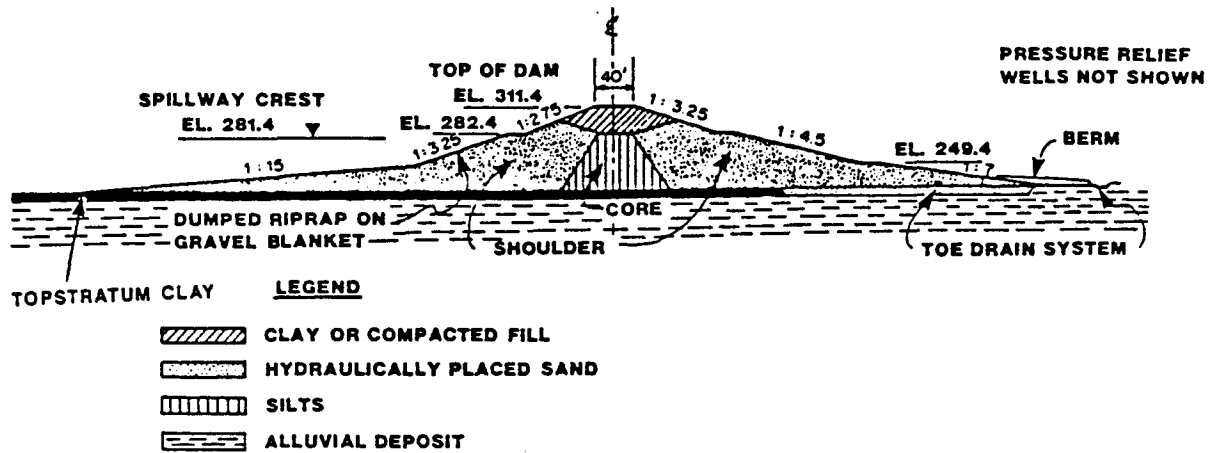


Figure 2.1: Typical Section of Sardis Dam (Finn et al., 1990a)

clays. During dam construction, the topstratum clay was removed from beneath the downstream portion of the dam to help control under seepage. The project was built in the late 1930's.

Hydraulic studies indicate that the probable maximum flood (PMF) would result in a reservoir level 3 m (10 ft) below the embankment crest. The limited discharge capacity of the outlet works prevents maintaining a specified reservoir level during periods of even moderate rainfall. The difficulty in maintaining a constant reservoir level has a significant impact on the feasibility of performing remedial work on the upstream slope.

Proximity of Sardis Dam, a hydraulic fill structure, to the New Madrid area, a region of significant historical seismicity, led to concern about the possibility of seismically induced liquefaction of portions of the dam and foundation and the stability of the dam

under seismic loading. The U. S. Army Corps of Engineers, Vicksburg District, undertook several studies to evaluate the probable behaviour of the dam during and after an earthquake . The results of these investigations indicated that some remedial measures were necessary to improve the stability of Sardis Dam during seismic loading.

Chapter 3

PREVIOUS SEISMIC STUDIES

3.1 Previous Investigation

Using the results of field and laboratory testing, conventional seismic assessment procedures (described in next chapter) were followed to predict the effects of the maximum credible earthquake on the structure. In Sardis dam, many borings were drilled and standard penetration tests(SPT) were performed both in the dam and the foundation soils. Laboratory testing of undisturbed samples taken from the borings included classification tests and static and cyclic triaxial tests.

From the previous investigations, it was concluded that the downstream stability of the dam is adequate during and after the earthquake. However, previous investigators found zones with the potential for liquefaction or significant strength loss which could threaten the upstream stability of the dam. These zones include the hydraulically placed silt core, and a discontinuous layer of weak clayey silt located in the foundation beneath the upstream slope of a 310 m (1000 ft) long portion of the dam. Preliminary field exploration also indicated the possible existence of discontinuous layers of weak clayey silt in other areas of the dam foundation. The upper 3 m (10 ft) to 9 m (30 ft) of sand shell along the lower portion of the upstream slope was also identified as having a potential for liquefaction; however, loss of strength in this zone has a relatively small effect on the stability of the dam.

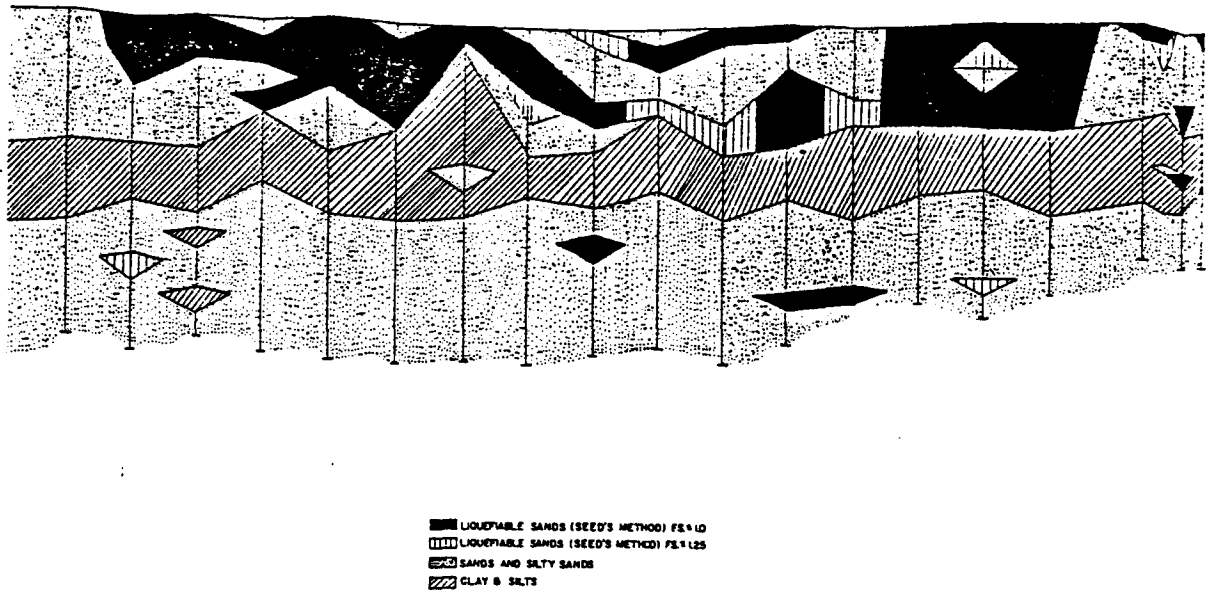


Figure 3.1: Longitudinal Section Showing Liquefiable Zones in Shell and Foundation Sands 139 m (450 ft) Upstream from Centerline (Finn et al., 1990a)

Fig. 3.1 shows zones of potential liquefaction within the shell and substratum sands where the predicted factor of safety against liquefaction is less than unity. This is a section about 139 m (450 ft) upstream. There was some concern that unacceptable excess porewater pressure might be generated in areas where the predicted factor of safety is between 1.0 and 1.25, and these zones are shown with hatched vertical lines. The study showed that liquefaction might occur in the upper portions of the upstream shell beginning between 31 m (100 ft) and 77 m (250 ft) upstream of the centerline and extending at least 139 m (450 ft) upstream.

The factor of safety with respect to upstream stability of the dam would still be adequate except in areas where the weak clayey silt layer occurs beneath the upstream slope

within 77 m (250 ft) of the centerline, even though the silt core might liquefy along the entire length of dam.

3.2 Potential for Liquefaction in Fine Grained Soils

Field data was evaluated and additional exploration and testing were conducted to locate any other zones of weak clayey silt. Discontinuous layers of the weak clayey silt were subsequently identified in two areas outside the original 310 m (1000 ft) long section.

Liquefaction potential of the weak clayey silt in the original investigation was determined using the Chinese criteria developed by Wang (1979). These criteria are :

- per cent finer than 0.005 mm \leq 20%
- liquid limit, LL \leq 35%
- natural water content \geq 0.9 LL
- liquidity index, $I_w \leq 0.75$

Liquefaction or significant loss of shear strength will occur for soils which satisfy all four criteria. In addition, any fine grained soils for which the standard penetration resistance $N \leq 4$ were also assumed to liquefy or suffer significant strength loss whether they satisfied the Chinese criteria or not. The Chinese criteria were applied strictly with no account taken of uncertainties in the measurement of the parameters in the criteria. In the later investigations these uncertainties are taken into account.

In the original investigation, the residual strength of the weak clayey silt in the foundation was established on the basis of judgement, the Seed's (1987) criterion, and laboratory vane tests. Sample disturbance and subsequent reconsolidation prior to testing resulted in higher values for the residual strengths determined by the laboratory vane tests than would be expected in situ. A more elaborate procedure was adopted for the later investigations involving use of cone penetration testing and field vane test data.

In the later investigation, Woodward Clyde consultants (1989) suggested that allowances should be made for uncertainties in the measured values of the parameters in the criteria. They recommended ignoring the liquidity index and making the following changes in the measured soil properties before applying the criteria:

- decrease per cent fines by 15%
- decrease LL by 5%
- increase water content by 3%

These changes increased significantly the extent of the soils vulnerable to liquefaction and strength loss so that almost the entire length of the dam required remediation. Therefore, the Vicksburg District engineers reviewed reports on the scatter in measured index properties in U.S. Corps of Engineers' laboratories over the last 30 years to determine the likely range of variation in test data. In addition they conducted tests on samples of standard soils of low to medium plasticity in their own laboratory to establish the scatter in their data. These standard soils are used to check comparability of testing procedures between different Corps of Engineers' laboratories and private laboratories. As a result of these studies the following changes in measured properties were adopted

before applying the Chinese criteria (again ignoring the liquidity index) :

- decrease the fines content by 5%
- decrease the liquid limit by 2%
- increase the water content by 2%

This change reduced the length requiring remediation to about 1700 m (5500 ft). The impact of the Chinese criteria on the extent of remediation necessary for stability appeared to be so critical that an investigation of Chinese procedures was undertaken by Koester (1990). The Chinese determine the liquid limit using a fall cone rather than the Casagrande device generally used in North America. Using a standard Chinese fall cone and following Chinese standard SD 128-007-84, Koester (1990) showed that the fall cone gives a liquid limit about 3% or 4% greater than the Casagrande device. The Koester study is not complete and findings relative to the liquid limit should be viewed as tentative.

On the basis of all the above studies the following changes in measured index properties were finally adopted to account for uncertainty before application of the Chinese criteria:

- decrease the fines content by 5%
- increase the liquid limit by 1%
- increase the water content by 2%

These changes reduced the length requiring remediation to about 926 m (3000 ft).

The zones in the topstratum clay vulnerable to strength loss based on the $N \leq 4$ Rule and the Chinese criteria and taking account of uncertainty are shown in plan, Fig. 3.2, and in longitudinal section at a location 76 m (250 ft) upstream from the centerline of the dam, Fig. 3.3. Those zones are designated as weak clayey silt layers found outside the 1988 remediation berms.

3.3 Conclusions Drawn from Previous Seismic Study

- 1.) The silt core of the dam may liquefy along the entire length of the dam.
- 2.) The post-liquefaction factor of safety with respect to the upstream stability of the dam would still be adequate except in areas where the weak clayey silt layer occurring beneath the upstream slope.
- 3.) The Chinese criteria for evaluating the potential for liquefaction or significant strength loss in clayey soils, based on liquid limit, water content and per cent fines ≤ 0.005 mm, can have a major impact on the extent of remedial measures necessary to achieve stability in earth structures with potentially liquefiable fine grained materials.
- 4.) Before applying the Chinese criteria the uncertainties in the measured soil properties should be taken into account in a reasonably conservative manner. This may be done by adjusting the measured water content, liquid limit, the fines content before applying the criteria. The amount of these adjustments should be based on the estimated



Figure 3.2: Plan View of Liquefiable Weak Clayey Silt Zones (Finn et al., 1990a)

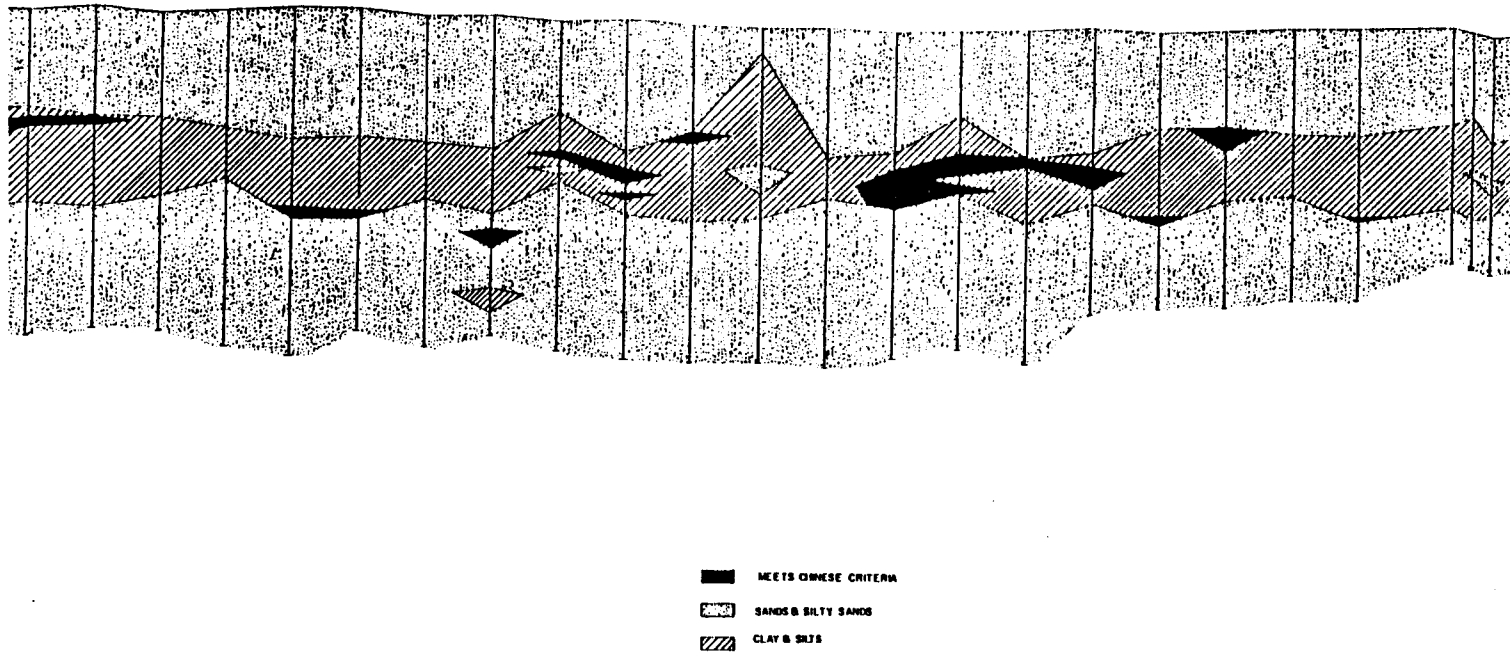


Figure 3.3: Longitudinal Section Showing Liquefiable Weak Clayey Silt Zones 139 m(450 ft) Upstream from Centerline (Finn et al., 1990a)

variability in data appropriate for the laboratory conducting the tests. In the absence of such specific information, the adjustments noted above of increasing the liquid limit by 1%, the water content by 2%, and decreasing the fines content by 5% may be considered. These adjustments reflect conservative estimates of the variability to be expected from very experienced personnel operating under high standards of quality control. Due note should be taken of the possible sensitivity of the liquefaction assessment to minor changes in the measured parameters.

5.) The zones of weak clayey silt vulnerable to strength loss are determined based on the $N \leq 4$ Rule and the Chinese criteria and taking account of uncertainty. Those zones are found outside the 1988 remediation berms and need to be remediated.

Chapter 4

THEORY OF POST LIQUEFACTION ANALYSIS

4.1 Conventional Static Equilibrium Method

The static equilibrium method is widely used to assess the stability of an earth dam after liquefaction in the dam or foundation. In this method, the factors of safety against shear failures along all potential failure surfaces are determined based on the residual strengths of the liquefied soils.

In the case of dams some deformations are acceptable although such deformations may indicate temporary factors of safety less than unity. Therefore, in accordance with the concept of designing dams for acceptable deformations proposed by Newmark (1965), there is a tendency to move away from the factor of safety concept and to evaluate the extent of necessary remedial measures on the basis of a tolerable amount of deformation for the low probability event specified by the design earthquake. This approach requires a reliable method of estimating post-liquefaction deformations.

4.2 The Deformation Analysis Theory

Post-liquefaction deformations for soil structures can be computed by using a nonlinear finite element code developed by Finn and Yogendrakumar (1989). This finite element

code is incorporated in the computer program TARA-3FL. The program has the capability of computing potential flow deformations. This flow deformation analysis method make it possible to assess the seismic behaviour of soil structures incorporating zones of liquefiable soils.

When a saturated or partially saturated soil structure undergoes an earthquake loading, the dynamic pore water pressures in the saturated soils increase, shear strengths of the saturated soil decrease. As the dynamic porewater pressures increase more and more, liquefaction may occur, and the shear strengths of the liquefied soils may reduce to steady state strengths or residual strengths.

In the present preliminary study, it is assumed that the residual strengths will be triggered in all soil elements that will liquefy according to the criteria developed by Seed et al. (1985), and the analysis is concentrated on the post-liquefaction behaviour only. In the deformation analysis involving soil liquefaction, the first requirement is a triggering criterion to switch the strength of any liquefiable soil in the dam to the residual strength at the proper time during the dynamic analysis. Two criteria are available , the peak strain criterion of Castro et al. (1989) and the stress ratio criterion of Vaid and Chern (1985). These criteria are not used in the present analysis. This analysis simply focuses on the fact that the residual strengths are reached but ignores when the residual strengths will be reached.

In the proposed deformation analysis, the soil structure is analyzed using initial or pre-earthquake soil strengths and moduli before applying a seismic loading. A stress-strain field prior to the earthquake loading is thus determined. When the seismic loading

is applied, increases in dynamic porewater pressures in saturated soils lead to reductions in shear strengths and shear moduli of the saturated soils which cause unbalanced shear stresses in the soil structure. As the unbalanced shear stresses are redistributed throughout the soil structure, a new stress-strain field is reached, and flow deformations are obtained for this level of shear strengths.

In any particular element in a dam, the shear stress-strain state which reflects pre-earthquake conditions is specified by a point P on the stress-strain curve as shown in Fig. 4.1. When liquefaction is triggered, the strength will drop to the steady-state value. The post-liquefaction stress-strain curve cannot now sustain the pre-earthquake stress-strain condition, and the unbalanced shear stresses are redistributed throughout the dam. In the liquefied elements, the stresses are adjusted according to the following equation,

$$\partial\tau = \frac{\partial f}{\partial\sigma'_m} d\sigma'_m + \frac{\partial f}{\partial\gamma} d\gamma \quad (4.1)$$

where $\tau = f(\sigma'_m, \gamma)$. This process leads to progressive deformation of dam until equilibrium is reached at the state represented by P_2 .

For static preliminary studies of flow deformations the basic idea is simulating the reduction sequence of the shear strengths in liquefied soils or non-liquefied soils by conducting a series of static finite element analyses. For each subsequent step of the deformation analysis, the previous shear strengths are reduced by a small percentage such as 5%. A final flow deformation configuration is determined as the final post-earthquake shear strengths (residual shear strengths) are reached in all liquefied elements. Since the deformation may become large, it is necessary to update progressively the finite element

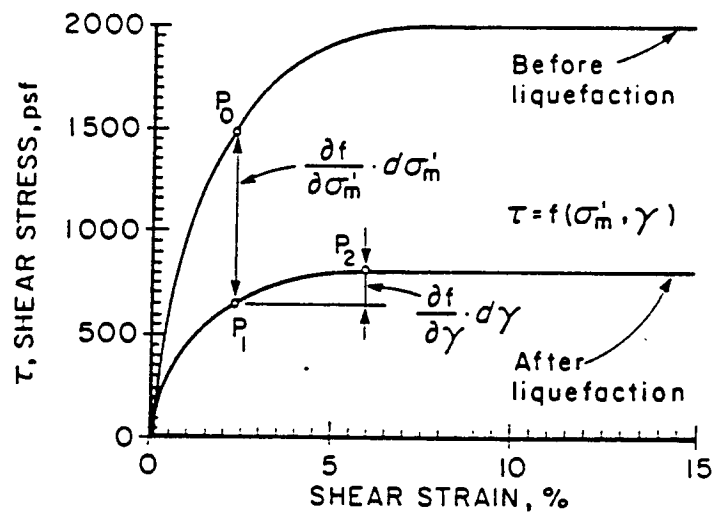


Figure 4.1: Adjusting Stress-Strain State to Post-Liquefaction Conditions (after Finn et al., 1990b)

mesh. Each calculation of incremental deformation is based on the current shape of the dam, not the initial shape as in a conventional finite element analysis. If the resulting flow deformations are not acceptable, the design must be not used. If they are acceptable, then the dynamic form of the analysis is used to check the design.

To model the nonlinear stress-strain behaviour of the soil material, an incremental elastic approach is used where the soil is assumed to be isotropic and elastic during the load increment. The two-dimensional stress-strain relationship is determined by a pair of elastic stiffness constants, tangent bulk modulus B_t and tangent shear modulus G_t . The bulk modulus can be expressed by:

$$B_t = K_b \cdot P_a \cdot \left(\frac{\sigma'_m}{P_a}\right)^n \quad (4.2)$$

where

K_b = bulk modulus constant

P_a = atmospheric pressure

σ'_m = effective mean normal stress

n = bulk modulus exponent

The constants K_b and n are determined by triaxial tests (Duncan and Chang, 1970). The tangent shear modulus G_t is determined by using a hyperbolic shear stress-strain model based on the maximum shear modulus, the shear strength, and the shear strain (Finn and Yogendrakumar, 1989). The maximum shear modulus G_{max} may be input directly if known or calculated by the program using the following equations (Seed and Idriss, 1970):

for sands,

$$G_{max} = K_{2max} \cdot P_a \cdot \left(\frac{\sigma'_m}{P_a}\right)^{0.5} \quad (4.3)$$

for clays,

$$G_{max} = K_c \cdot S_u \quad (4.4)$$

where S_u is the undrained shear strength and K_{2max} and K_c are parameters to be estimated or determined. The maximum shear modulus may be determined based on laboratory tests or on the shear wave velocity from conventional seismic crosshole tests. If direct data are not available, the maximum shear modulus of soil can be estimated based on the relative density of sands or on the level of shear strain for clays (Seed and Idriss, 1970).

Chapter 5

RESIDUAL SHEAR STRENGTH

5.1 Introduction

Liquefaction involves large unidirectional shear deformations. When the soil is strained beyond the peak strength, the undrained strength drops to a value that is maintained constant over a large range in strain, as illustrated by curve 1 in Fig. 5.1. The steady state of deformation for any mass of particles is that state in which the mass is continuously deforming at constant volume, constant normal effective stress, constant shear stress, and constant rate of shear strain. The steady state is achieved only after the structure is completely remolded and all particle orientation effects have reached a steady state condition and after all particle breakage, if any, is complete. The steady state exists only during deformation. The shear strength under steady state condition is called the undrained steady state strength or residual strength.

If the driving shear stresses due to gravity on a potential slip surface through liquefied materials in an embankment are greater than the undrained steady state strength, deformations will occur until the driving stresses are reduced to values compatible with static equilibrium (Fig. 5.2). The more the driving stresses exceed the steady state strength the greater the deformations to achieve equilibrium. The driving shear stresses to be used in analyzing liquefaction are not the shear stresses resulting from placement or consolidation of the soil, but rather are the minimum shear stresses that are necessary

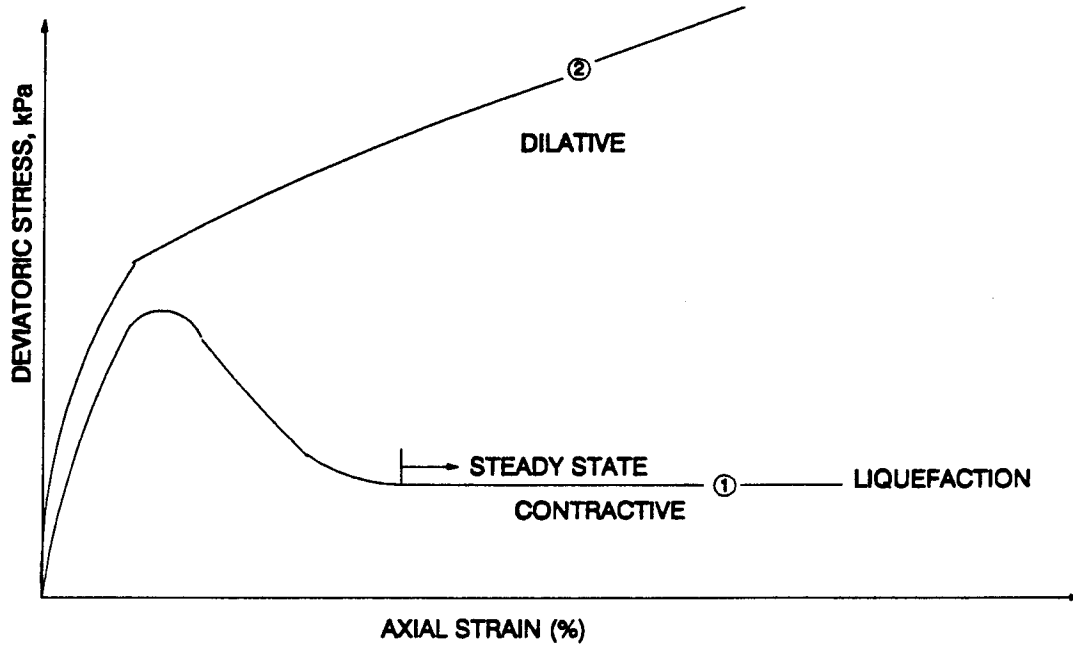


Figure 5.1 Types of Stress Strain Curve for Consolidated Undrained Triaxial Tests on Clean Sand

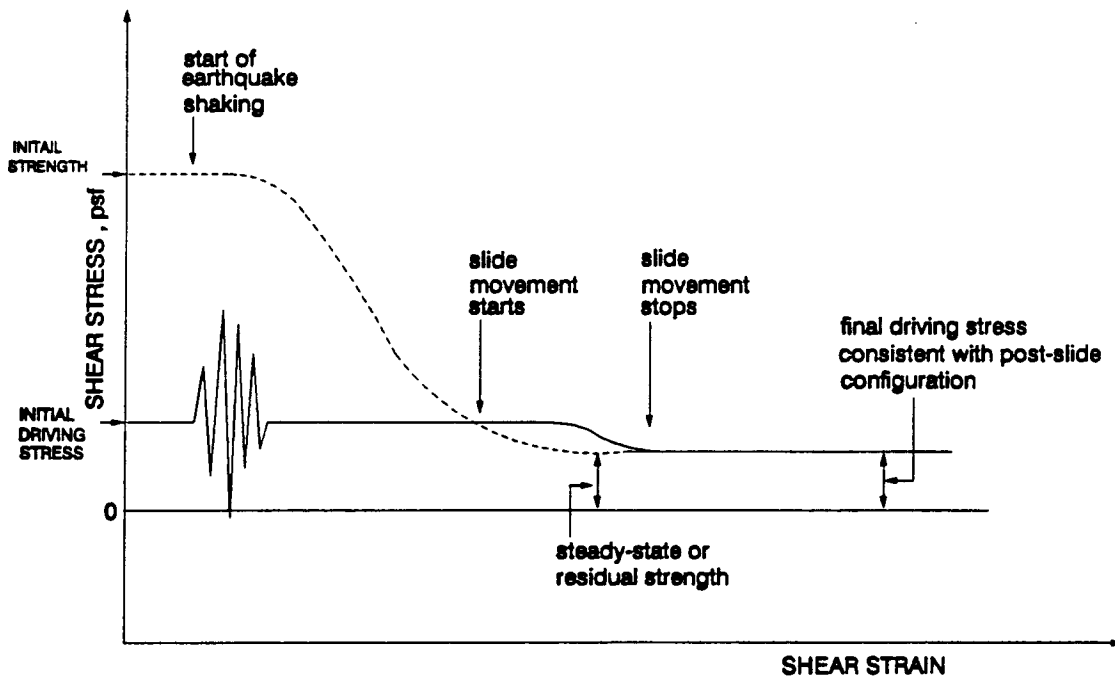


Figure 5.2 Changes in Driving Stresses and Undrained Shear Strength During an Earthquake

to maintain equilibrium of soil mass under external or body forces. The driving shear stresses that should be compared to the steady state shear strength are shear stresses which will continue to be applied to soil as deformation occur.

The residual strength is the crucial element controlling post- liquefaction deformations. Therefore available procedures in determining the residual strength are critically discussed below.

5.2 Determination of Residual Strengths

5.2.1 Steady state concept

Casagrande (1936) in his classic paper discussed the significance of the critical void ratios of cohesionless soils. In his paper, Casagrande pointed out that a sand with a void ratio greater than the critical void ratio tends to contract upon monotonic shearing, whereas a sand with a void ratio less than the critical value tends to expand. Thus, when a saturated sand is sheared in an undrained state, positive pore pressures are developed if the void ratio is greater than this critical value (loose sands). The development of positive pore pressures leads to a reduction in the effective normal stress and consequently to a reduction in shearing strength. It was found that the critical void ratio varied with the effective confining pressure. The line describing such a relation on a critical void ratio versus effective confining pressure plot is unique for a given sand and is called the steady state line. The undrained steady state shearing strength is represented by the strength corresponding to the effective confining pressure on the steady state line and the associated void ratio.

Since it is the steady state shear strength that is needed for a liquefaction analysis , it is convenient to plot the results of the undrained triaxial tests in terms of void ratio versus undrained steady state strength on the failure plane, as shown in Fig. 5.4, rather than in terms of σ'_{3s} , as shown in Fig.5.3. The corresponding steady state, undrained strength of the soil, S_{us} , can be determined from the Mohr diagram and expressed in the following form:

$$S_{su} = \frac{\sin\phi' \cdot \cos\phi'}{1 - \sin\phi'} \sigma'_{3s} \quad (5.1)$$

where ϕ' is the effective friction angle , and σ'_{3s} the effective minor principle stress, corresponding to the steady state condition.

The steady state strength of liquefied sands, S_{us} , generally can not be determined directly by undrained shear tests on undisturbed samples from the field . Such contractive soils are very difficult to sample. They are likely to densify during sampling, transportation and the process of setting up the tests. Therefore the tests cannot be conducted at the field void ratio. A procedure for dealing with this problem has been proposed by

Poulos et al. (1985). In the procedure the steady state strength of a good quality undisturbed sample is determined at the laboratory void ratio after reconsolidation in the laboratory. It is then assumed (1) that there is a unique relationship (the steady state line) between steady state strength and void ratio ; (2) that the slope of the steady state line is the same for reconstituted samples of that sand as for undisturbed samples; and (3) that the slope of the steady state line is independent of the method by which samples are reconstituted in the laboratory. Thus by performing tests on reconstituted samples,

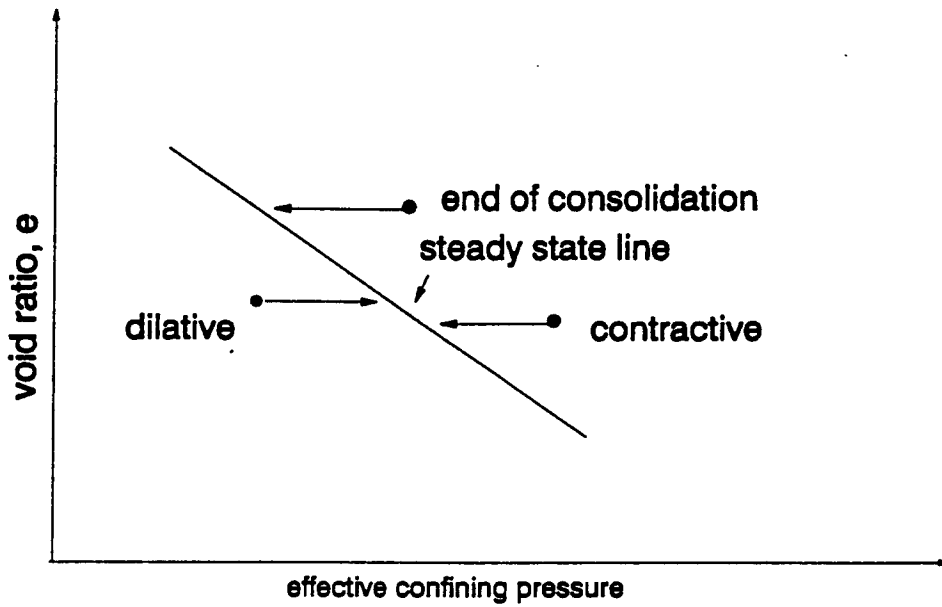


Figure 5.3 Steady State Line (void ratio vs effective confining pressure)
(after Poulos et al., 1985)

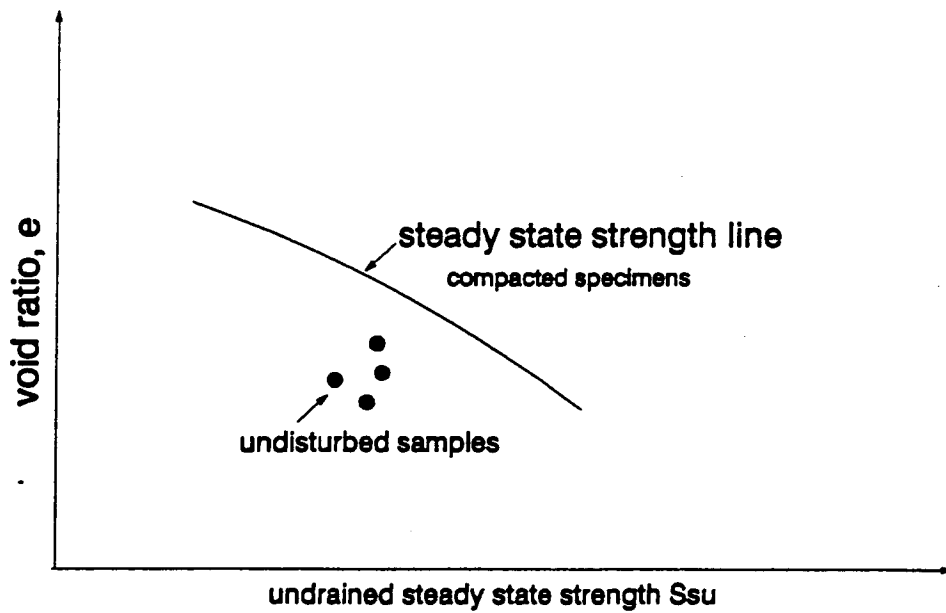


Figure 5.4 Steady State Line (void ratio vs steady state strength)
(after Poulos et al., 1985)

the slope of the steady state line for these samples can be established and used to predict the steady state strength of the undisturbed sample at the void ratio corresponding to its in-situ condition. The procedure for the accomplishing this is illustrated in Fig. 5.5.

The steady state line in $e - \log S_{su}$ space is obtained by tests on reconstituted samples at different void ratios. Then S_{su} is measured in undrained compression tests on good quality undisturbed samples from the field. A representative value of this laboratory steady state strength, $(S_{su})_L$ is plotted in Fig. 5.5 at the void ratio at failure in the laboratory, e_L . A line is drawn through the point $((S_{su})_L, e_L)$ parallel to the line for reconstituted samples and the strength corresponding to the field void ratio, e_f , given by this line, is taken as the steady state strength in the field, $(S_{su})_f$.

There are some difficulties with the use of this procedure. First the differences between the steady state lines of the field samples can be very wide. It is clear that selection of a representative steady state strength poses significant problem for a designer or analyst. Secondly there is controversy over whether the undrained steady state strength is stress path dependent or not.

Castro et al. (1985) hold the view that steady state strength is independent of the stress path. Vaid et al. (1990) conducted an extensive test program on Ottawa sand and a tailings sand to investigate the effects of stress path on steady state strength using extension and compression tests. They found that the steady state strength was greatest in compression. In the case of loose Ottawa sand, the ratio of steady state strength in compression to the strength in extension was 10:1; for the loose tailings sand, the ratio was about 6:1. Furthermore the range in void ratios exhibiting contractive behaviour in extension is much larger than in compression. These tests were conducted on water

pluviated sands to simulate the depositional process in nature. Such sands are inherently anisotropic and their response to loading depends on the orientation, β , of the major principal stress relative to the plane of deposition. The data strongly suggest that the steady state or residual strength of soils in the field is a function of β (Vaid et al., 1990).

The dependence of S_{su} on β has important practical implications. The angle β varies along the curved failure surface of an embankment from $\beta = 0$ (compression loading) near the crest to $\beta = 90$ degree (extension loading) at the toe (Fig. 5.6). Therefore steady state strength based on data from compression tests would appear to be applicable only near the upper part of the failure surface. The strength should decrease and reach its lowest value in extension near the toe. Thus the average steady state strength in the

liquefied zone of the lower San Fernando dam may be much less than that value measured in laboratory compression tests. Seed et al. (1988) have shown from back analysis of the San Fernando dam that the average steady state strength in situ was substantially less than the average strength measured in compression tests.

Discrepancies between steady state strength in compression measured on undisturbed samples and the average steady state strength computed by back analysis of the San Fernando slide are credited almost entirely to densification. The quantitative effect of stress path in steady state strength suggested by the work of Vaid et al. (1990) may account for a substantial part of the difference noticed in the San Fernando dam studies. This effect is also crucial to a reliable stability analysis.

There are clearly sharp differences between recent research finding and current practice in the determination of steady state strength from laboratory tests. The key assumption underlying current practice that the steady state strength is a function of void ratio

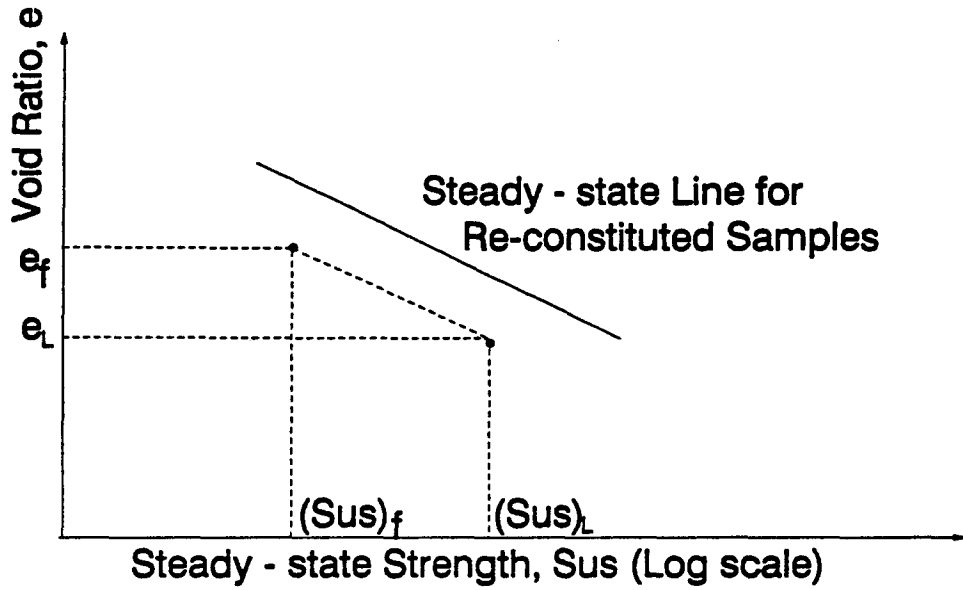


Figure 5.5 Poulos Procedure for Determining Steady State Strength (after Poulos et al., 1985)

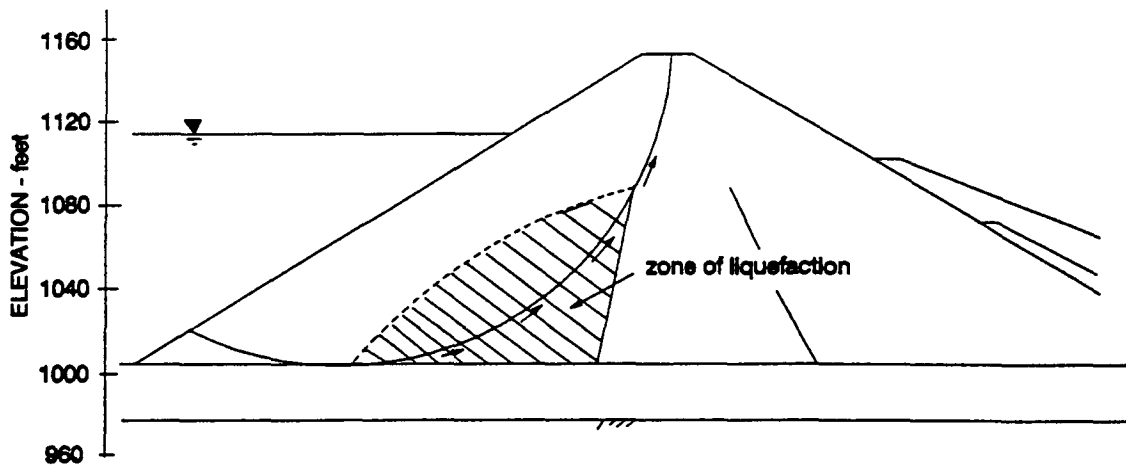


Figure 5.6 Cross Section of Lower San Fernando Dam Showing Liquefaction Zone (after Seed et al., 1988)

only needs further investigation. More studies on the effects of stress path are needed to establish a generally acceptable position on this very important problem.

5.2.2 A correction between residual strengths and SPT blowcounts

Seed (1987) developed an alternative approach to determining steady state strength. He analyzed the stability of a number of field cases in which large deformations occurred after liquefaction and developed a correlation between in situ steady state strength and representative $(N_1)_{60}$ values. This correlation was updated in 1987 by refining some of the previous analyses and incorporating new data from embankment failures during the Chilean earthquake of 1985 (De Alba, et al., 1987). The latest version of the correlation is shown in Fig. 5.7.

There are two challenges for the designer in using this correlation. The first is related to the range in strength at a given penetration resistance. At the low penetration resistances associated with very contractive materials the range in strength is many times the minimum value. This makes it very difficult to decide on an appropriate value for residual strength at low penetration resistances. The second challenge relates to the selection of a representative $(N_1)_{60}$. The dispersion of $(N_1)_{60}$ values can be very wide in the field. This dispersion can be particularly troubling when analyzing case histories to determine steady state strengths. An excellent discussion of all the difficulties associated with the analysis of case histories of flow deformation to determine steady state strength may be found in Seed et al. (1988).

5.3 Evaluation of Residual Strength on Sardis Dam

The residual shear strength in the liquefied silt core in Sardis Dam was estimated to be 5 kPa (100 psf) based on Seed's correlation between corrected standard penetration resistance $(N_1)_{60}$ and residual strength shown in Fig. 5.7; see Seed et al, 1988.

In the original investigation, the residual strength of the weak clayey silt in the foundation was established on the basis of judgement, the Seed (1987) criterion, and laboratory vane tests. Sample disturbance and subsequent reconsolidation prior to testing resulting in higher values for the residual strengths determined by the laboratory vane tests than would be expected in situ. In the later investigation, the peak and residual in situ strength of the weak clayey silt were determined by field vane tests in the top-stratum clay. These residual strength (Fig. 5.8), however, were not used in the stability assessment prior to 1988 because cone penetration tests in adjacent locations appeared

to indicate the presence of silt and sand lenses that might have allowed some drainage during the vane tests. Such drainage would result in higher strength values. Woodward Clyde Consultants (1989) reviewed the results of classification tests conducted on samples of the soils tested by the field vane and concluded that lenses of sand or silt sufficient to cause significant internal drainage were not present. Furthermore, they concluded that even if lenses small enough not to have been detected in the classification were present, they were unlikely to have allowed significant drainage at the typical rates for conducting the vane tests (about 6 degree per minute in the post-peak phase of the test).

The field vane tests were used to estimate the ratios of peak undrained strength, S_u , and residual strength, S_{su} , to the effective overburden pressure σ'_{vo} and the sensitivity S_u/S_{su} . The peak undrained strength was also estimated from cone penetration test data

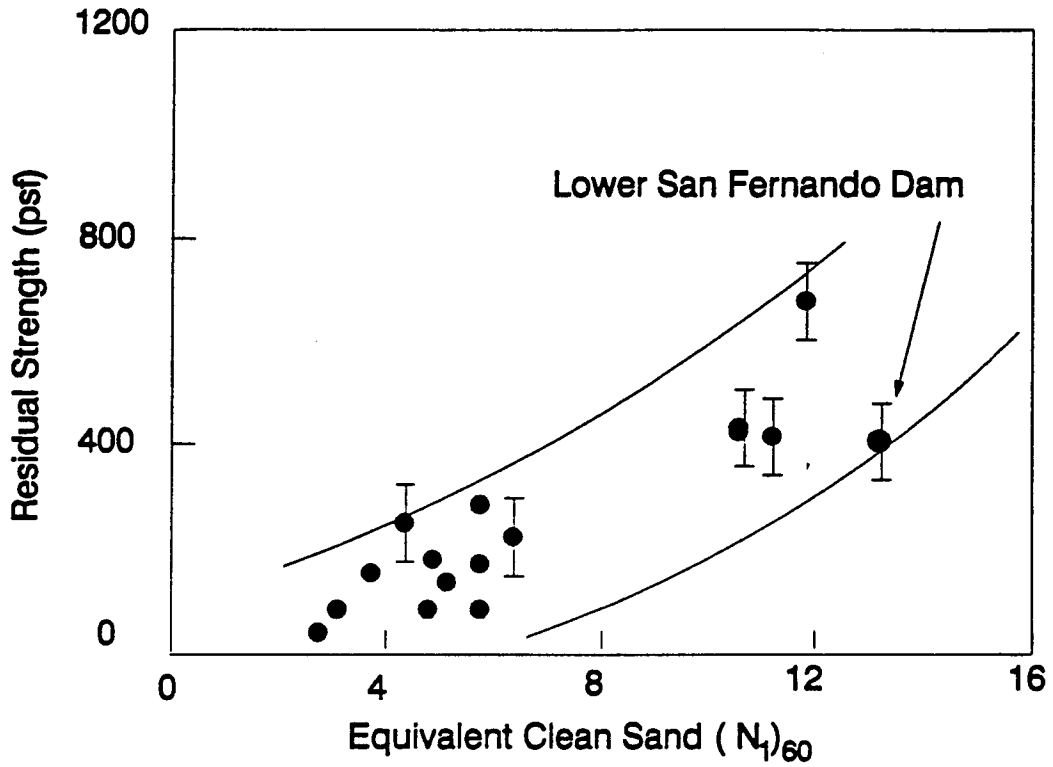


Figure 5.7 Tentative Relationship Between Residual Strength and SPT N Values for Sands (after Seed et al., 1988)

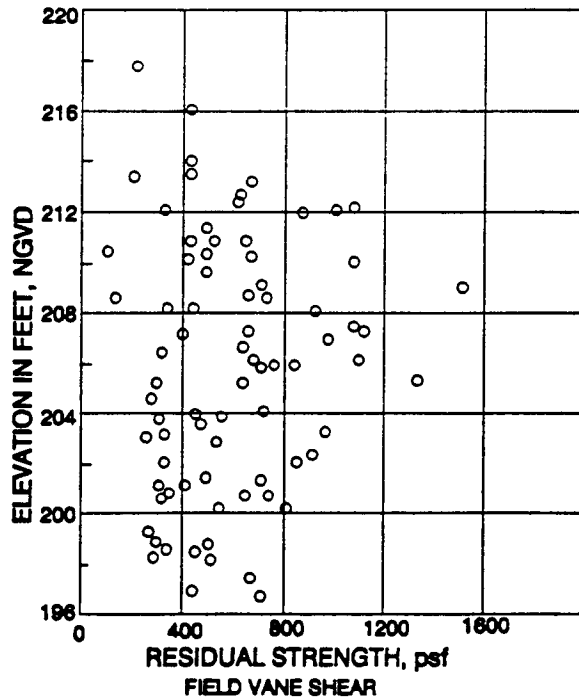


Figure 5.8 Residual Strength in Topstratum Clay - Sardis Dam (after Finn et al., 1990a)

using the equation developed by Robertson and Campanella (1983),

$$S_u = \frac{q_c - \sigma_{vo}}{15} \quad (5.2)$$

where q_c = cone tip resistance and σ_{vo} = total overburden pressure. In addition, estimates were obtained of the undrained strength required to give factor of safety in the range of 1.5 to 2.0. This range in factor of safety was considered appropriate for the pre-earthquake condition of the dam. A conservative assessment of all these results suggested an average S_u/σ_{vo} ratio for the weak clays and silts of about 0.2 to 0.3 . Based on these results for S_u/σ_{vo} , the work of Pyles (1981) on the shearing resistance of cohesive soils at large strains, the S_{su}/σ_{vo} ratios and sensitivities from the field vane tests, a conservative value of the residual strength for the weak clayey silt was estimated to be $S_{su}/\sigma'_{vo} = 0.075$.

The residual shear strength of the non-liquefiable top stratum clay was estimated at 100 kPa (2000 psf) on the basis of undrained triaxial tests.

Chapter 6

LIQUEFACTION DEFORMATION ANALYSIS

6.1 Initial Stress Conditions in Dam and Foundation

The mechanical behaviour of Sardis dam is simulated by modelling the performance of a typical cross section . The actual three dimensional problem is simplified as a two dimensional plane strain problem. Both initial stresses after the construction and the deformations after liquefaction were computed by using the computer program TARA-3FL (Finn and Yogendrakumar, 1989) described earlier. The basic theory has been reported by Finn (1985,1990) and Finn et al. (1990).

6.1.1 Finite element mesh

For the purposes of simulating the initial stress conditions and the subsequent liquefaction behaviour of the dam , a finite element mesh is constructed as shown in Fig. 6.1 and Fig. 6.2, which show the element and node numbers of the mesh. This finite element mesh consists of 576 nodes and 502 quadrilateral elements.

The boundary conditions for analyzing the construction of dam and foundation are defined along all boundaries. The surfaces of the dam and the free field are free to move horizontally and vertically.

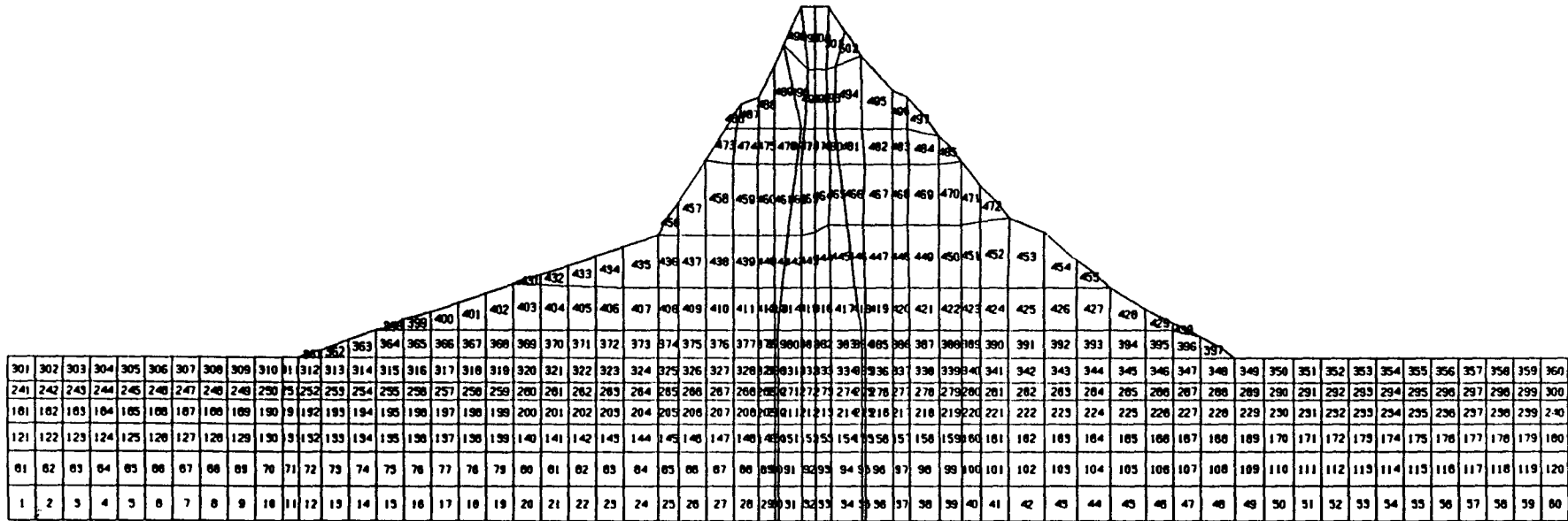


Figure 6.1: Finite Element Mesh Showing Element Distribution

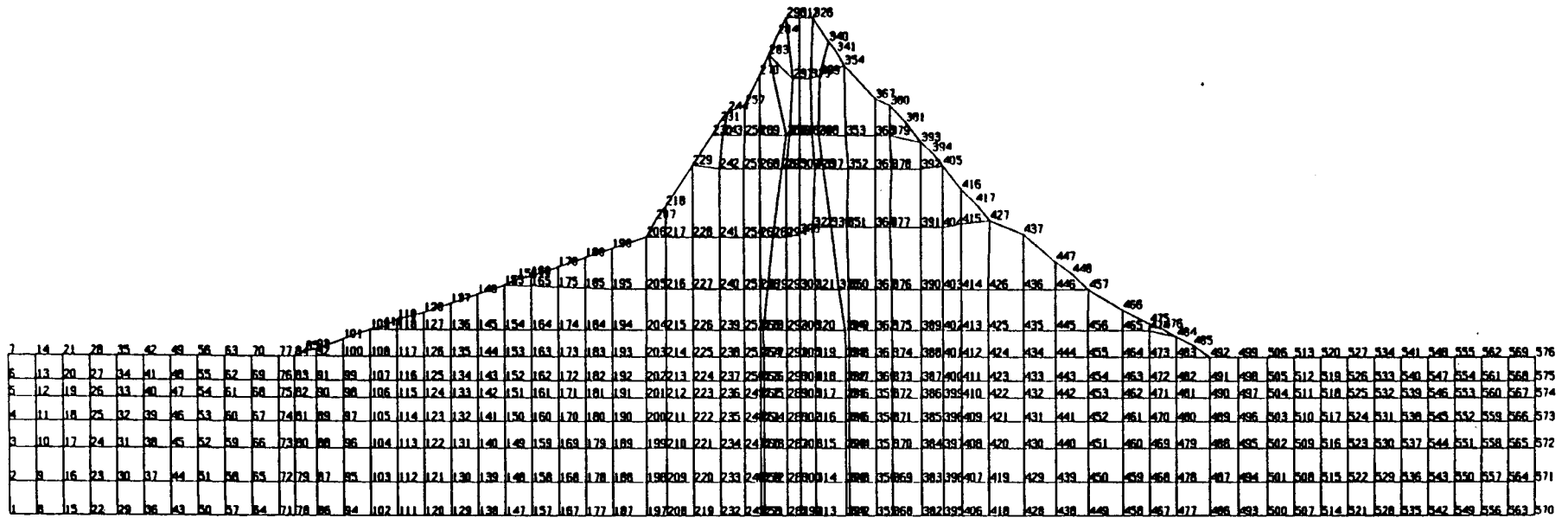


Figure 6.2: Finite Element Mesh Showing Node Distribution

Nodes on the base are fixed in both directions. At the two side boundaries the nodes are free to move vertically but are fixed horizontally. Therefore, the two side boundaries have to be far enough so that the building of the dam could not cause significant horizontal movements at the two side boundaries.

The rest of the nodes in the mesh are set free to move in both X and Y directions.

6.1.2 Soil material properties

Parameters defining material properties are assigned to each element to reflect realistic strengths and moduli. Generally the elements are grouped to represent zones of different materials. In each zone, the same material parameters are used. Fig. 6.3 shows the distribution of these material zones.

The dam foundation consists of a 10 to 20-foot thick zone of natural silty clay, designated as top stratum clay and modelled as material #2 and #5. The top stratum clay is underlain by pervious alluvial sands, designated as substratum sands and modelled as material #1, approximately 40-foot thick. The substratum sands are underlain by tertiary silts.

Sardis Dam consists of a central silt core, constructed by hydraulic filling. The saturated (liquefiable) and drained (above water table) parts of the silt core were modelled as material #8 and #9, respectively. The silt core is surrounded by a sand shell. The drained part of the sand shell was modelled as material #10. The saturated part of the sand shell was modelled as material #6 (non-liquefiable) and #7 (liquefiable). The crest of the dam consists of a compacted clay fill which was modelled as material #11.

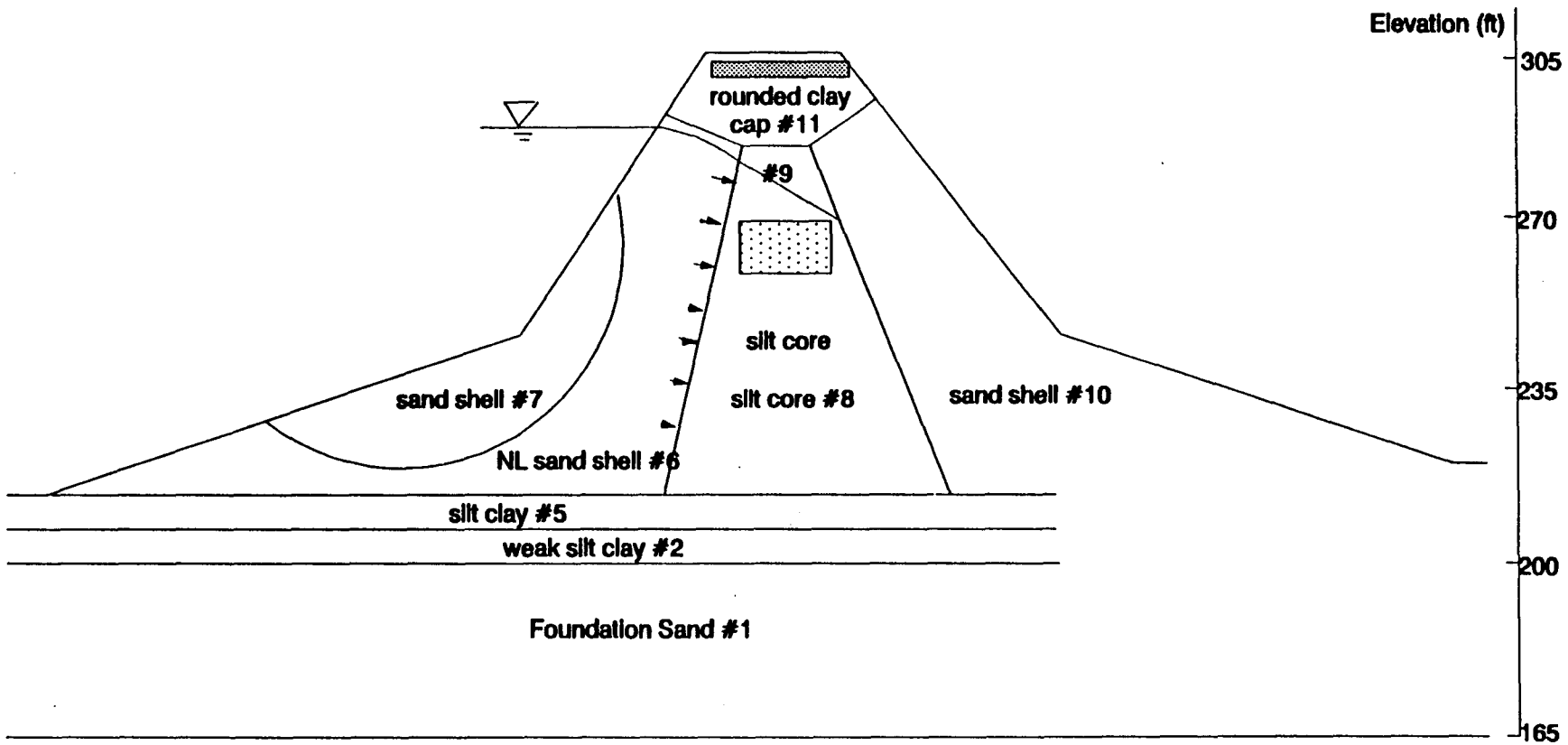


Fig. 6.3 Distribution of Soil Material Zones

Table 6.1: Parameters of Strength and Stiffness Used in the Construction Analysis

Material#	ϕ°	C (psf)	K_b	n	K_c	K_{2max}	γ (pcf)
1	35	0	6182	0		61	125
2	0	2000	13230	0	1400		120
5	0	2000	13230	0	1400		120
6	35	0	6182	0		61	125
7	35	0	6182	0		61	125
8	20	300	4054	0		40	120
9	20	300	4054	0		40	120
10	35	0	5067	0		50	125
11	0	750	5150	0	1453		115

Materials:

- #1 - foundation sand
- #2 - weak clayey silt
- #5 - clayey silt
- #6 - sand shell (non-liquefiable)
- #7 - sand shell (liquefiable)
- #8 - silt core (liquefiable)
- #9 - silt core (above water table)
- #10 - sand shell (above water table)
- #11 - rounded clay cap

In the program TARA-3FL, soil materials have been classified into two types : sands and clays. For the construction sequence, drained strength and modulus parameters are used for sands, and undrained strength and modulus parameters are used for clays. After liquefaction, undrained strengths and moduli are used for all materials. Table 6.1 shows the soil parameters used in the construction sequence, which are obtained from the previous study. The parameters used for the liquefaction analysis will be presented in section where post-liquefaction analysis is considered.

6.1.3 Pool water level and water force

The conservation level of the reservoir is at elevation 277 ft. In this thesis, the performance of the dam after liquefaction was examined at this reservoir elevation. The dam crest is at elevation 312 ft, for an initial freeboard of 35 ft. If the material is submerged below the phreatic line (Fig. 6.3), the buoyant unit weight is used in analyses.

The water forces acting on left side of the relatively impermeable silt core should be included in the initial stress analysis of the construction. These forces shown in Fig. 6.3 are perpendicular to the core face. The distributed water forces are replaced by equivalent concentrated normal forces at the nodes and then resolved in the vertical and horizontal directions in an approximately representation of reservoir effects during liquefaction.

The construction of the foundation and the dam was modelled by a 13-layer construction sequence, where incremental stresses, strains and deformations were computed after the placement of each new layer. Final results of static analysis during construction stage were printed out by the program. In this way , the initial stress conditions in the dam before liquefaction were determined.

6.2 Description of Liquefaction Analysis

6.2.1 Liquefiable materials

Previous investigators had determined the zones with potential liquefaction or significant strength loss. These are :

- Hydraulically placed silt core (saturated) - material #8;
- Upper 10 to 30-foot of sand shell along the upstream slope - material #7;
- Discontinuous layer of weak clayey silt 5 ft thick located approximately 7 ft into top stratum clay - material #2.

The residual strength for the liquefied silt core is 100 psf, for the liquefied sand shell is 400 psf, and for the weak clayey silt is $0.075\sigma'_{vo}$, where σ'_{vo} is the effective vertical stress. Table 6.2 shows the variation of residual strengths in the weak clayey silt with locations in the dam foundation, a minimum value of 100 psf of the residual strengths was used in the analysis.

6.2.2 Soil properties after liquefaction

The maximum shear modulus and bulk modulus for sands can be calculated by following equations:

$$G_{max} = 21.7K_{2max}P_a\left(\frac{\sigma'_m}{P_a}\right)^{0.5} \quad (6.1)$$

$$B = K_bP_a\left(\frac{\sigma'_m}{P_a}\right)^n \quad (6.2)$$

where P_a is atmospheric pressure, 2117 psf; σ'_m is the mean normal stress. The other constants are shown in Table 6.1.

Using the appropriate mean normal stress from the final results of the construction analysis, we can calculate the maximum shear modulus G_{max} and bulk modulus B at the end of construction for the drained parameters. When drained strengths and moduli are shifted into undrained parameters, undrained strengths and moduli are approximated by

Table 6.2: Variations of Residual Strengths in the Weak Clayey Silt (psf)

<i>Element</i>	<i>WT277 model</i>
241-255	100
256	100
257	109
258	121
259	133
260	147
261	160
262	173
263	186
264	211
265	246
266	287
267	342
268	398
269	449
270	504
271	549
272	597
273	621
274	671
275	728
276	766
277	742
278	687
279	610
280	551
281	515

Table 6.3: Parameters of Strength and Stiffness after Liquefaction

Material#	ϕ°	C (psf)	K_b	n	K_c	K_{2max}	γ (pcf)
1	35	0	6182	0		61	125
2	0	$0.075\sigma'_{vo}$	13230	0	1400		120
5	0	2000	13230	0	1400		120
6	35	0	6182	0		61	125
7	0	400	6182	0	3825		125
8	0	100	4054	0	1384		120
9	20	300	4054	0		40	120
10	35	0	5067	0		50	125
11	0	750	5150	0	1453		115

maintaining the same values of these parameters. For the liquefaction or undrained condition, the bulk modulus exponent n is usually set to be zero and K_b adjusted accordingly. The moduli expressions for undrained parameters are :

$$G_{max} = K_c \cdot S_u \quad (6.3)$$

$$B = K_b \cdot P_a \quad (6.4)$$

The undrained equivalent shear modulus constant K_c and bulk modulus constant K_b could easily be evaluated by using equations (6.3) and (6.4) given the initial undrained values of G_{max} , B , and undrained strength.

There are three potential zones of liquefaction which are grouped as materials #2, #7 and #8. The soil parameters after liquefaction are shown in Table 6.3.

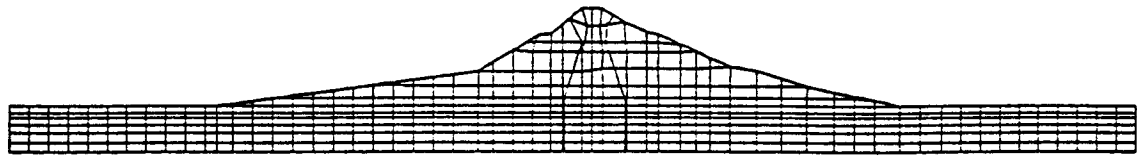
For Sardis Dam, the reduction of shear strengths and moduli of the liquefied weak clayey silt in the top stratum clay (material #2) mainly controls the final deformations

of the dam. The loss of strength and stiffness in the upstream sand shell after its liquefaction has a relatively minor effect. The strengths of the liquefied soils were reduced by 5% for each step in the sequence of strength reduction from initial undrained strength to residual strength. This led to a corresponding decrease in the undrained shear modulus. When the residual strength in any zone is reached, the residual strength is used as the shear strength in this zone for the subsequent steps of the analyses. For each new run, the calculated finite element mesh and stresses from the previous run were taken as the input data for the next run.

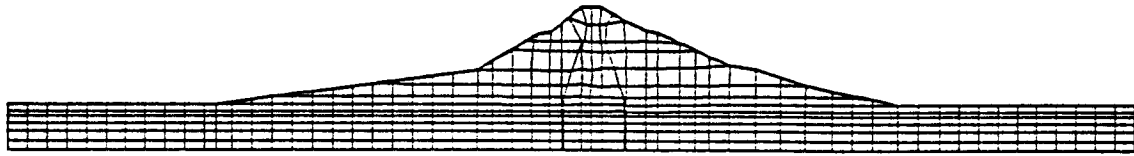
6.2.3 Results of liquefaction analyses

When the shear strength of the weak clayey silt decreases from 2000 psf to residual strengths, large deformations are induced in the dam. The water level of the dam is assumed to be at the elevation of 277 ft, and it is termed as the WT277 model. Fig. 6.4 shows the development of the deformed shape of the dam as the shear strengths in the weak clayey silt are reduced.

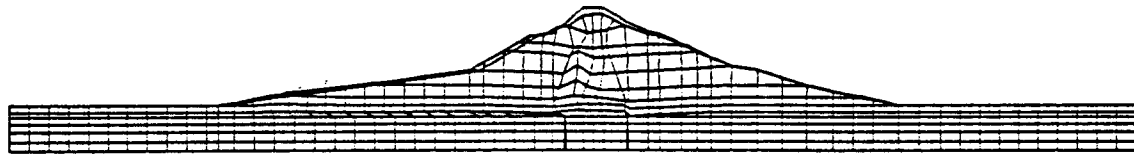
The variation of the loss of freeboard is illustrated in Fig. 6.5 for various levels of minimum residual strength. The residual strengths of the weak clayey silt vary depending on the initial effective stresses. The minimum value of these residual strengths in this layer for the current liquefaction step is designated as the minimum residual strength. The increase in the loss of freeboard is gradual with the decrease in the minimum residual strength. For the WT277 model, the loss of freeboard begins to increase very rapidly after the minimum residual strength drops to 400 psf. When the minimum residual strength reaches 100 psf, a crest vertical displacement of 45.5 ft is predicted from the analysis.



Minimum Residual Strength 2000 psf



Minimum Residual Strength 500 psf



Minimum Residual Strength 200 psf



Minimum Residual Strength 100 psf

vertical scale two times horizontal scale

horizontal scale (ft)

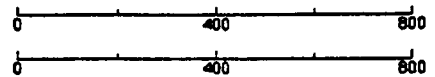


Figure 6.4: Variation of Post Liquefaction Configurations with Minimum Residual Strength - WT277 model

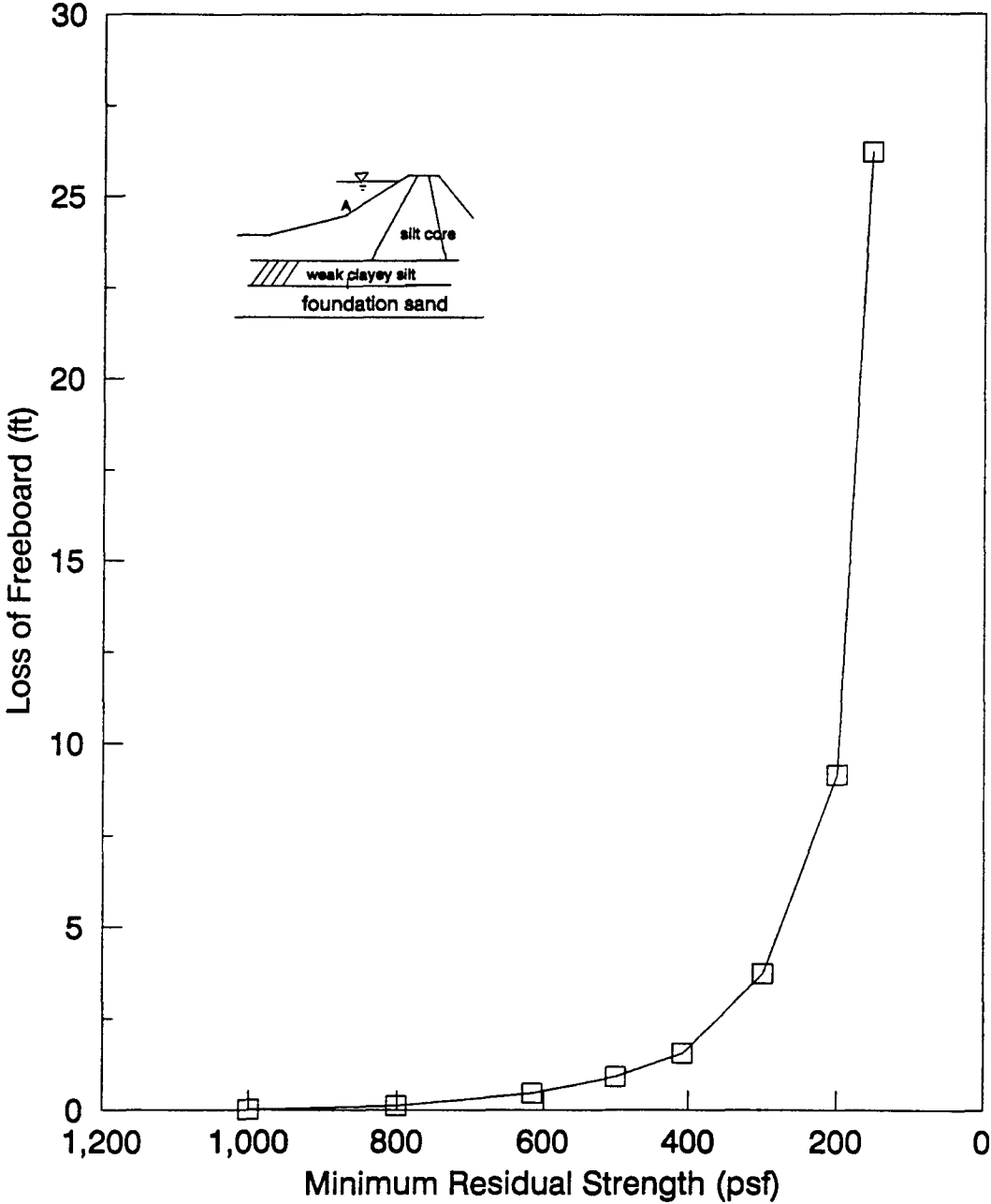


Fig. 6.5 Variation of Loss of Freeboard with Minumum Residual strength

Based on the original configuration of the dam for the WT277 model, the water level of the dam is at elevation 277 ft and the dam crest at elevation 312 ft, for an initial freeboard of 35 ft. Again from Fig. 6.5, the dam is predicted to overtop at minimum residual strength 120 psf of the weak clayey silt. Hence, remediation measures are required if an adequate freeboard is to be maintained.

The variations of horizontal displacements at the midpoint of the upstream slope (point A) are shown in Fig. 6.6 for various levels of minimum residual strengths. The horizontal displacements increase dramatically when the minimum residual strength is less than 400 psf. When the minimum residual strength drops to 100 psf, the horizontal displacement of 100 ft is predicted.

Fig. 6.7 illustrates the variations of maximum ratios of the shear stress to the shear strength in the weak clayey silt. This ratio increases constantly with the reduction of the minimum residual strength and reaches the steady state value of 1.0 at the minimum residual strength of 615 psf. This implies that the weak clayey silt fails before the minimum residual strengths 100 psf are reached.

Tables 6.4 summarizes the final results from the liquefaction analysis. The overall performance of the dam is very poor after liquefaction with its original configuration. The loss of freeboard is 45.5 ft after liquefaction. The maximum horizontal displacement of the dam is 100 ft. The dam will fail along the weak clayey silt layer under the upstream slope. Therefore, remediation measures are required to maintain an adequate freeboard of the dam. A zone of improved soil must be created in the dam to resist the upstream movements after liquefaction. Certain requirements of strength and stiffness of this zone

Table 6.4: Summary Results of Liquefaction Analysis (WT277 model)

<i>Residual Strength (psf)</i>	<i>Loss in Freeboard(ft)</i>	<i>Horiz. Disp. (ft)</i>	<i>Shear Stress / Su</i>
1000	0.015	0.001	0.574
800	0.114	0.005	0.76
615	0.463	0.052	1.00
500	0.911	0.229	1.00
408	1.56	0.717	1.00
300	3.72	3.500	1.00
200	9.15	21.80	1.00
154	26.2	50.90	1.00
120	38.7	81.28	1.00
100	45.5	100.8	1.00

have to be met to keep an adequate freeboard of the dam and to prevent a shear failure along the weak layer.

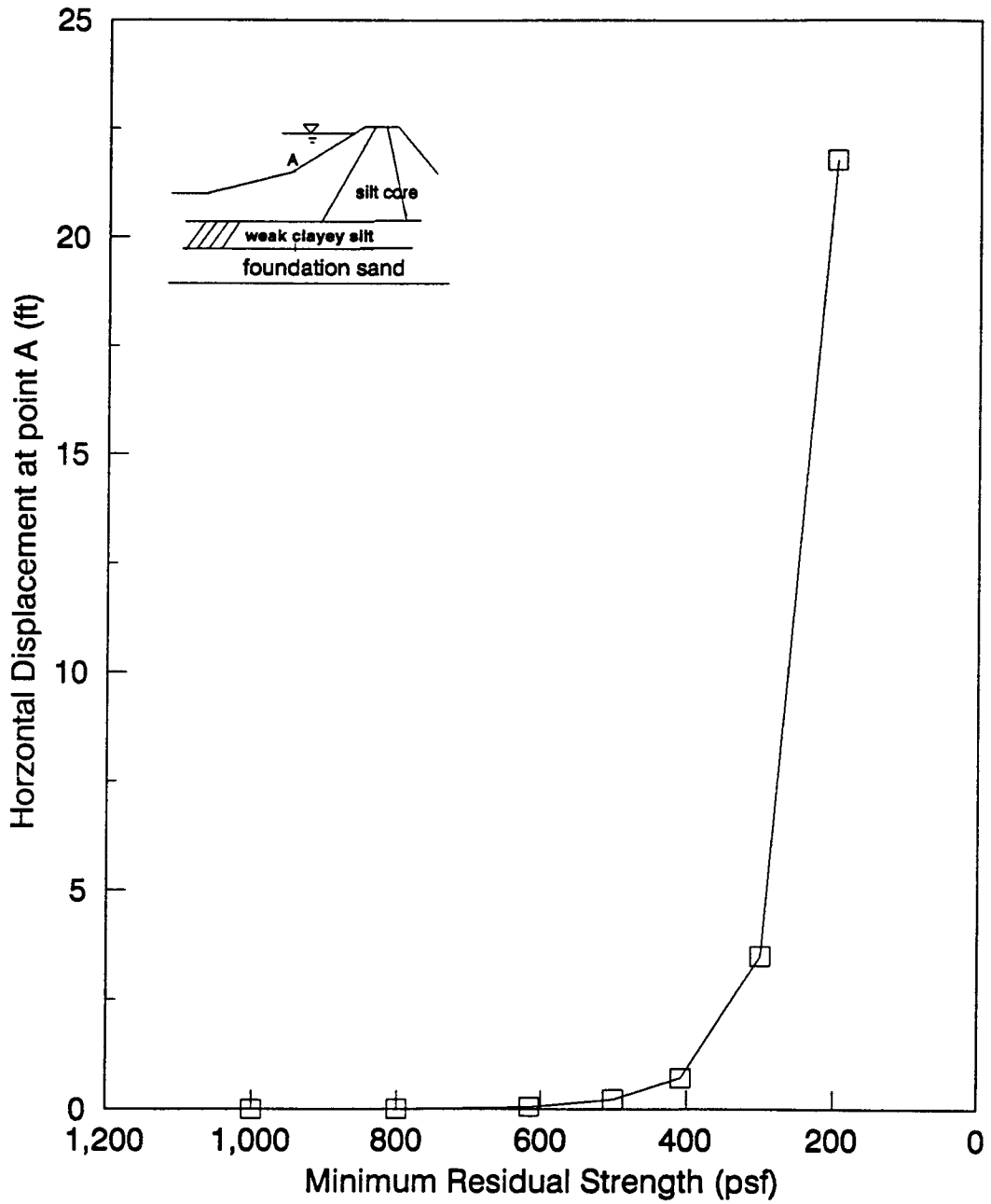


Fig. 6.6 Variation of Horizontal Displacement with Minimum Residual strength

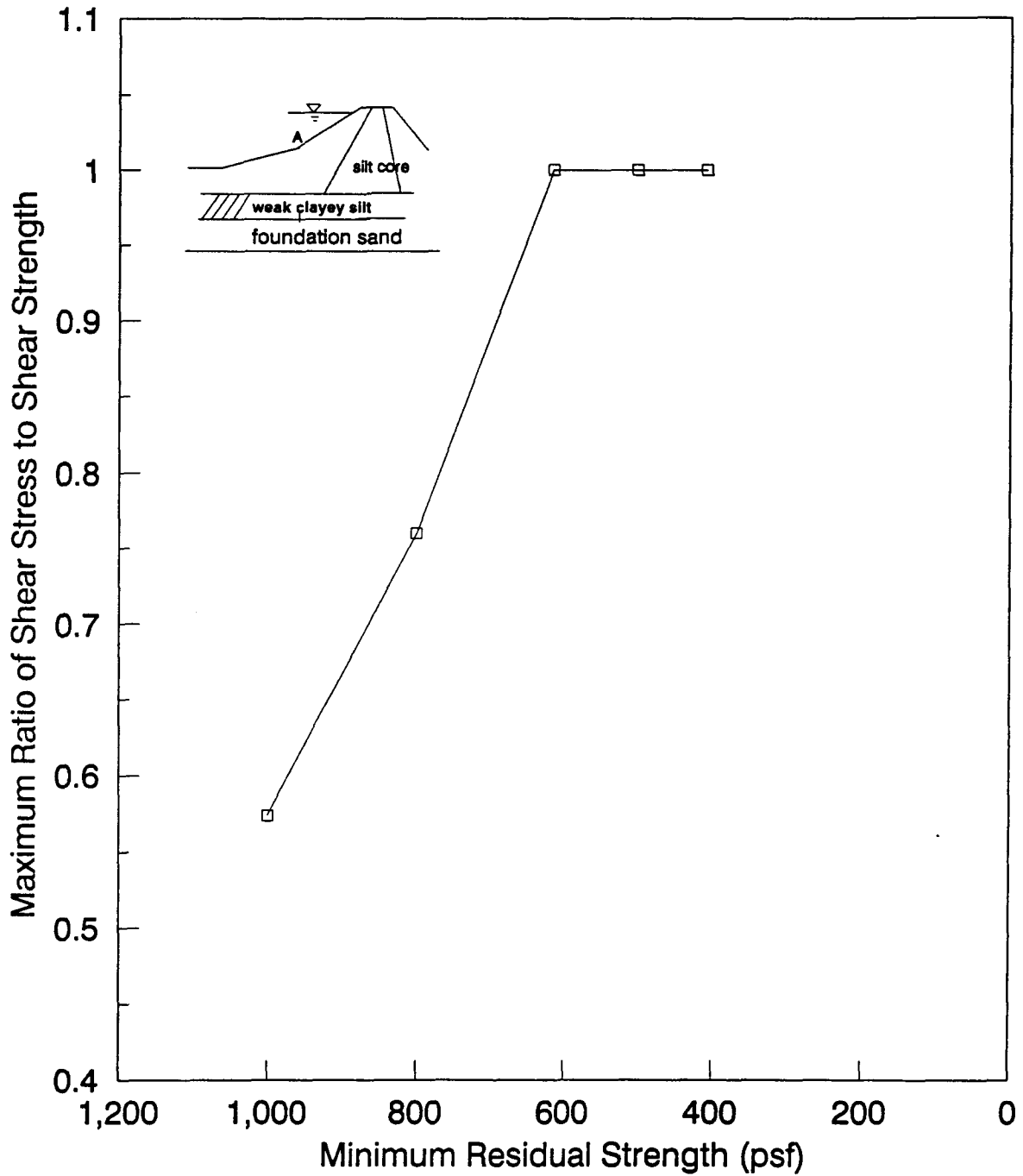


Fig. 6.7 Maximum Ratio of Shear Stress to Strength in Weak Clayey Silt versus Minimum Residual Strength

Chapter 7

GENERAL REMEDIATION STUDY OF SARDIS DAM

7.1 General Remediation Schemes

The remediation must fulfil two functions. The remediated zone must have a sufficient strength to prevent shear failure along the level of the weak clayey silt and also have sufficient stiffness to prevent deformations that may lead to a significant loss of freeboard. If the remediated zone is not stiff enough, bending deformations, with or without cracking, may allow significant crest settlements. Therefore the aim of the remediation study is to establish the average strength and stiffness combination of the proposed remediation zone that will limit the loss of freeboard as economically as possible. The analysis presented here is based on tolerable deformations rather than the factor of safety.

One of the key issues concerning the remediation is to select the best location to perform the remediation. Fig. 7.1 shows the location of the zone to be remediated in the cross section of the dam. Rip-rap protection exists on the upper part of the upstream slope of the dam. To avoid both the rip-rap and the deep water in the construction, the zone to be remediated is selected to be adjacent to the slope break on the upstream slope, which was controlled by the conservation level of the pool during construction.

As the location of the remediation zone was determined, studies were made to determine general requirements of strength, stiffness and width of the remediated zone to

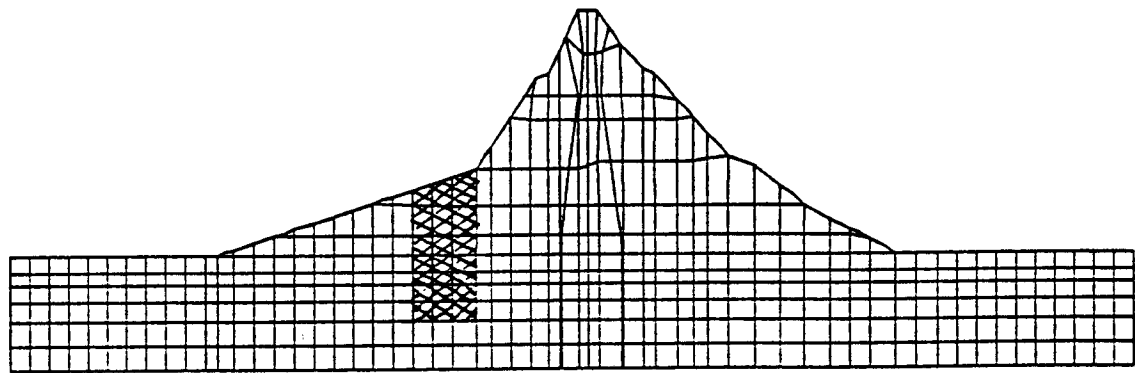


Figure 7.1: Finite Element Mesh Showing Location of Remedial Pile Plug

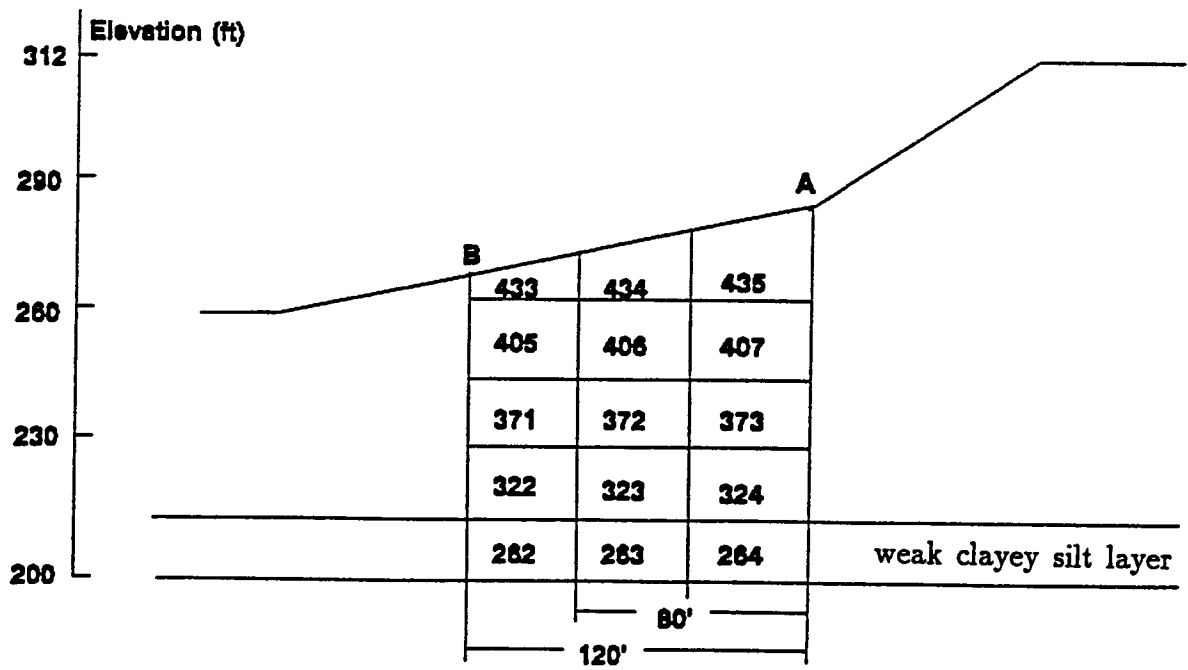


Figure 7.2: Detailed Distribution of Remedial Elements

provide enough resistance to flow deformations. For this purpose, the remediated zone is idealized to be a zone of uniform material which has constant shear modulus and shear strength. This idealized zone is called the remediated plug or plug. Fig. 7.2 shows the distribution of the elements in the remediated zone and the size of the plug. The plug penetrates 15 ft down into the foundation sand from the bottom of the weak clayey silt layer. Note that the same finite element mesh used in the construction and the original liquefaction analyses was used in the post-liquefaction analysis of the remediated dam.

The residual strengths for the liquefied soils have the same values as those used in the previous liquefaction analysis. During shaking by the design earthquake, the saturated portion of the core and the weak foundation clayey silt outside the remediated plug are still expected to liquefy. The residual strength in the silt core is taken as 100 psf. The residual strengths in the liquefied weak clayey silt are assumed to be $0.075\sigma'_{vo}$, where σ'_{vo} is the initial effective vertical stress. A minimum value of 100 psf of the residual strengths of this weak layer was adopted. The original strengths of this weak clayey silt layer are estimated to be 2000 psf, with a shear modulus constant 1400 and therefore a maximum shear modulus of 2800 tsf.

The amount of pore water pressure generated in the non-liquefiable sand shell during earthquake shaking, the plug width (80ft or 120 ft) and the plug strength and stiffness will have a significant effect on the performance of the dam during the earthquake shaking. The comparison study of these key factors is summarized below and shown in Table 7.1.

- Effect of pore water pressure in the non-liquefiable (NL) sand shell – PWP effect.

Table 7.1: Different Plug Remediation Schemes

	<i>PWP</i>	<i>plug width</i>	<i>plug strength(psf)</i>	<i>plug modulus (psf)</i>
PWP	No PWP	120 ft	3000	900,000
	50% PWP	120 ft	3000	900,000
plug width	50% PWP	80 ft	3000	900,000
	50% PWP	120 ft	3000	900,000
	50% PWP	80 ft	2000	600,000
	50% PWP	120 ft	2000	600,000
plug strength	50% PWP	120 ft	1000	300,000
	50% PWP	120 ft	2000	600,000
	50% PWP	120 ft	3000	900,000
	50% PWP	120 ft	4000	1200,000
	50% PWP	120 ft	8000	2400,000

Plug width 120 ft, plug strength 3000 psf, comparing a) No PWP with b) 50% PWP .

- Plug width effect – for plug with strengths of 3000 psf and 2000 psf, 50% PWP in the NL sand shell , comparing a) plug width 80 ft with b) plug width 120 ft.
- Plug strength effect – plug width 120 ft, 50% PWP in the NL sand shell, comparing the plug strengths of a) 1000 psf; b) 2000 psf; c) 3000 psf; d) 4000 psf; e) 8000 psf.

In the liquefaction analysis with the remedial plug, the placement of the plug was modelled during the construction sequence which is conservative. The remedial plugs have the same shear modulus constant of 300 . Since the shear modulus is the product of the shear modulus constant and the shear strength, the shear moduli of the plugs increase as the strengths of the plugs increase.

7.2 Effect of the Pore Water Pressure of the Non-Liquefiable Sand Shell

During shaking, dynamic pore water pressure will be generated in the non-liquefiable sand shell (material #6). Recall Fig. 6.3 that shows the distribution of the soil material zones. From previous seismic investigations, this sand shell was not identified as a liquefiable material, but it is expected to build up some amount of dynamic pore water pressure during the earthquake. As the seismic pore water pressure increases by a ratio of r_u to the initial effective vertical stress σ'_{vo} , i.e. $r_u = u/\sigma'_{vo}$, the shear resistance or the shear strength is reduced to $(1 - r_u)\sigma'_{vo}\tan\phi'$ because of the reduction of the effective vertical stress. An alternative way of reducing the shear strength would be keeping the effective vertical stress unchanged and adjusting the friction angle of the soil. This assumption is equivalent to using the initial effective vertical stress and a modified equivalent friction angle, ϕ'_{eq} , where $\tan\phi'_{eq} = (1 - r_u)\tan\phi'$. To investigate the influence of the PWP amount in these areas on the performance of the dam during the shaking, the following cases are examined:

- 50% PWP model: Assume a 50% pore water pressure ratio is generated during the shaking, corresponding to an reduction of the friction angle from 35° to 19.2° in the non-liquefiable (NL) sand shell;
- No PWP model: Assume no pore water pressure generated in the non-liquefiable sand shell during the shaking. The friction angle of the non-liquefiable sand shell keeps unchanged and has a value of 35° .

7.2.1 Loss of freeboard

The loss of freeboard is a useful index of the overall performance of the dam after soil liquefaction. The amount of vertical movement in the center point of the dam crest corresponding to Node 312 in the finite element mesh is designated as the loss of freeboard. Comparison of the loss of freeboard with the minimum residual strength in the weak clayey silt is plotted in Fig. 7.3. When the residual strengths drop to their appropriate minimum values, the loss of freeboard for the 50% PWP model is 4.50 ft and for the No PWP model is 2.36 ft. The loss of freeboard when 50% PWP is developed in the sand shell is approximately double the loss of freeboard when there is no porewater pressure development. Both models show losses of freeboard with the mobilization of the residual strengths.

7.2.2 Horizontal pressures against the plug

The plug is expected to prevent the upstream slope from sliding due to soil liquefaction. The horizontal pressures or stresses against the downstream face of the plug are much greater than those against the upstream face of the plug. For the design purpose, the difference between the horizontal stresses or pressures of the downstream face and the upstream face would be used to estimate the necessary depth of penetration of the plug into the foundation sand. The penetration of the plug should be deep enough to provide a sufficient resistance to the plug rotation or translation. The greater the pressure difference, the deeper the plug needs to penetrate into the foundation sands. Fig. 7.4 shows the horizontal stresses on the downstream side (side A) of the plug after liquefaction.

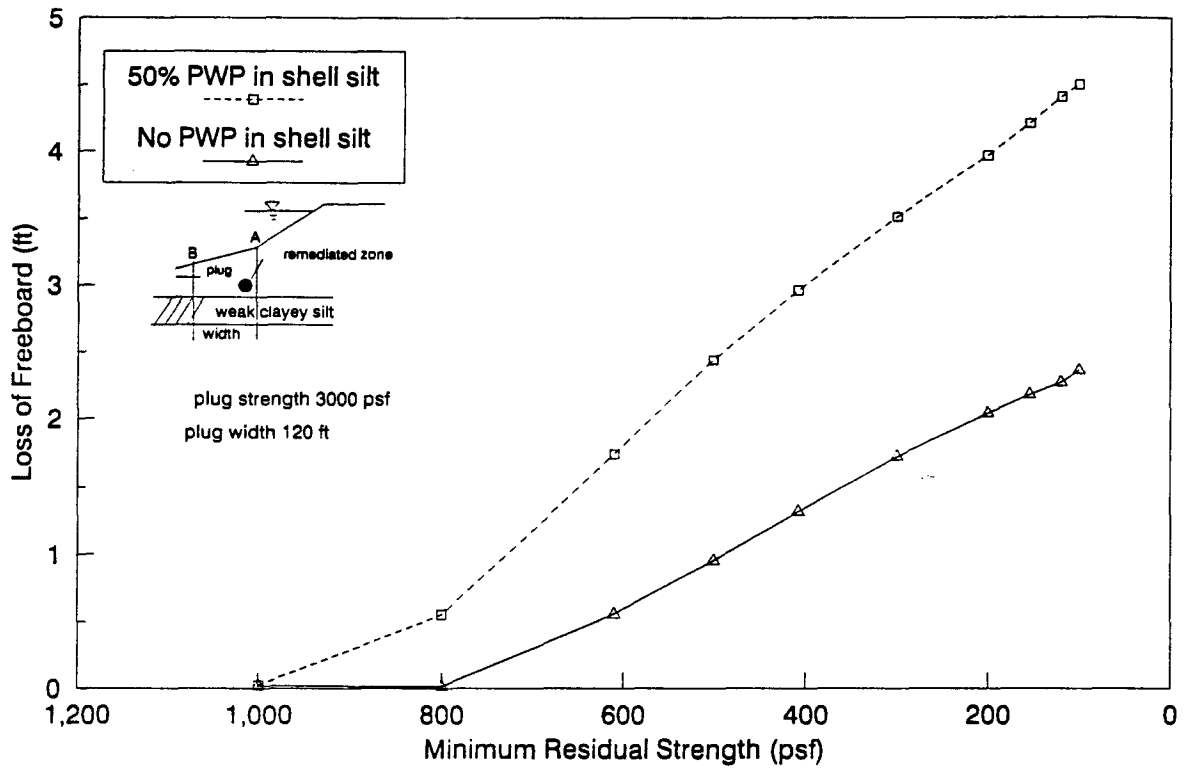


Figure 7.3 Variation of Loss of Freeboard with Residual Strength (PWP effect)

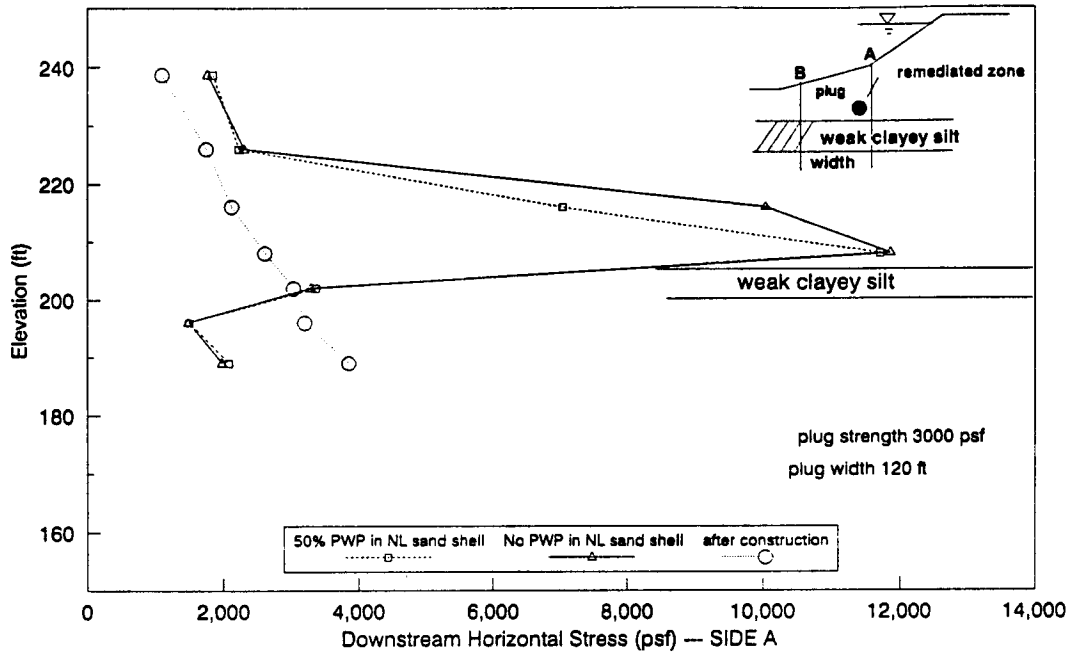


Figure 7.4 Pressure Distribution on Downstream Face of Remediated Section (PWP effect)

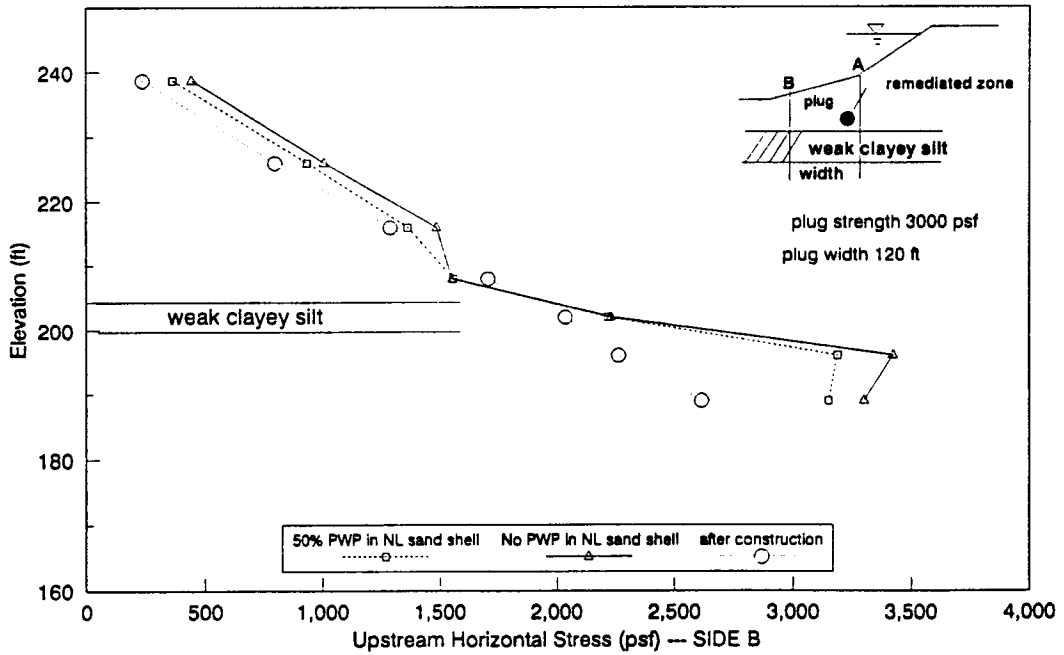


Figure 7.5 Pressure Distribution on Upstream Face of Remediated Section (PWP effect)

7.2.3 Ratio of shear stress to strength of the plug

One aim of the remediation study is to determine an appropriate combination of the strength and stiffness which would provide sufficient strength at the level of the weak clayey silt layer to prevent a shear failure along the plug. The ratio of the shear stress occurring in the plug to the shear strength of the plug is an index of the possibility of a shear failure of the plug. A value of unity or close to unity of this ratio indicates that the shear stress induced inside the plug reaches the shear strength of the plug, and a shear failure may occur. Fig. 7.6 shows the ratio of the shear stress to the shear strength in the plug versus elevations as the minimum residual strength in the weak clayey silt drops to 100 psf. It can be observed that the maximum value of 0.74 occurring at the elevation of the weak clayey silt layer. This observation provides useful information for the design of the plug section. The plug should have a strong section with a relatively high shear strength and stiffness at the location around the weak clayey silt layer.

Since the maximum shear stress occurs at the downstream side of the weak clayey silt layer, the ratio of the shear stress at this location (element 265 in FE mesh) to the strength of the plug is designated as the maximum ratio of the shear stress to the shear strength in the plug. Fig. 7.7 shows the development of the maximum ratio of the shear stress to the shear strength in the plug for the variations of residual strengths. This ratio increases dramatically when the minimum residual strength drops from 800 psf to 100 psf.

7.2.4 Horizontal displacement of the plug

The horizontal movement of the plug depends on both the shear strength and the stiffness of the plug. A large displacement at the level of the weak clayey silt layer implies

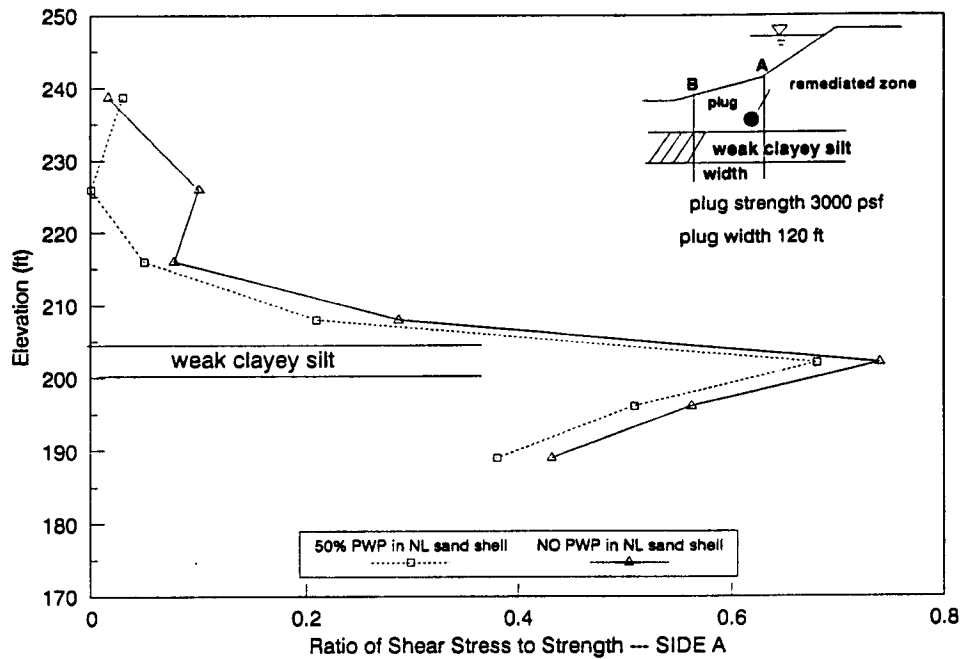


Figure 7.6 Distribution of Ratio of Shear Stress to Strength at Downstream Face of Remediated Section (PWP effect)

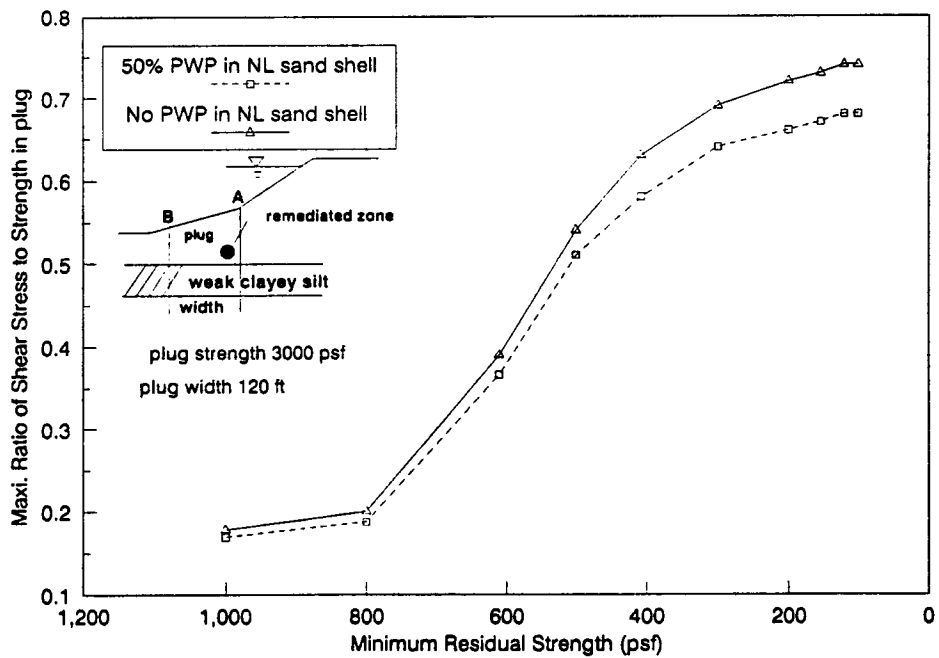


Figure 7.7 Maximum Ratio of Shear Stress to Strength in Remediated Section versus Residual Strength (PWP effect)

a shear failure of the plug. The displacement has to be limited for the design purpose. Fig. 7.8 shows the horizontal displacements on the downstream side of the plug (side A). The maximum displacement occurs around the weak clayey silt layer with maximum values of 0.32 ft for the No PWP model and 0.24 ft for the 50% PWP model. Pore water pressures in the non-liquefied sand shell significantly reduce the ability of the sand shell to transfer loads to the plug; so the maximum displacement of the 50% PWP model is less. Sharp curvature of the plug developed from the bottom to the top of the weak zone indicates that a great internal moment is accumulated inside the plug. Gradual increase of the horizontal displacement at the downstream edge of the plug was observed as the shear strengths in the weak clayey silt decrease; see Fig. 7.9.

7.3 Effect of Plug Width

In this section, the effect of the plug width on the performance of the dam is studied by calculating the displacements for plug widths of 80 ft and 120 ft using plug strengths of 3000 psf and 2000 psf.

7.3.1 Loss of freeboard

The loss of freeboard for different plug widths is plotted in Fig. 7.10. Essentially, the two models have no difference in the loss of freeboard. The loss of freeboard is 4.50 ft as the minimum residual strength drops to 100 psf.

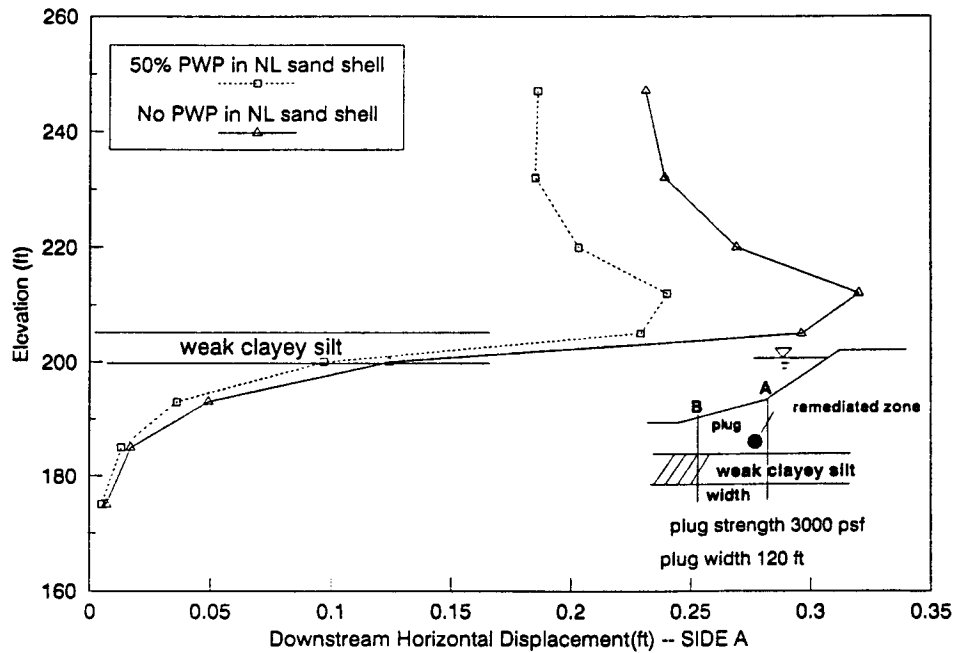


Figure 7.8 Distribution of Downstream Horizontal Movement of Remediated Section (PWP effect)

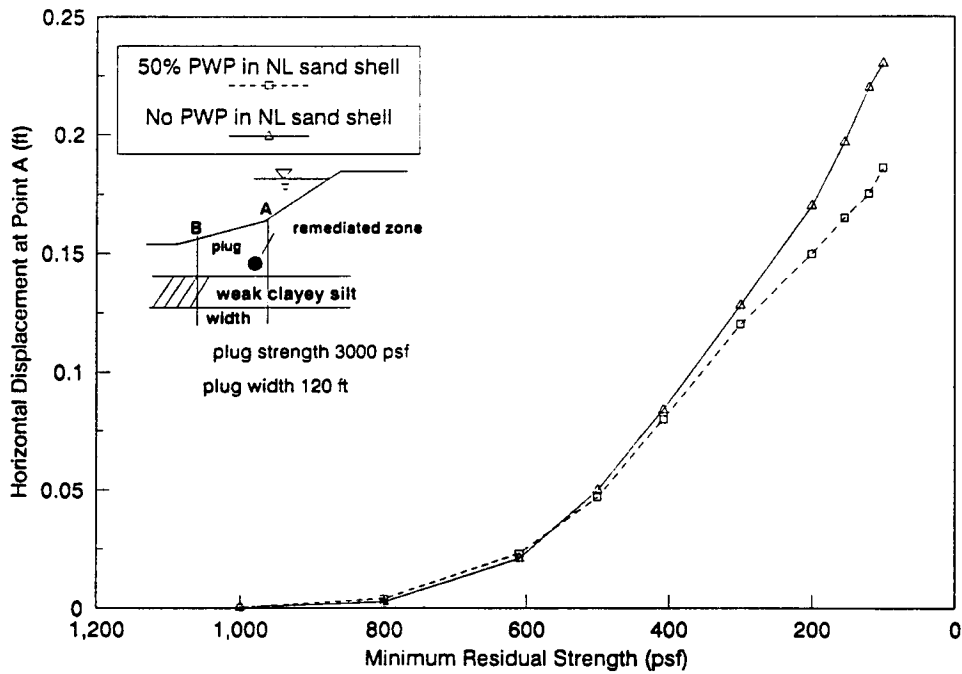


Figure 7.9 Horizontal Displacement at Downstream Edge with Residual Strength (PWP effect)

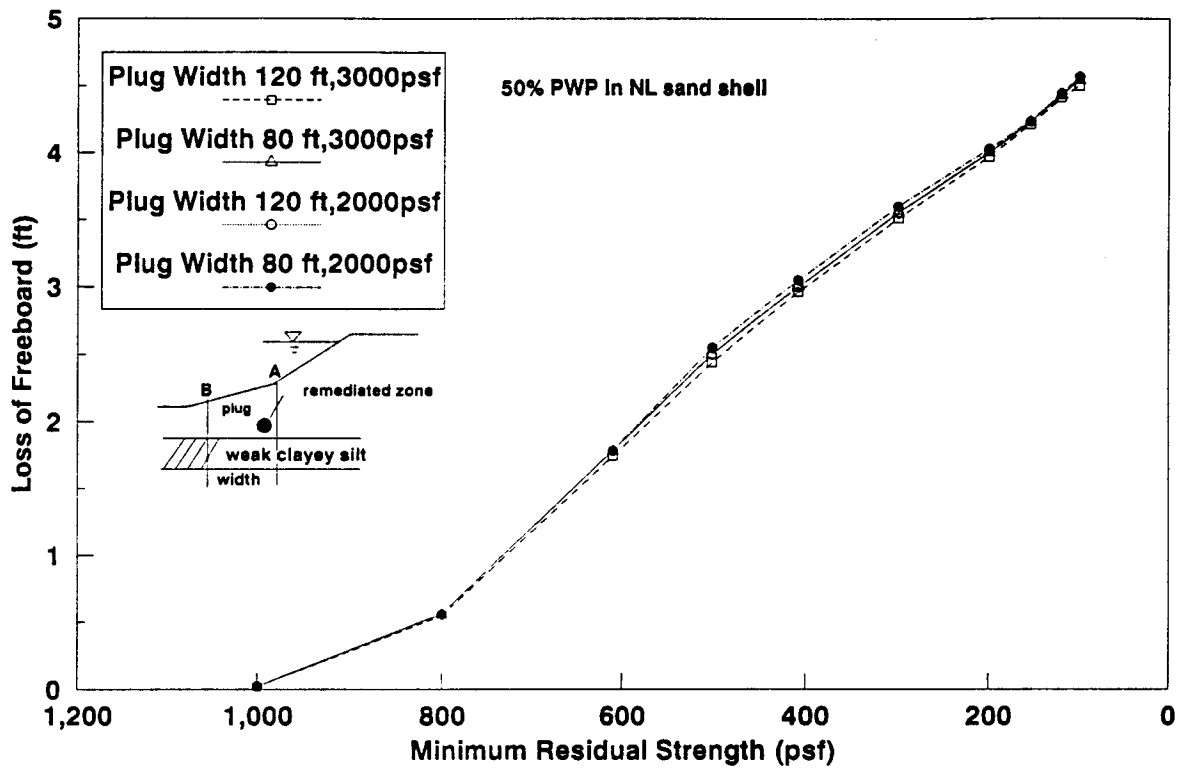


Figure 7.10 Variation of Loss of Freeboard with Residual Strength (Plug width effect)

7.3.2 Horizontal pressures against the plug

Fig. 7.11 and Fig. 7.12 shows the horizontal stresses on the remediation zone for between the two different plug widths. The horizontal stresses against the downstream side (side A) greatly increase after soil liquefaction, by a maximum increment of 9240 psf. The horizontal stresses reach the maximum value around the weak clayey silt. It should be noted that 80% or more of the total driving forces are carried by the plug section within and close to the weak clayey silt zone. The very low strength and stiffness in the weak zone causes a stress concentration in this area. For the plugs with same strengths, the horizontal stresses against the downstream face are essentially the same regardless of the plug width because the total loadings coming from the downstream of the dam is the same as long as the plug is wide enough to prevent failure or large deformation.

7.3.3 Ratio of shear stress to strength of the plug

The plug width has little influence on the shear stresses in the plugs with same strengths. Fig. 7.13 illustrates the ratio of the shear stress to the shear strength at the downstream face of the plug after liquefaction. Because of the stress concentration in the weak clayey silt zone, the shear stresses in this area increase very much. The ratios of the shear stress to the shear strength increase rapidly with the decrease of elevation and reach their maximum value of 0.68 at the weak clayey silt layer.

The maximum ratio of the shear stress to the shear strength in the plug increases as the residual strengths decrease from 800 psf to 300 psf, as shown in Fig. 7.14. As the minimum residual strength in the weak clayey silt layer is greater than 800 psf, the driving force is carried mainly by the soil. When the minimum residual strength of the

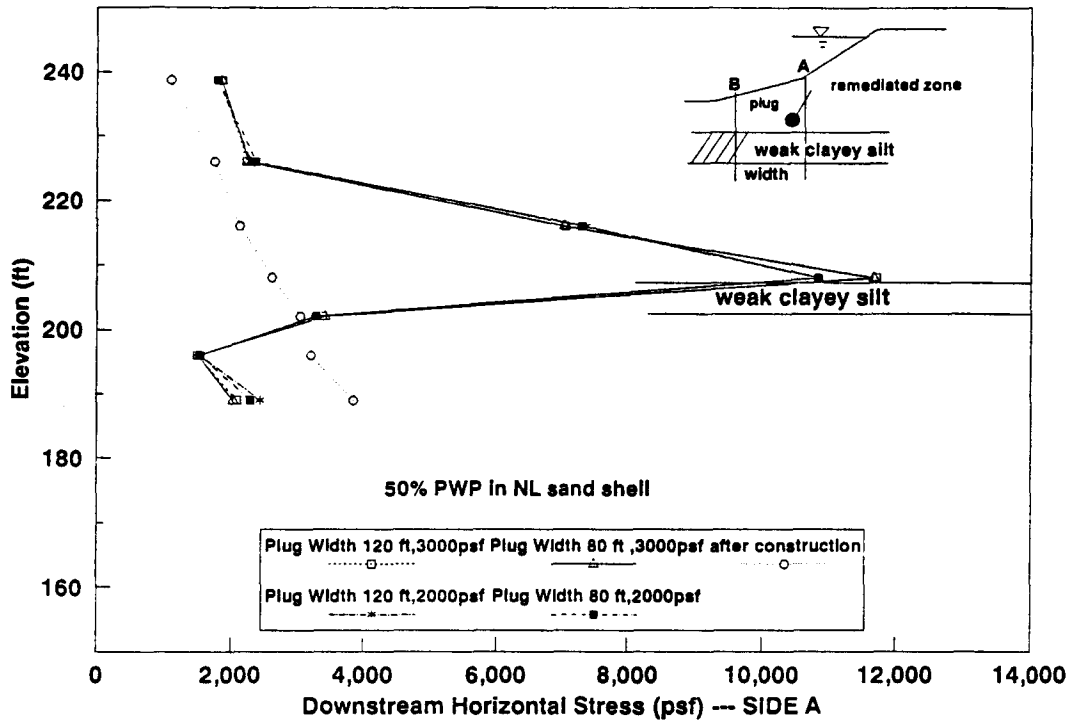


Figure 7.11 Pressure Distribution on Downstream Face of Remediated Section (Plug width effect)

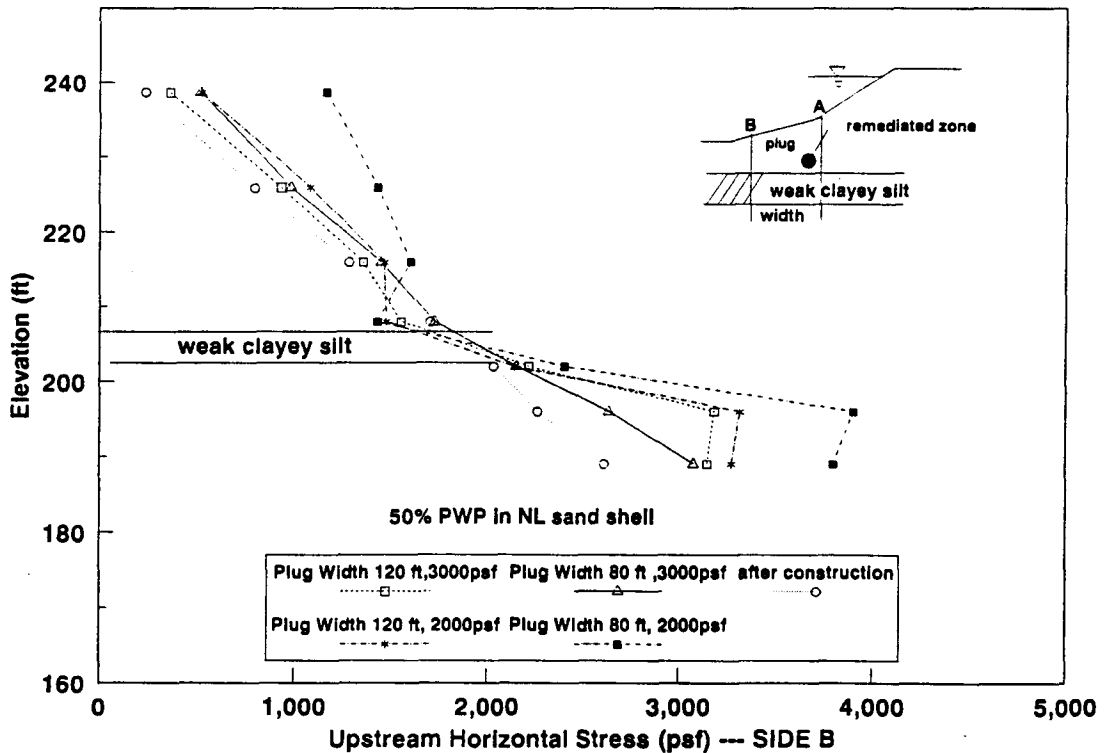


Figure 7.12 Pressure Distribution on Upstream Face of Remediated Section (Plug Width effect)

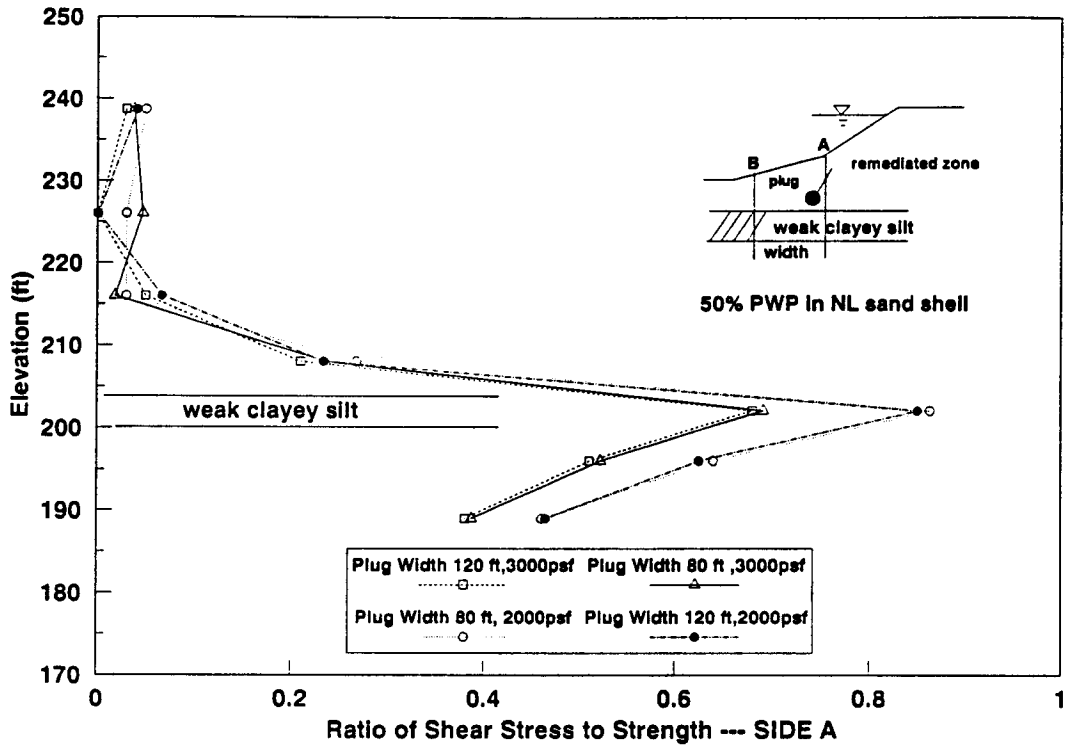


Figure 7.13 Distribution of Ratio of Shear Stress to Strength at Downstream Face of Remediated Section (Plug width effect)

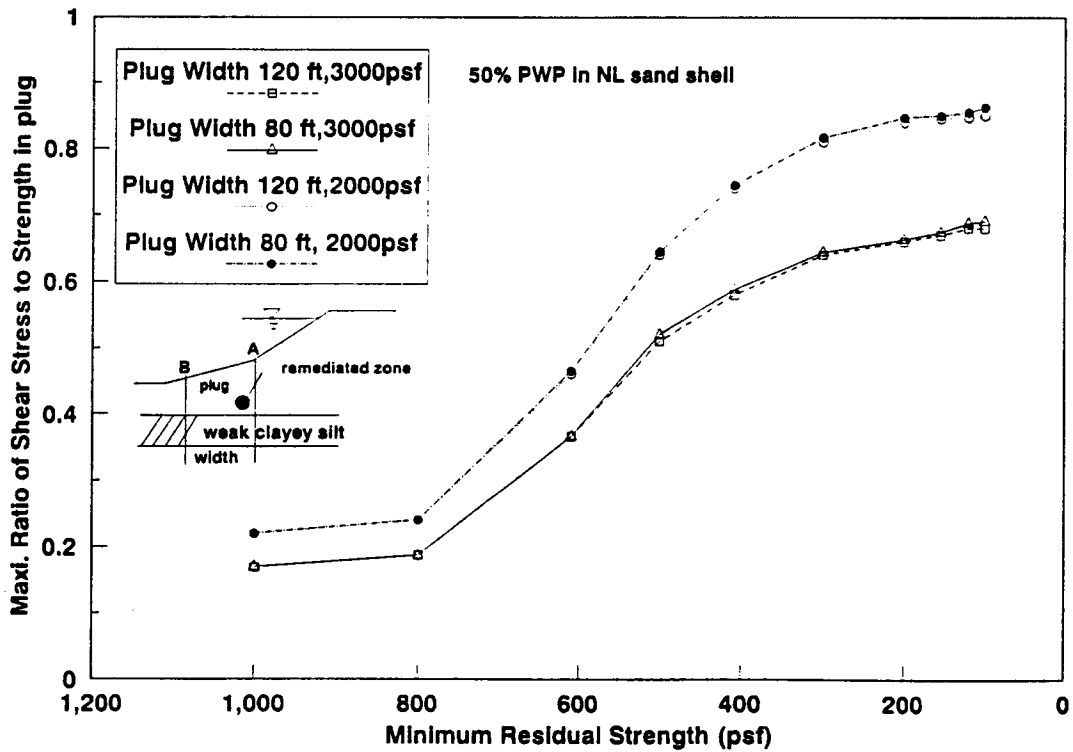


Figure 7.14 Maximum Ratio of Shear Stress to Strength in Remediated Section versus Residual Strength (Plug width effect)

weak clayey silt is less than 300 psf, almost all of the driving forces are carried by the remedial plug section, and the curve goes flat.

7.3.4 Horizontal displacement of the plug

The maximum horizontal displacement occurs around the weak clayey silt layer. Fig. 7.15 illustrates the response of horizontal displacements on the downstream side of the plug (side A). It is interesting to note that the horizontal movement of the plug along the weak clayey silt is larger than the horizontal movements on the upper half of the plug.

Although a plug section with a large width could reduce the horizontal movement by some extent, the shear strength of the plug has a stronger control on the horizontal movement. A plug with a shear strength of 3000 psf and a width of 80 ft would provide a much stronger resistance to the horizontal forces than a plug with a shear strength of 2000 psf and a width of 120 ft does. For plugs with the shear strength of 3000 psf, the maximum horizontal displacements are 0.26ft and 0.24 ft for the plug width of 80 ft and 120 ft, respectively. For plugs with the shear strength of 2000 psf, the maximum horizontal displacements are 0.52 ft and 0.48 ft for the plug width of 80 ft and 120 ft, respectively.

Fig.7.16 shows the development of the horizontal movement at the downstream edge of the plug with the variation of the minimum residual strength. The horizontal displacement increases at a constant rate after the minimum residual strength is less than 600 psf.

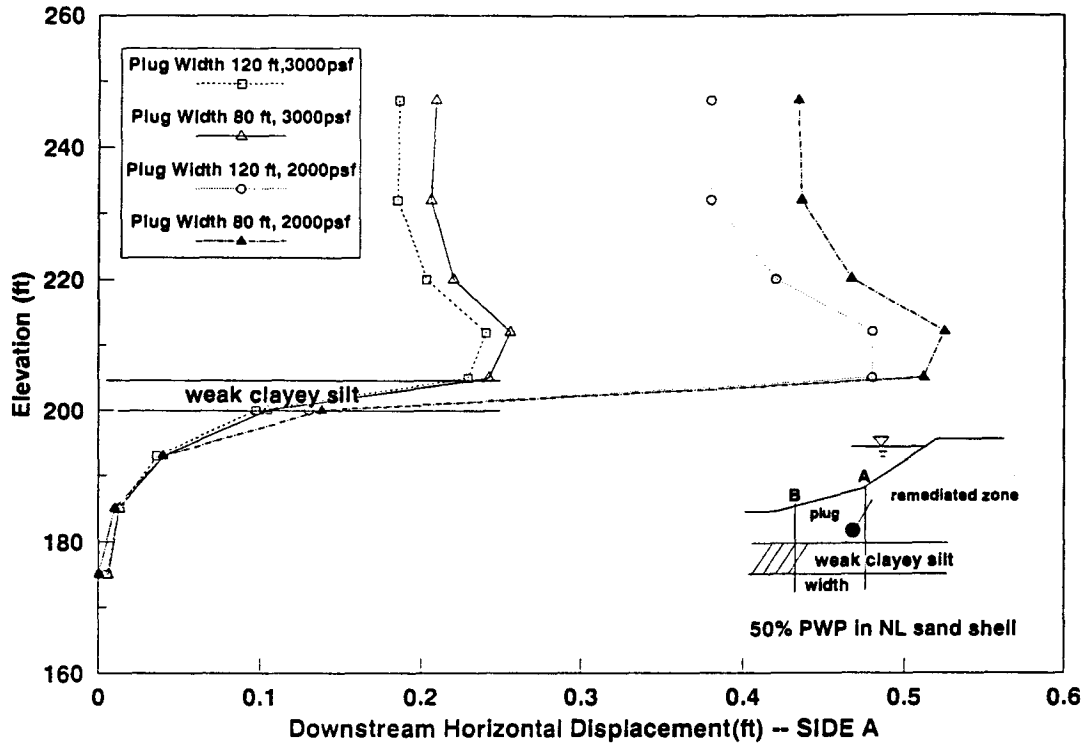


Figure 7.15 Distribution of Downstream Horizontal Movement of Remediated Section (Plug width effect)

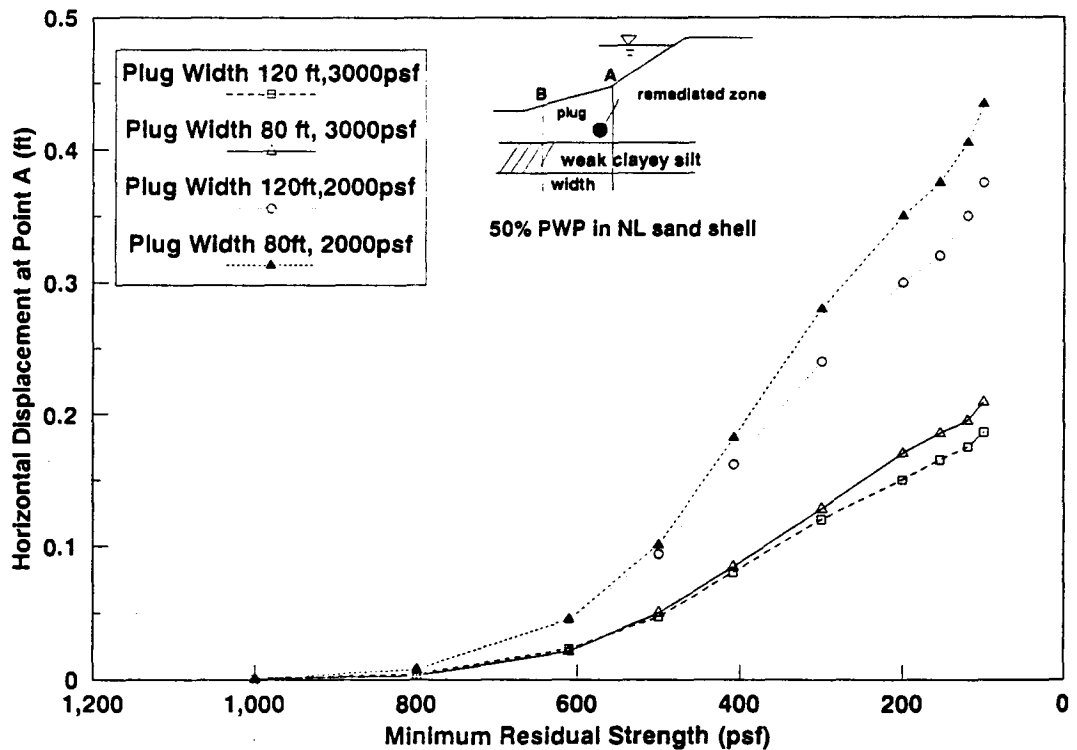


Figure 7.16 Horizontal Displacement at Downstream Edge with Residual Strength (Plug width effect)

7.4 Effect of Plug Strength

A parametric study is made to examine the effect of the strength of the plug on the performance of Sardis Dam after the remediation. The plug width of 120 ft and the 50% PWP in NL sand shell are kept unchanged during this comparison study. The strengths of the plug are 1000 psf, 2000 psf, 3000 psf, 4000 psf and 8000 psf.

7.4.1 Loss of freeboard

The variation of the loss of freeboard with the minimum residual strength in the weak clayey silt is illustrated in Fig. 7.17 for the five plug strengths chosen. The strength models of 2000 psf , 3000 psf , 4000 psf and 8000 psf have a very close response in the loss of freeboard. However, the stronger shear strength in the plug the smaller its drop of the dam crest. The difference in the loss of freeboard is not significant because the plugs of 120 ft width with strength greater than 2000 psf provide sufficient resistance against driving forces from the downstream of the dam. The loss of freeboard is around 4.5 ft for these cases as the minimum residual strength drops to 100 psf. But when the strength of the plug drops to 1000 psf, the loss of freeboard of the dam is 5.7 ft. The average strength of 1000 psf in the remediation plug was not considered acceptable.

7.4.2 Horizontal pressures against the plug

Fig. 7.18 and Fig. 7.19 show the horizontal stress responses against the downstream side (side A) and the upstream side (side B). The horizontal stresses increase after soil liquefaction compared to those before soil liquefaction at the elevations above the weak clayey silt layer and decrease at the elevations below the weak clayey silt layer. The

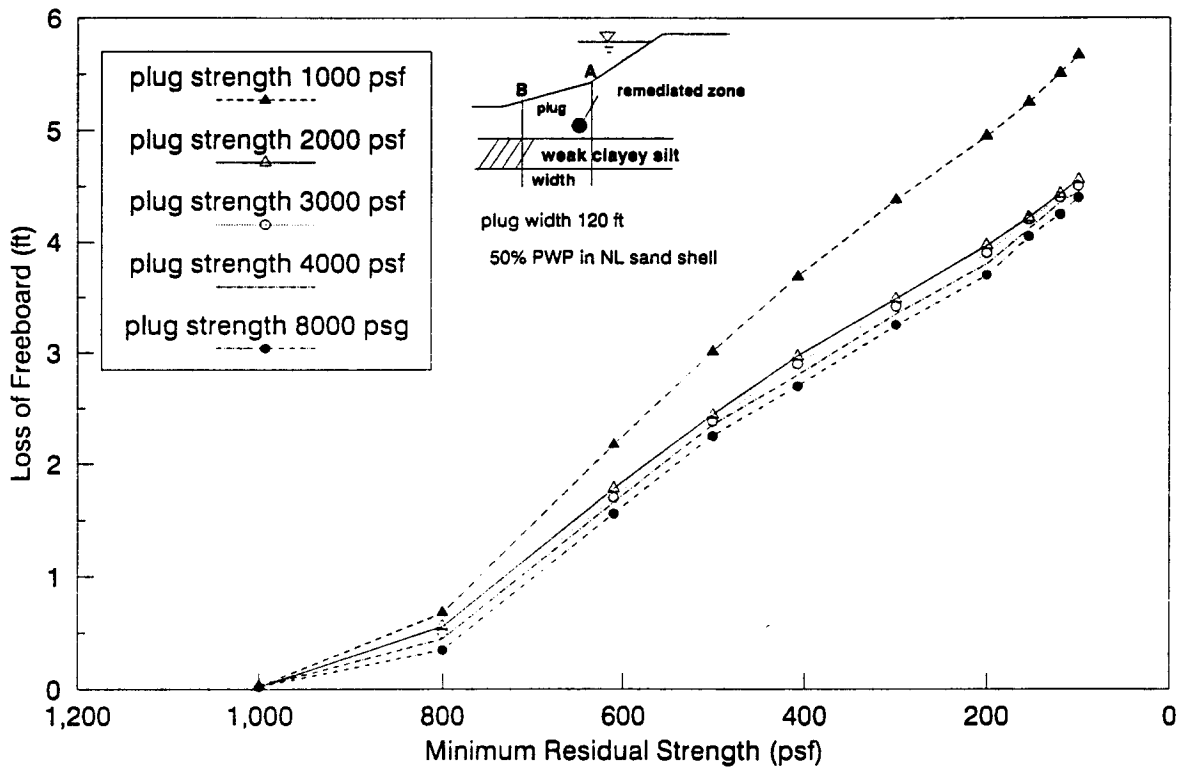


Figure 7.17 Variation of Loss of Freeboard with Residual Strength (Plug strength effect)

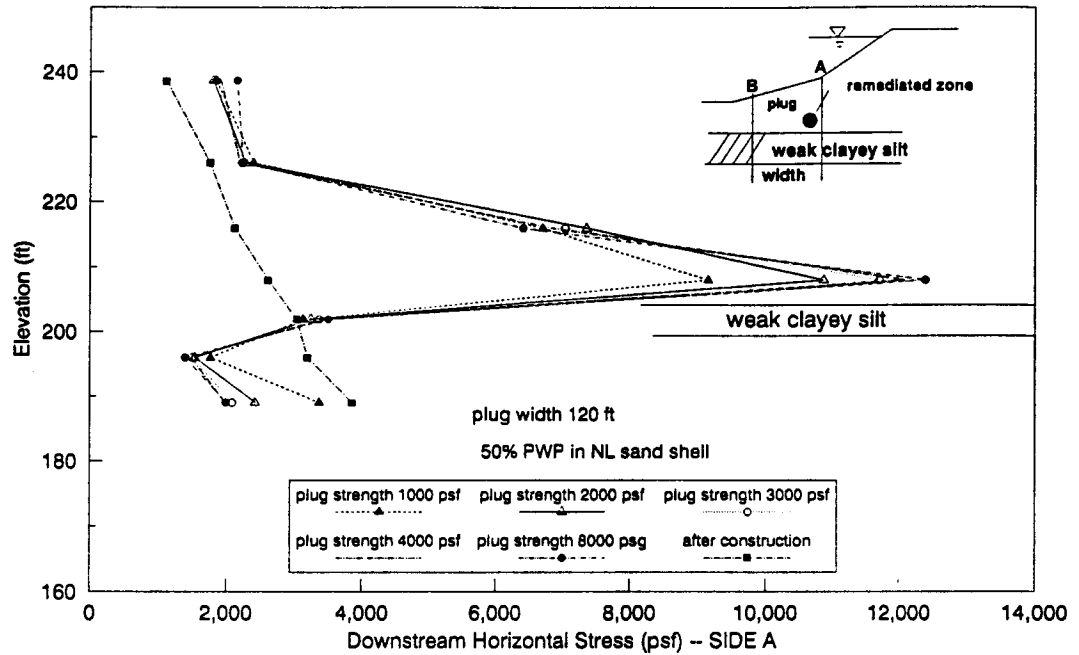


Figure 7.18 Pressure Distribution on Downstream Face of Remediated Section (Plug strength effect)

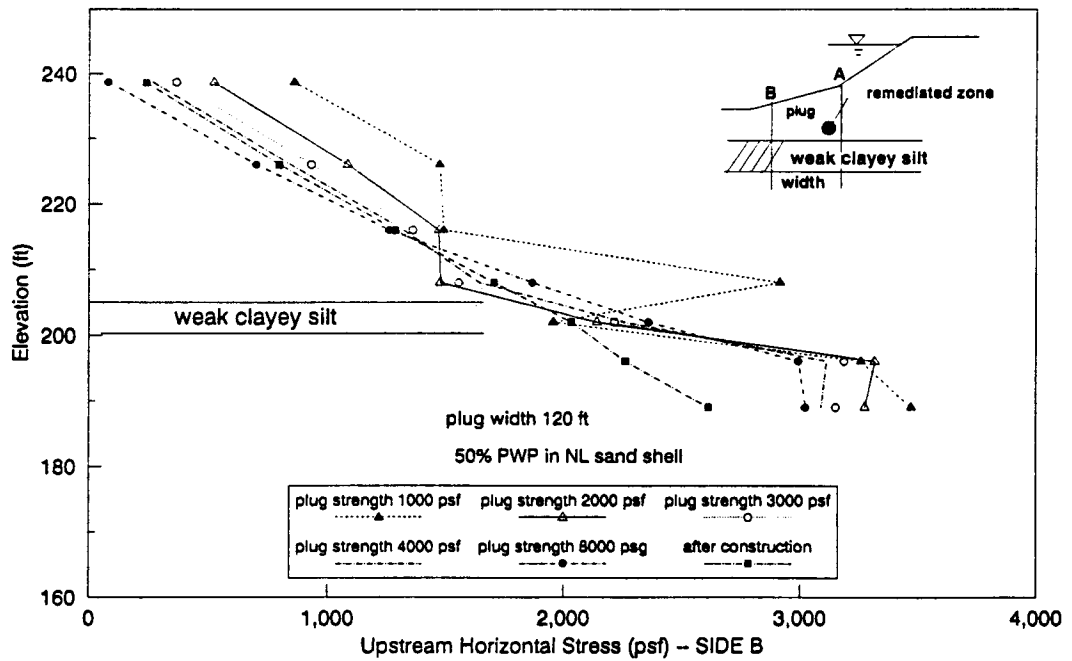


Figure 7.19 Pressure Distribution on Upstream Face of Remediated Section (Plug strength effect)

horizontal stresses show a triangular distribution along the downstream face of the plug after liquefaction. The maximum horizontal stresses against the downstream faces of the plugs occur just above the weak clayey silt layer. These maximum horizontal stresses are 9160, 10866, 11710, 12100, 12405 psf for the plugs with the shear strengths of 1000 psf, 2000 psf, 3000 psf, 4000 psf and 8000 psf, respectively.

The plug with a higher shear strength needs to penetrate deeper to provide sufficient moment resistance. The pressures against the downstream face of the stronger plugs are higher than those on the weaker plugs. The higher the plug strength is, the more the horizontal stresses against the downstream face of the plug increase after liquefaction. On the other hand, the pressures against the upstream face of the strong plug are less than those of the weak plugs. Therefore, the overturning moments about the point at which the plug intersects with the foundation sands are high for the plug with a high shear strength.

7.4.3 Ratio of shear stress to strength of the plug

A comparison of the ratios of the shear stress to the shear strength in the plugs for the five different plug strengths is given in Fig. 7.20. The maximum ratios of the shear stress to the shear strength in the plug decrease as the strengths of the plugs increase. Fig. 7.21 shows the relationship between these maximum ratios and the reduction of the minimum residual shear strength of the weak clayey silt. These maximum ratios have the values of 0.1 to 0.4 before liquefaction occurs, and they increase after liquefaction. When the minimum residual strength is less than 300 psf, the curve goes flat and most of the shear force is carried by the plug. The final maximum ratios of the shear stress to the shear strength are 0.99 (failure), 0.85, 0.68, 0.55 and 0.29 for the plugs with strengths of 1000 psf, 2000 psf, 3000 psf, 4000 psf and 8000 psf, respectively.

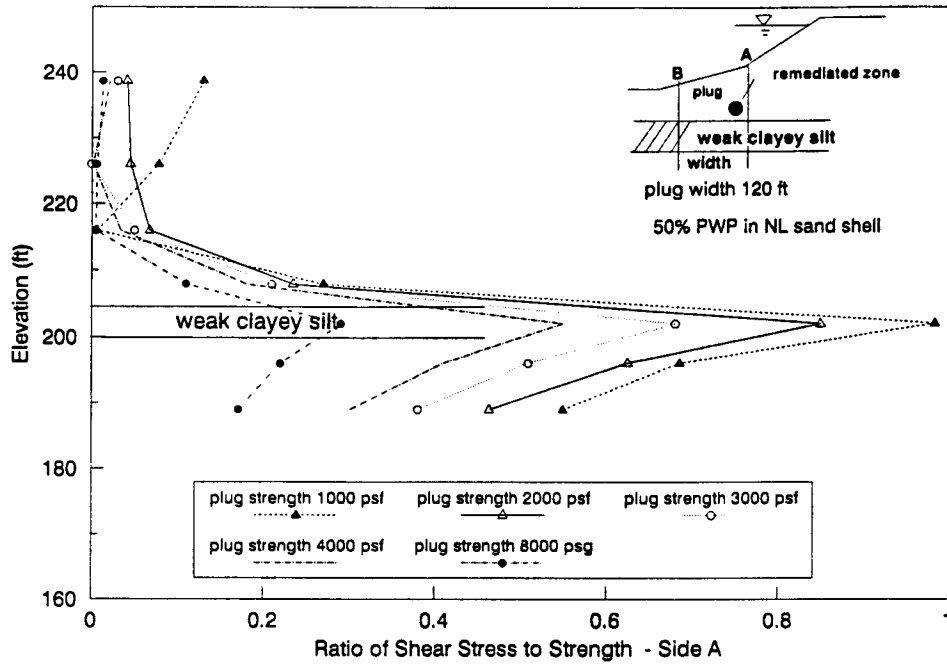


Figure 7.20 Distribution of Ratio of Shear Stress to Strength at Downstream Face of Remediated Section (Plug strength effect)

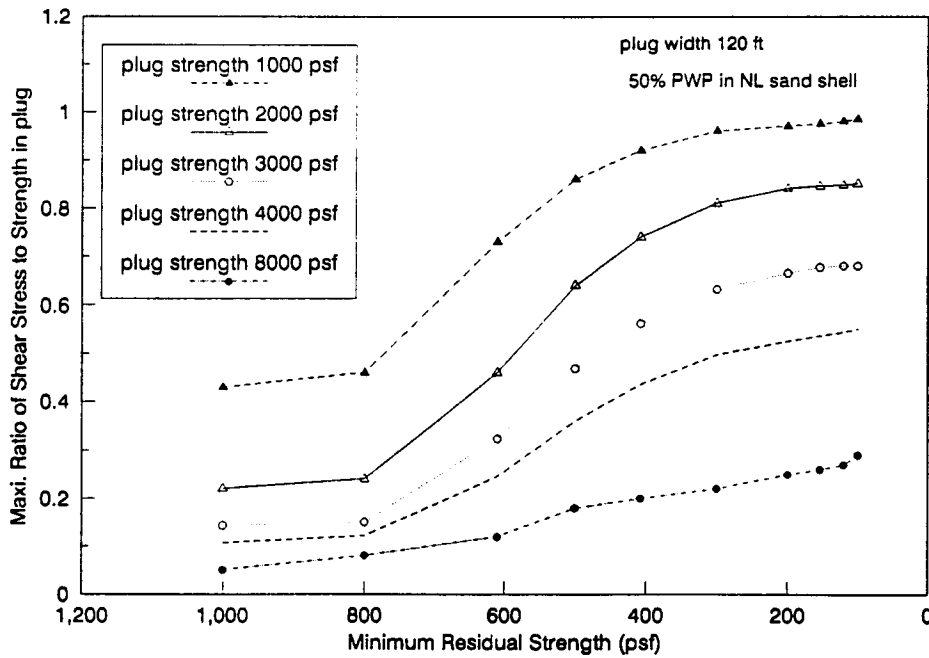


Figure 7.21 Maximum Ratio of Shear Stress to Strength in Remediated Section versus Residual Strength (Plug strength effect)

7.4.4 Horizontal displacement of the plug

Fig. 7.22 illustrates the distribution of the horizontal displacements in the plug with elevation. Above the weak clayey silt which is located at the elevations between 200 ft and 205 ft, the horizontal movements are essentially constant for the plugs with high strength such as 4000 psf or 8000 psf. The plug with strength of 2000 psf deflects much more than those plugs with the strengths of 3000 psf, 4000 psf and 8000 psf.

The increasing rate of horizontal movement becomes high when the plug strength is less than 2000 psf; see Fig. 7.23. The maximum horizontal movements are 3.29ft, 0.48ft, 0.24ft, 0.16ft and 0.07 ft for the plugs with strengths of 1000 psf, 2000 psf, 3000 psf, 4000 psf and 8000 psf, respectively.

The large horizontal displacement and the rapid increase of the horizontal displacement were observed for the plug with strength of 1000 psf.

7.5 Summary on General Remediation Studies

The results on the general remediation study are summarized in Table 7.2. Plug strength 1000 psf is too weak to provide enough resistance after liquefaction. This plug strength results in a large horizontal displacement and a low factor of safety against a shear failure of the plug. Plug strength 3000 psf may restrain the maximum horizontal displacement of 0.24 ft and the maximum ratio of shear stress to strength of 0.68. Plug strength 3000 psf would be an appropriate strength of the remedial plug. On the other hand, plug

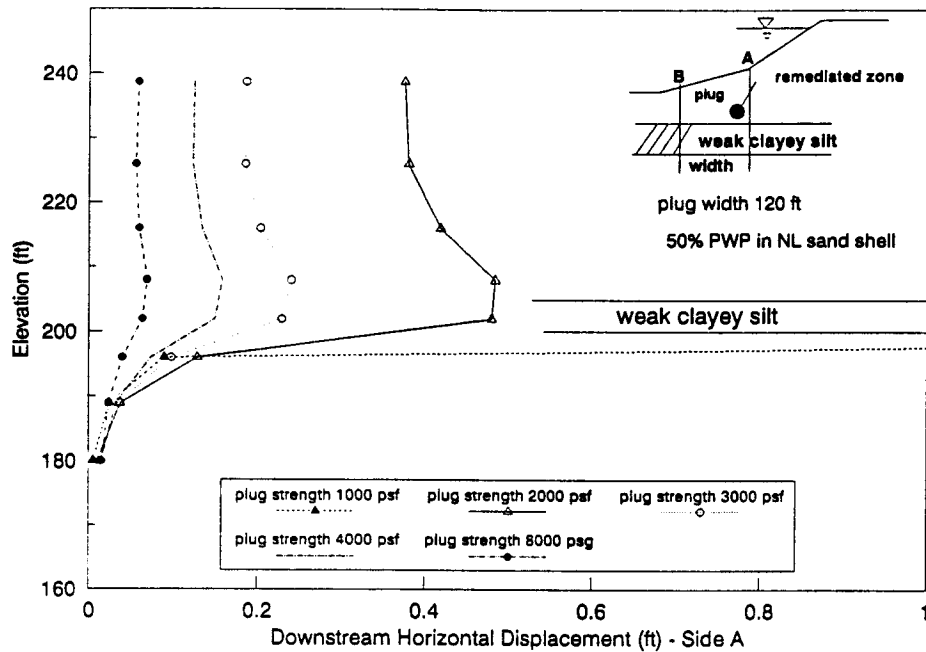


Figure 7.22 Distribution of Downstream Horizontal Movement of Remediated Section (Plug strength effect)

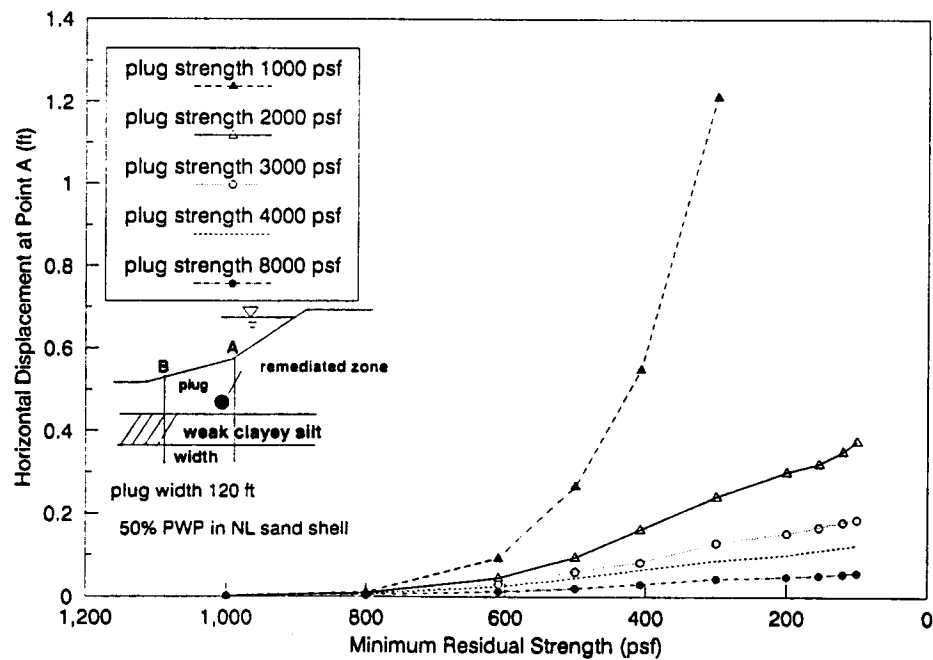


Figure 7.23 Horizontal Displacement at Downstream Edge with Residual Strength (plug strength effect)

Table 7.2: Summary Results of Plug Remediation Studies

	<i>plug</i> strength(psf)	<i>loss of</i> Freeboard(ft)	<i>Maximum</i> $\frac{\tau}{s_u}$ ratio in plug	<i>Maximum Hori.</i> Displacement(ft)
width 120ft 50% PWP	1000	5.67	0.99	3.29
	2000	4.56	0.85	0.48
	3000	4.50	0.68	0.24
	4000	4.49	0.55	0.16
	8000	4.40	0.29	0.07
width 80ft 50% PWP	2000	4.56	0.86	0.52
	3000	4.54	0.69	0.26
width 120ft No PWP	3000	2.36	0.74	0.32

strength higher than 3000 psf is not necessary for the remediation of this dam.

From the variation of the loss of freeboard with plug strength, Fig. 7.24, plug strength 2000 psf is appropriate to control the loss of freeboard of the dam. Plug strength 2000 psf may cause the maximum ratio of the shear stress to strength of the plug as high as 0.85; see Fig. 7.25. Hence it is reasonable to select plug strength 3000 psf to limit this ratio to a range of 0.70 which may be adequate for an engineering design. Fig. 7.26 shows the maximum horizontal displacement in the plug versus plug strength. When the plug strength is less than 2000 psf, the maximum horizontal displacement in the plug increases dramatically with the decrease of the plug strength. Again plug strength of 3000 psf would be adequate to meet design requirements on the displacement of the plug. Plug width 120 ft is reliable to meet all design purposes.

Therefore plug strength of 3000 psf (with modulus 900,000 psf) and plug width of 120 ft are selected to be the general requirements of the remediated zone of Sardis Dam to provide a satisfactory control on both the loss of freeboard and the shear failure along

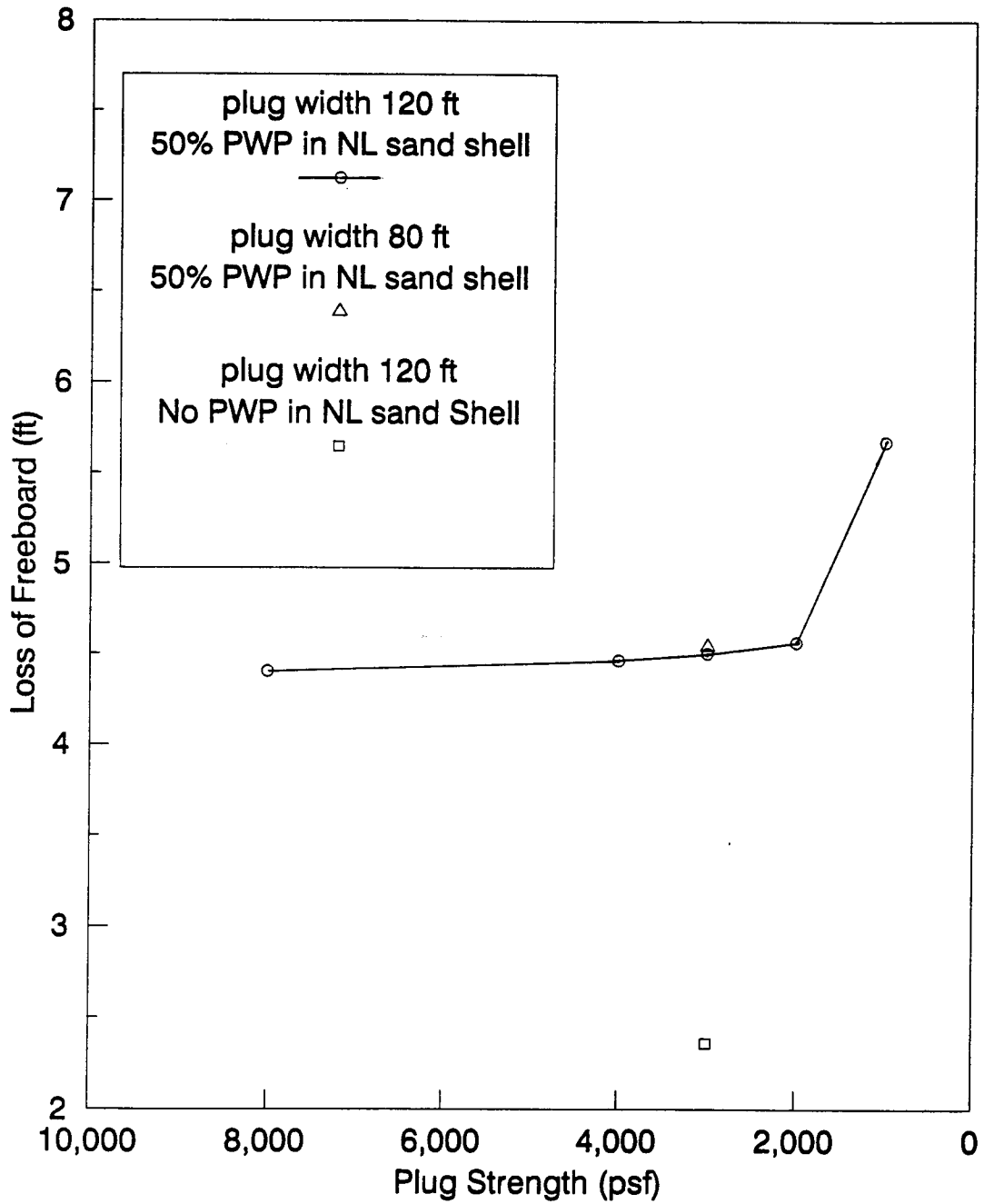


Figure 7.24: Loss of Freeboard versus Plug Strength

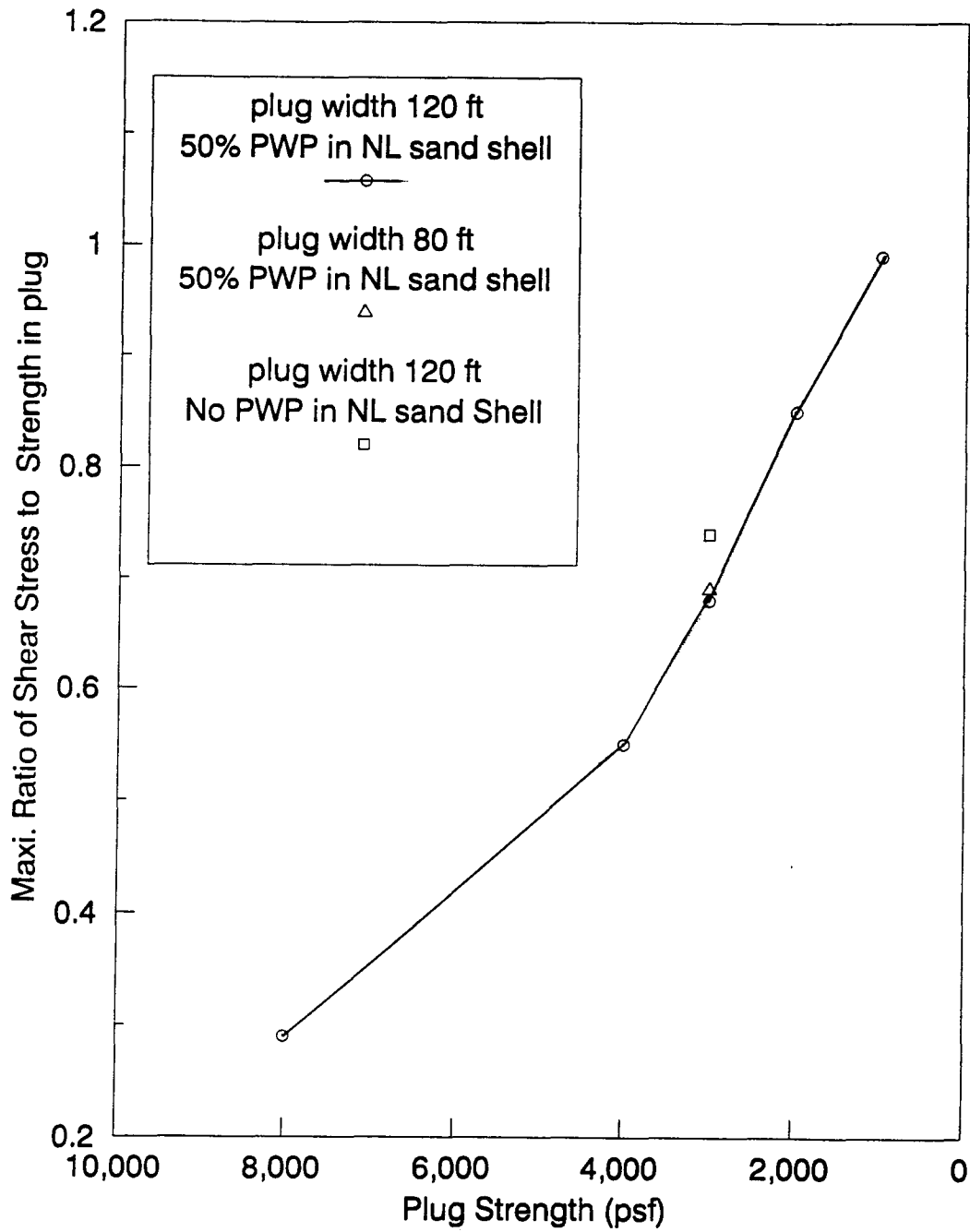


Figure 7.25: Maximum Ratio of Shear Stress to Strength in Plug versus Plug Strength

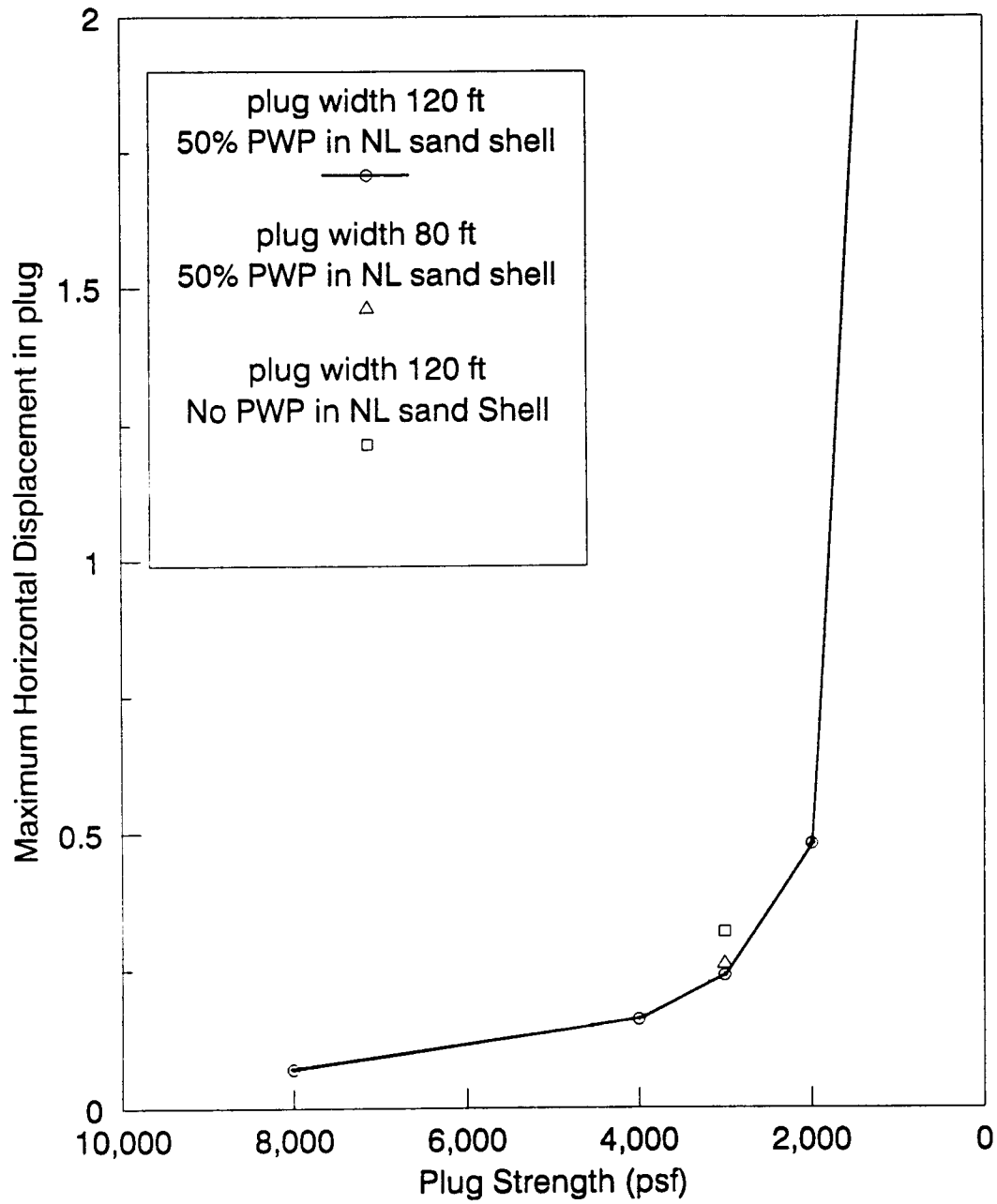


Figure 7.26: Maximum Horizontal Displacement in Plug Versus Plug Strength

the weak layer.

The plug with strength of 3000 psf and width of 120 ft was adopted to remediate Sardis Dam. The overall improvement on the performance of the dam after liquefaction is evident; see Fig. 7.27. After remediation, the loss of freeboard is 4.50 ft, and the maximum horizontal displacement of the dam is 0.24 ft. Although the overall configuration of the dam does not change very much, significant distortions in the liquefied silt core are observed.

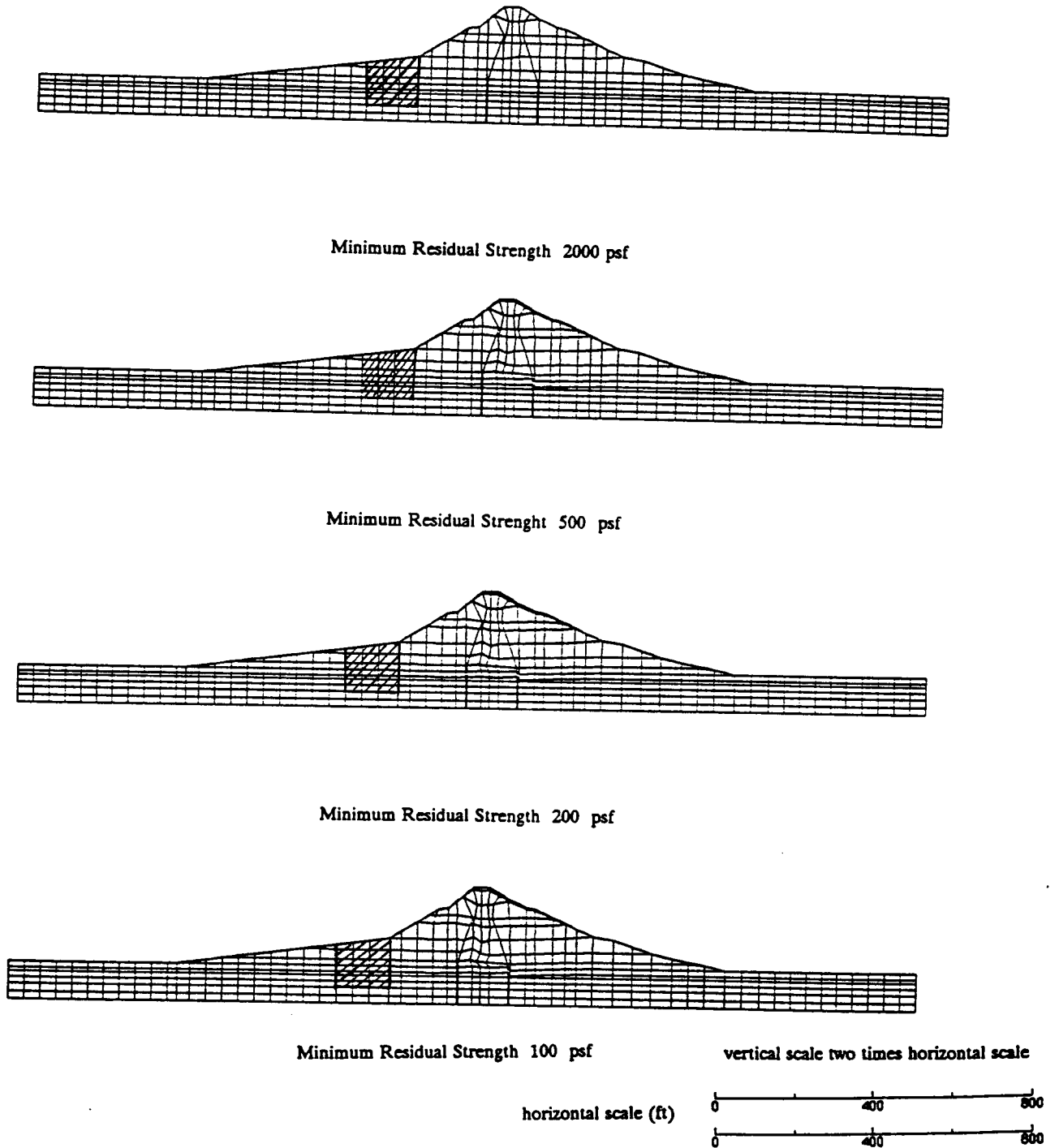


Figure 7.27: Variation of Typical Post liquefaction Configurations after Remediation - Plug Strength 3000 psf, Plug Width 120 ft)

Chapter 8

REMEDICATION STUDY OF PILE-REINFORCED SECTION

8.1 Equivalent Composite Material Properties of the Pile Reinforced Section

In practice, the remediation requirements of Sardis Dam can be met by driving piles through the section to be remediated. The proposed layout of the remediation piles is shown in Fig. 8.1 and Fig. 8.2. The width of the pile-reinforced zone is 120 feet. 24-inch square prestressed concrete piles are arranged in the remediation zone with a center-to-center spacing of 12 feet in two cross horizontal directions. The remediation piles need to penetrate 15 feet into the foundation sand from the bottom of the weak clayey silt layer.

Since the reinforced pile group distributes loads in both horizontal and vertical directions, the problem involves a three dimensional pile-soil interaction system. 3-D flow analysis is not available yet, so 2-D plane strain analysis was employed to simulate the pile-soil system. Again finite element code TARA was used, which contains 2-D plane strain bilinear isoparametric elements. For this purpose equivalent composite material properties are required for the pile-reinforced section.

Woodward-Clyde consultants (1991) conducted a 3-D analysis on a single pile, which provided the composite stress strain curves for the pile-reinforced zone. In their study, the 3-D nonlinearity finite element code, NONSAP, developed by Bath et al. (1974) was

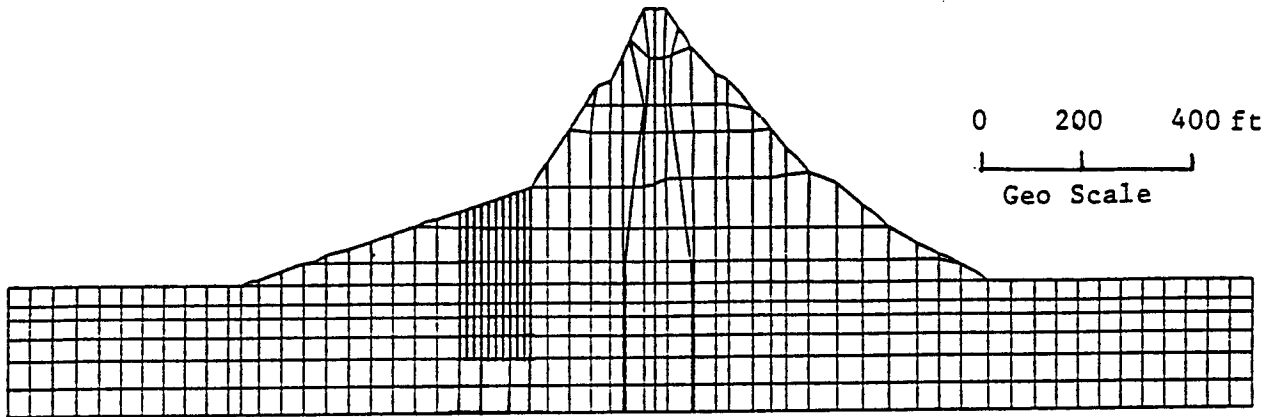


Figure 8.1: Cross Section of Sardis Dam Showing Remediation Piles

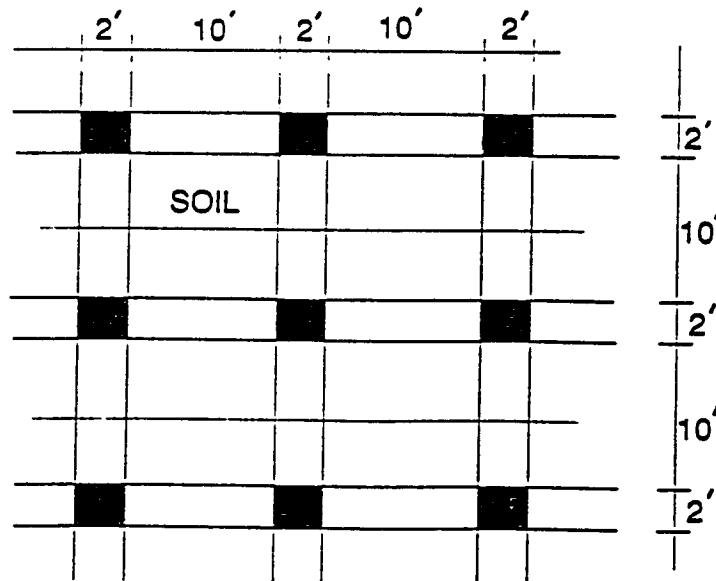


Figure 8.2: Plane View of Layout of Remediation Piles

used. Since the program does not have a beam element, the 3-D 8-node isoparametric element was chosen to model the pile and its surrounding soils. The single pile-soil system consists of a 24-inch-square prestressed concrete pile embedded about 15 feet into the dense foundation sand with a pile center-to-center spacing of 12 feet; see Fig. 8.3. This single pile-soil system was loaded laterally. The lateral loads were assumed to distribute triangularly along elevation; see Fig. 8.4. In their study the baseline load was defined to be the shear force that can cause shear stresses of 230 psf in the weak clayey silt layer, i.e, 33 kips for the single pile case (12 by 12 feet area). Load levels were increased by multiplying the baseline load by different integer numbers. The compression strength of prestressed concrete was assumed to be 6000 psi in their analysis. After performing 3-D analysis on the single pile-soil system with various load levels, they developed the shear stress-strain relationships shown by the solid lines in Fig. 8.5 through Fig. 8.13 for use in the finite element analysis of the global deformation of the dam.

The composite shear stress-strain curves obtained by Woodward-Clyde consultants (1991) are used to represent the composite shear stress-strain characteristics of the pile-reinforced zone of remediated soil. Since the hyperbolic stress-strain relationship is used in TARA, those composite shear stress-strain curves were approximated by hyperbolic curves. These hyperbolic curves are shown by the dashed lines in Fig. 8.5 through Fig. 8.13.

The shear strength and shear modulus (initial modulus) obtained from the hyperbolic model are designated as the composite shear strength and the composite shear modulus. Those composite strengths and moduli for different elevations of the reinforced zone are shown in Table 8.1. Fig. 8.14 presents the variation of the composite shear strengths in the pile-reinforced section versus elevations. The composite shear strengths vary from

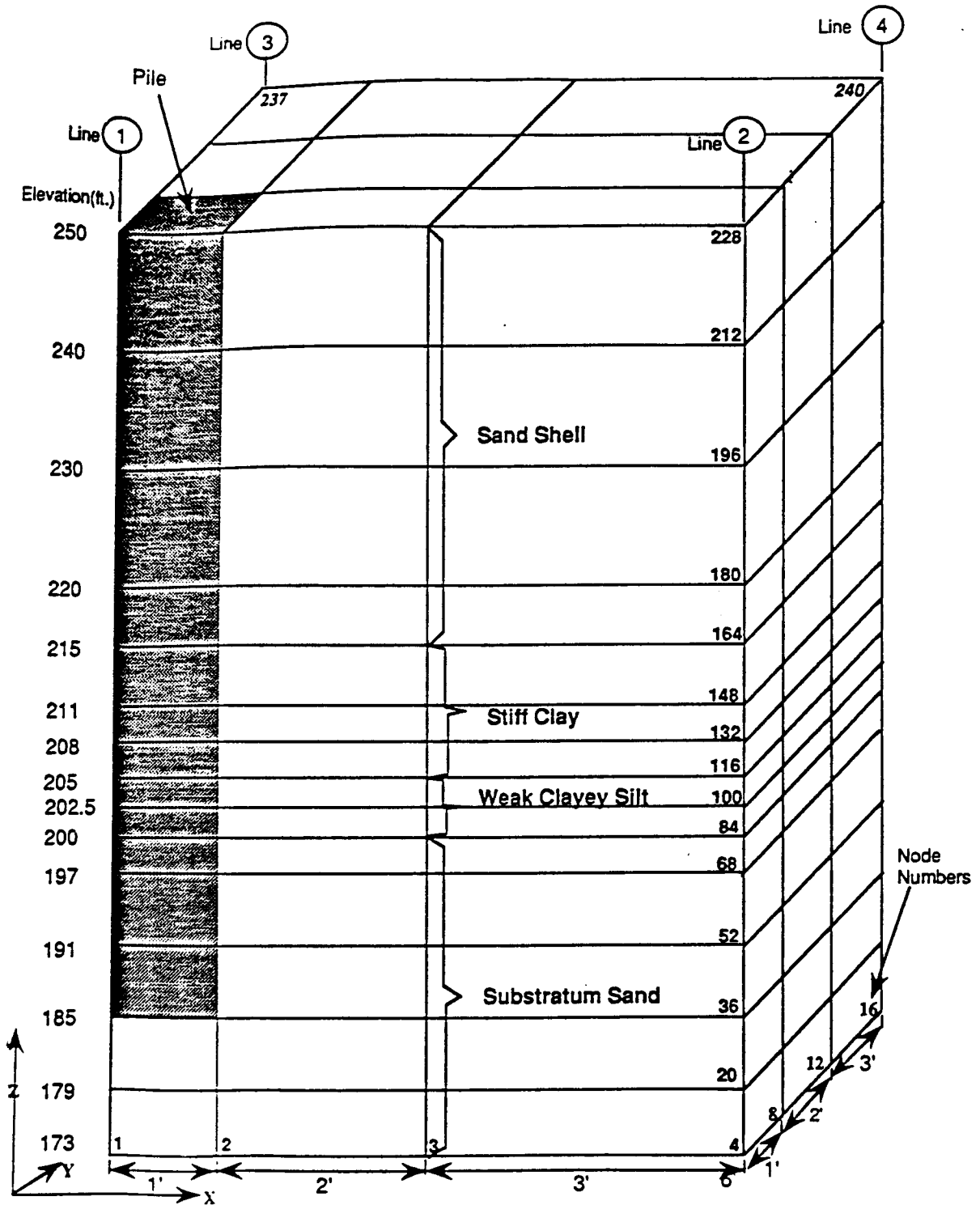


Figure 8.3: Finite Element Model of Single Pile-Soil System

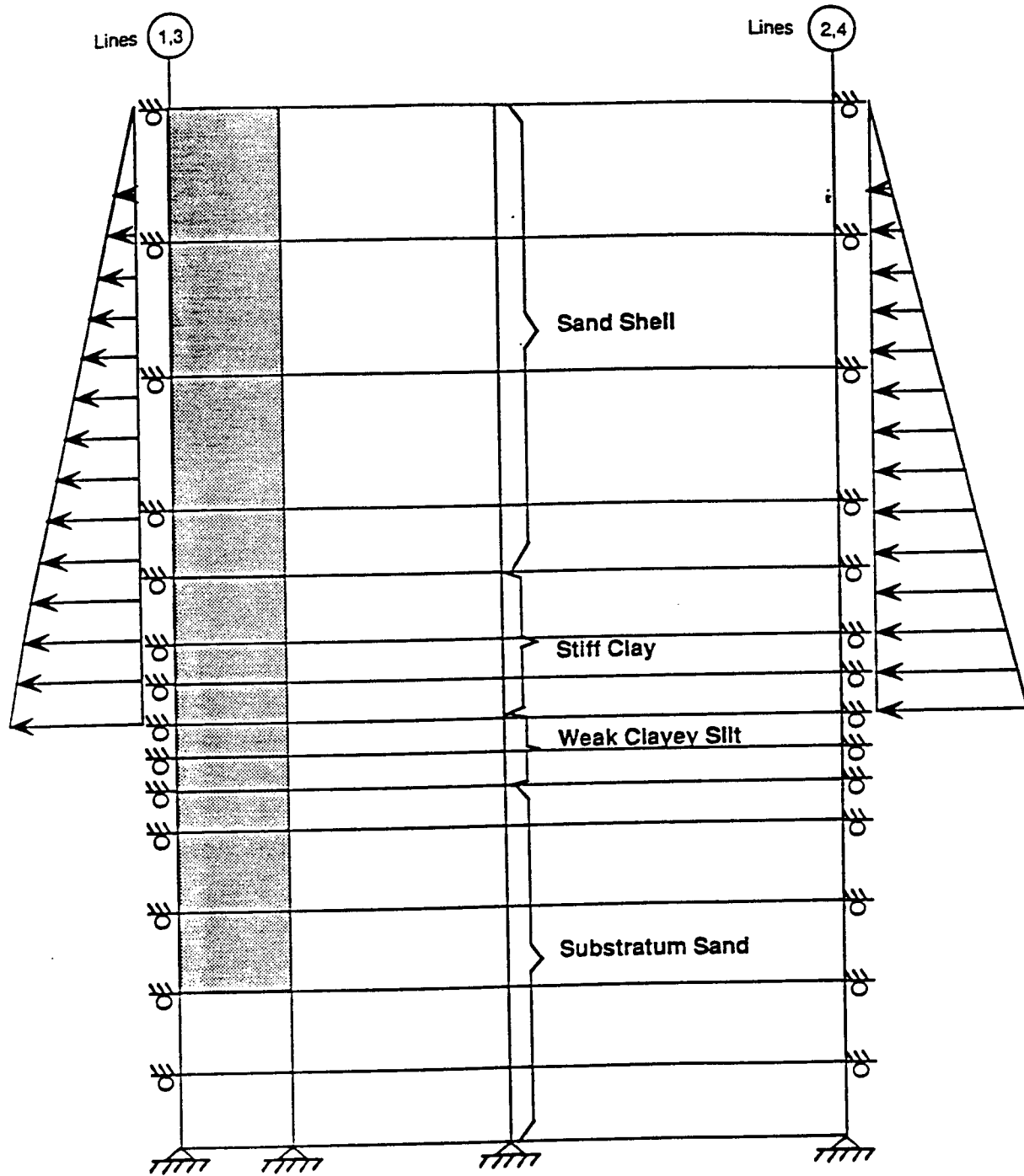


Figure 8.4: Boundary Conditions and Loading Distribution of Single Pile-Soil System

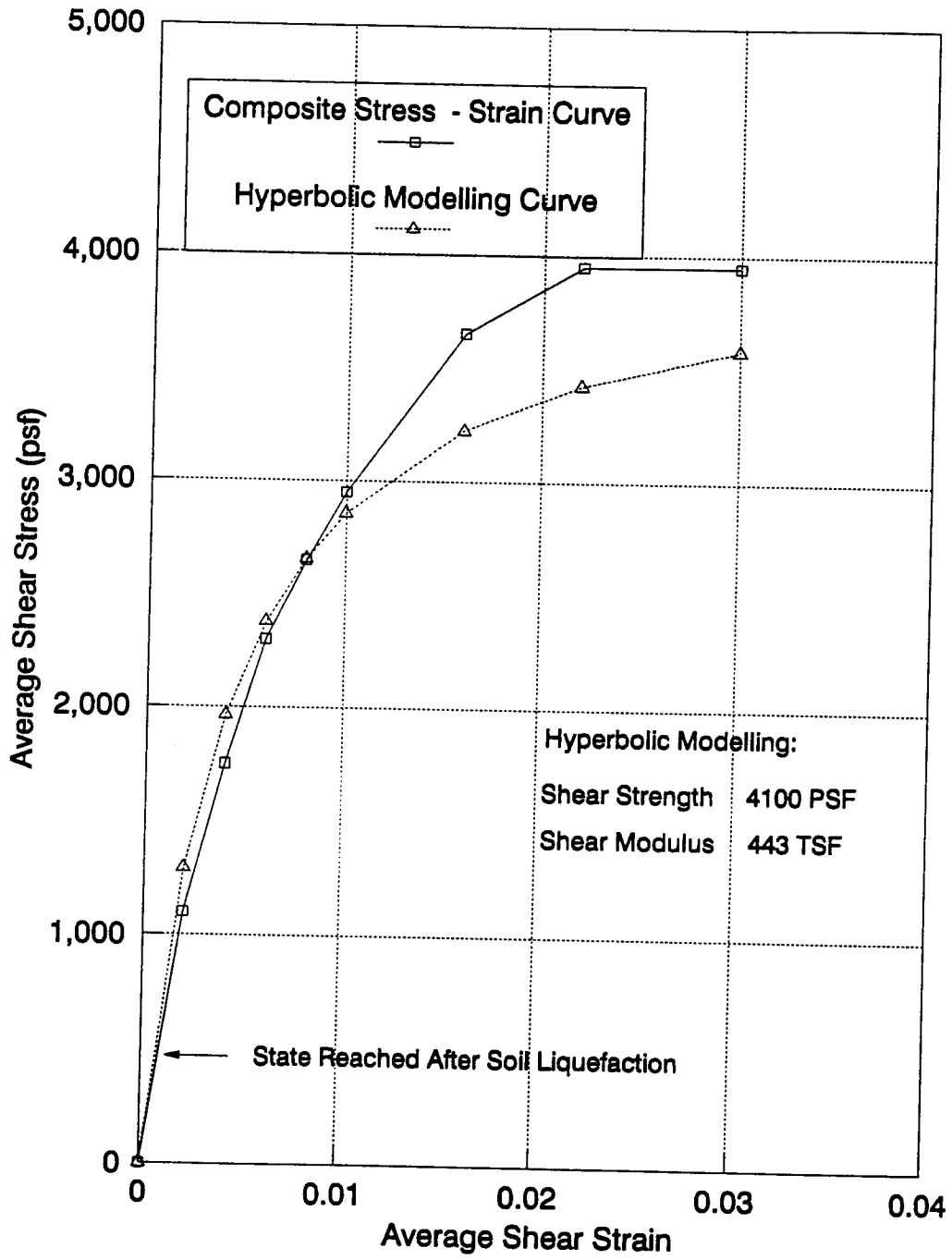


Figure 8.5: Shear Stress - Strain Relationship for the Pile-Reinforced Section, Elevation 173 to 185 ft

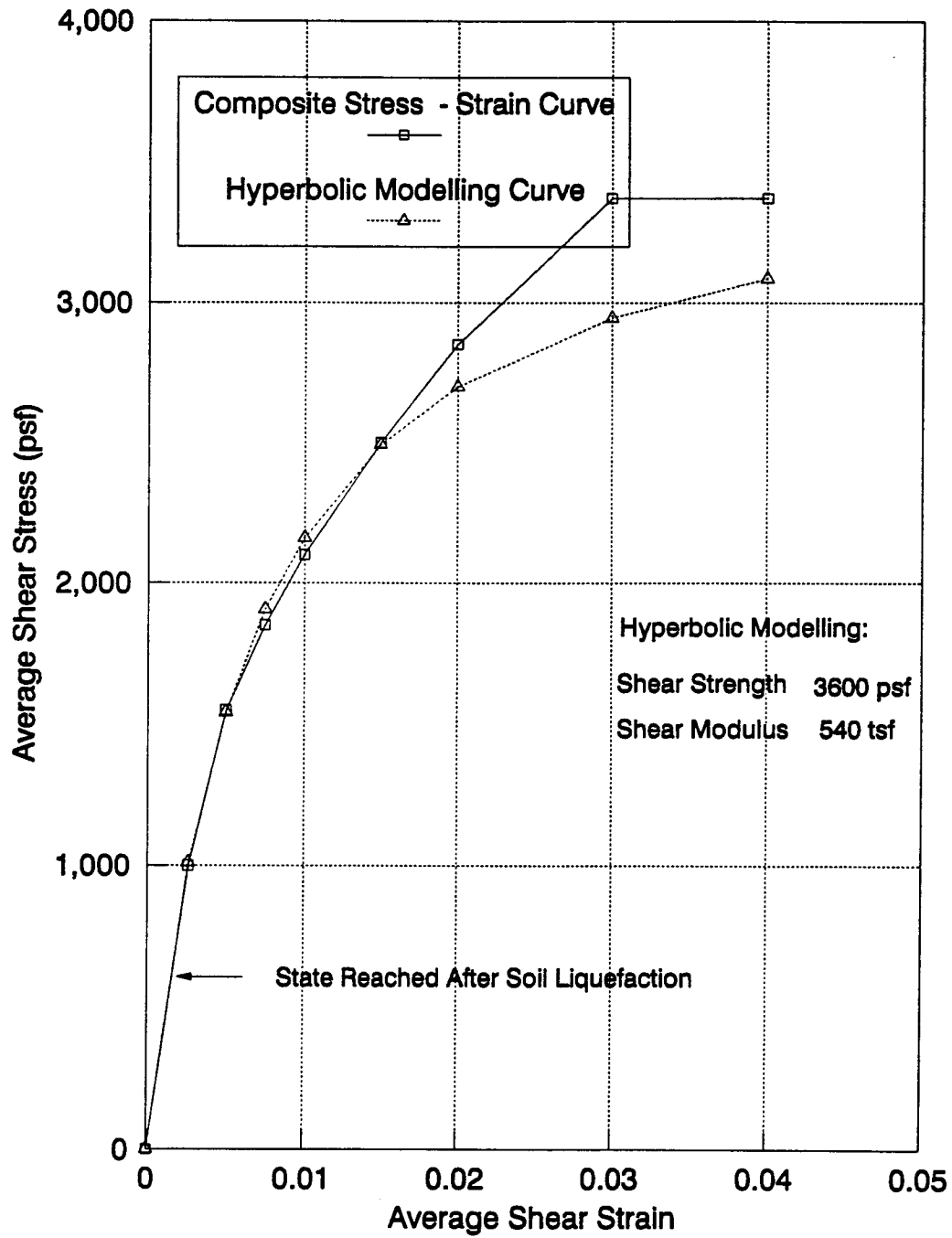


Figure 8.6: Shear Stress - Strain Relationship for the Pile-Reinforced Section, Elevation 185 to 191 ft

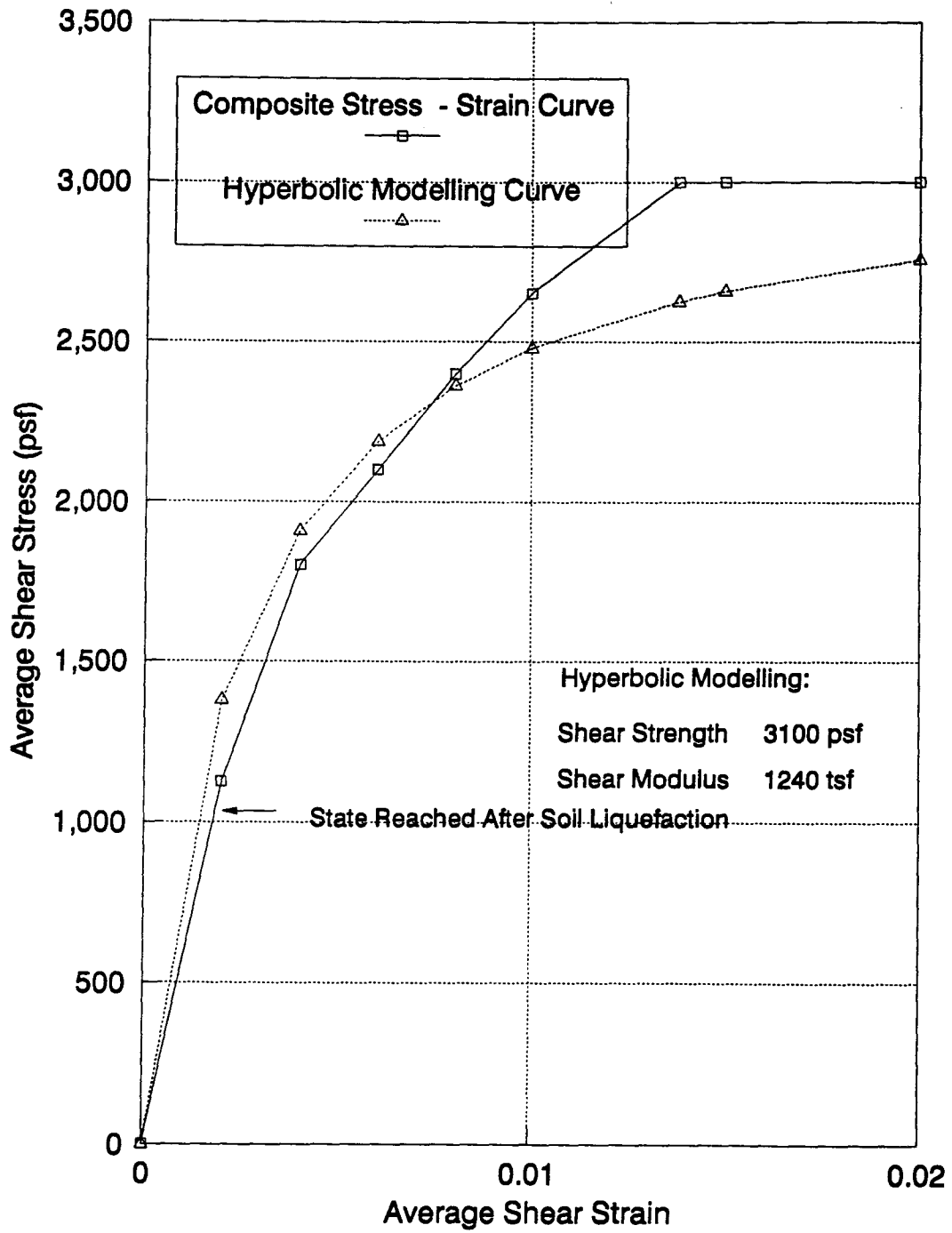


Figure 8.7: Shear Stress - Strain Relationship for the Pile-Reinforced Section, Elevation 191 to 200 ft

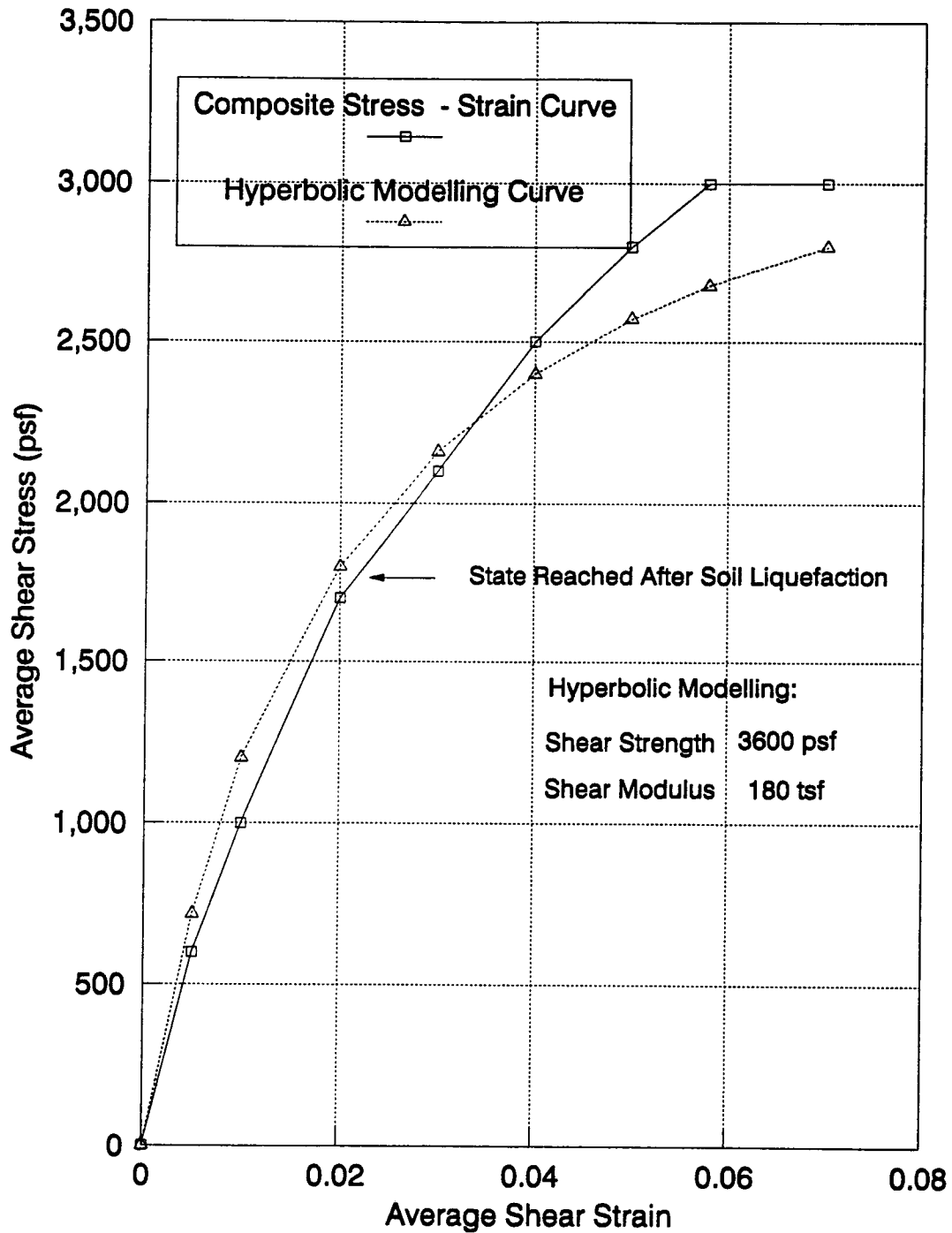


Figure 8.8: Shear Stress - Strain Relationship for the Pile-Reinforced Section, Elevation 200 to 205 ft

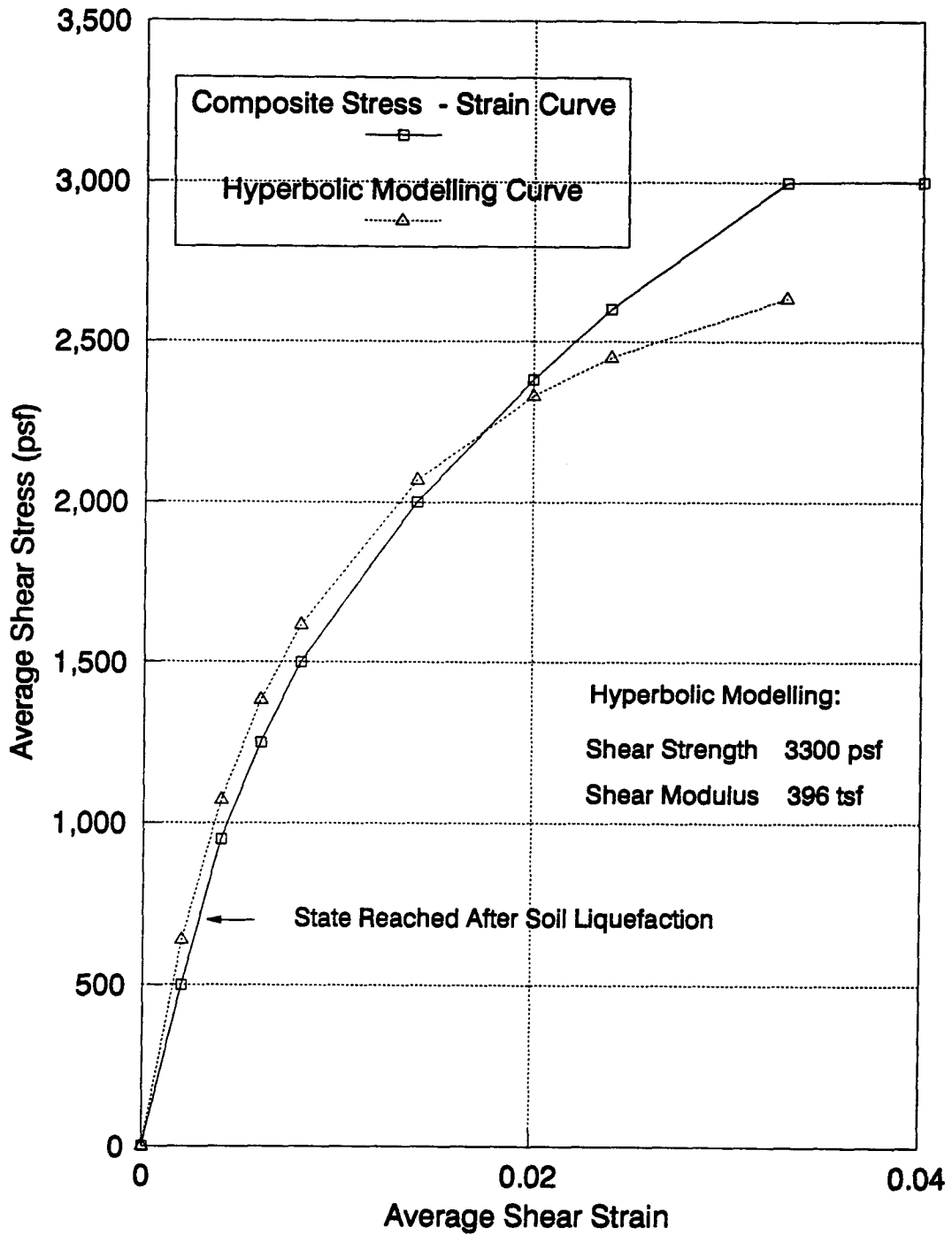


Figure 8.9: Shear Stress - Strain Relationship for the Pile-Reinforced Section, Elevation 205 to 215 ft

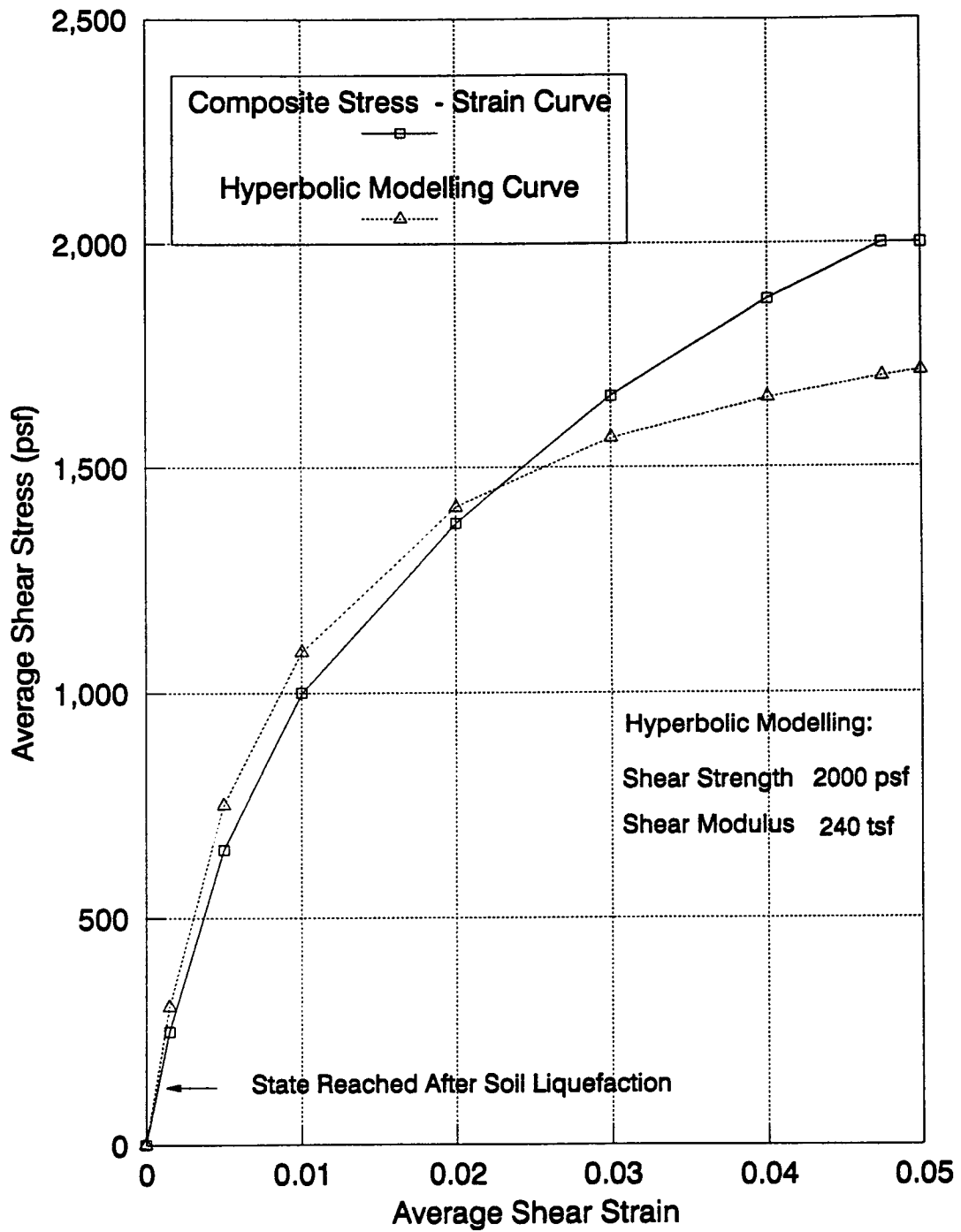


Figure 8.10: Shear Stress - Strain Relationship for the Pile-Reinforced Section, Elevation 215 to 220 ft

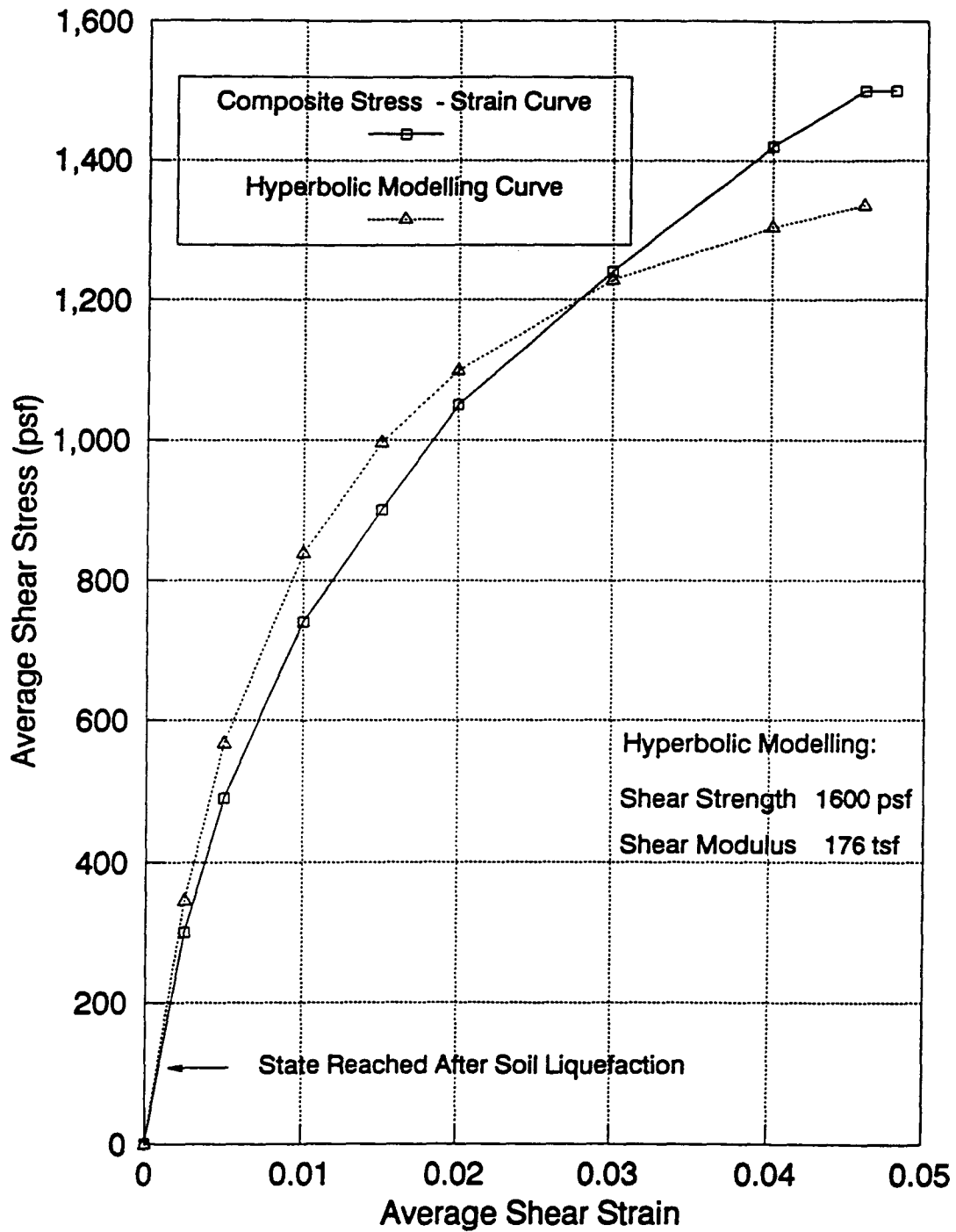


Figure 8.11: Shear Stress - Strain Relationship for the Pile-Reinforced Section, Elevation 220 to 230 ft

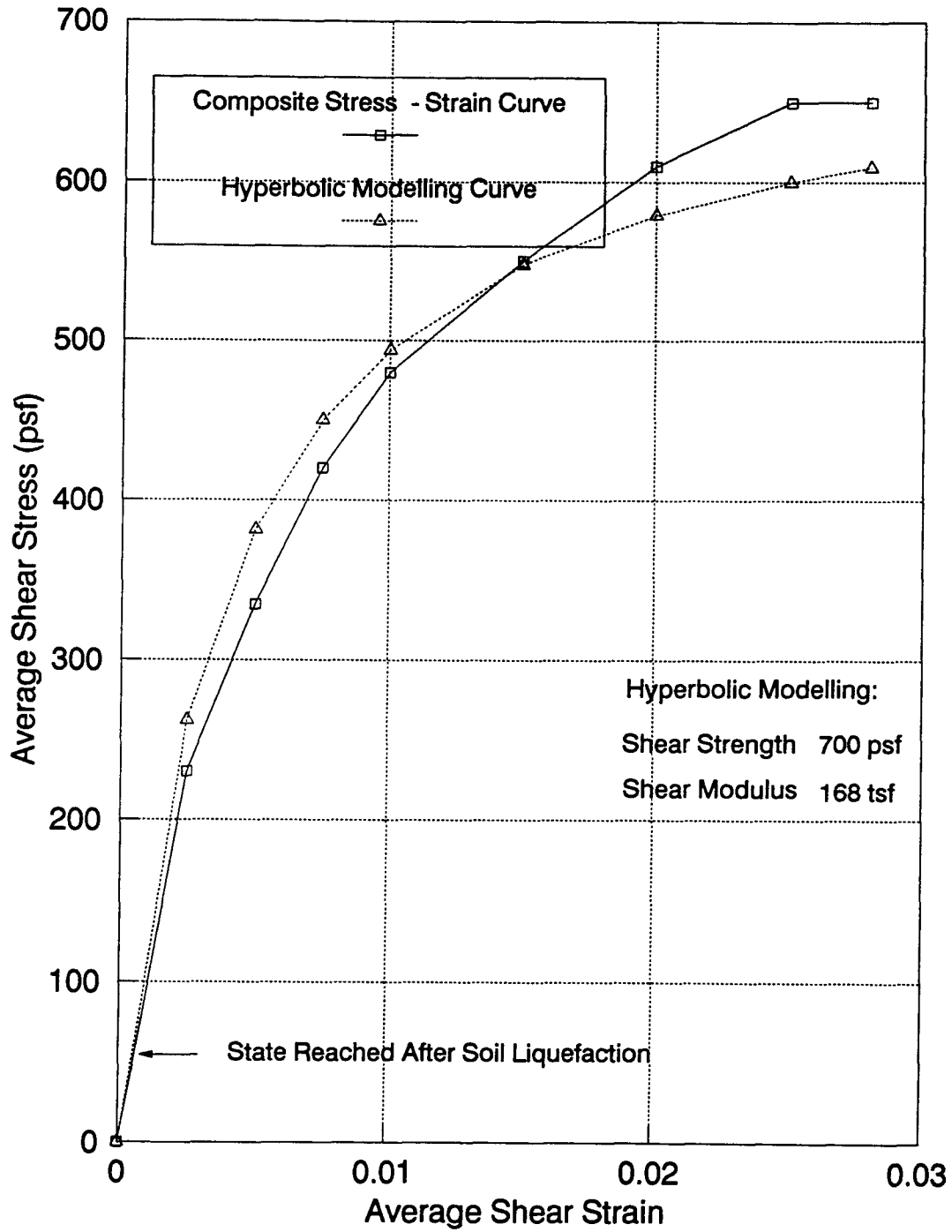


Figure 8.12: Shear Stress - Strain Relationship for the Pile-Reinforced Section, Elevation 230 to 240 ft

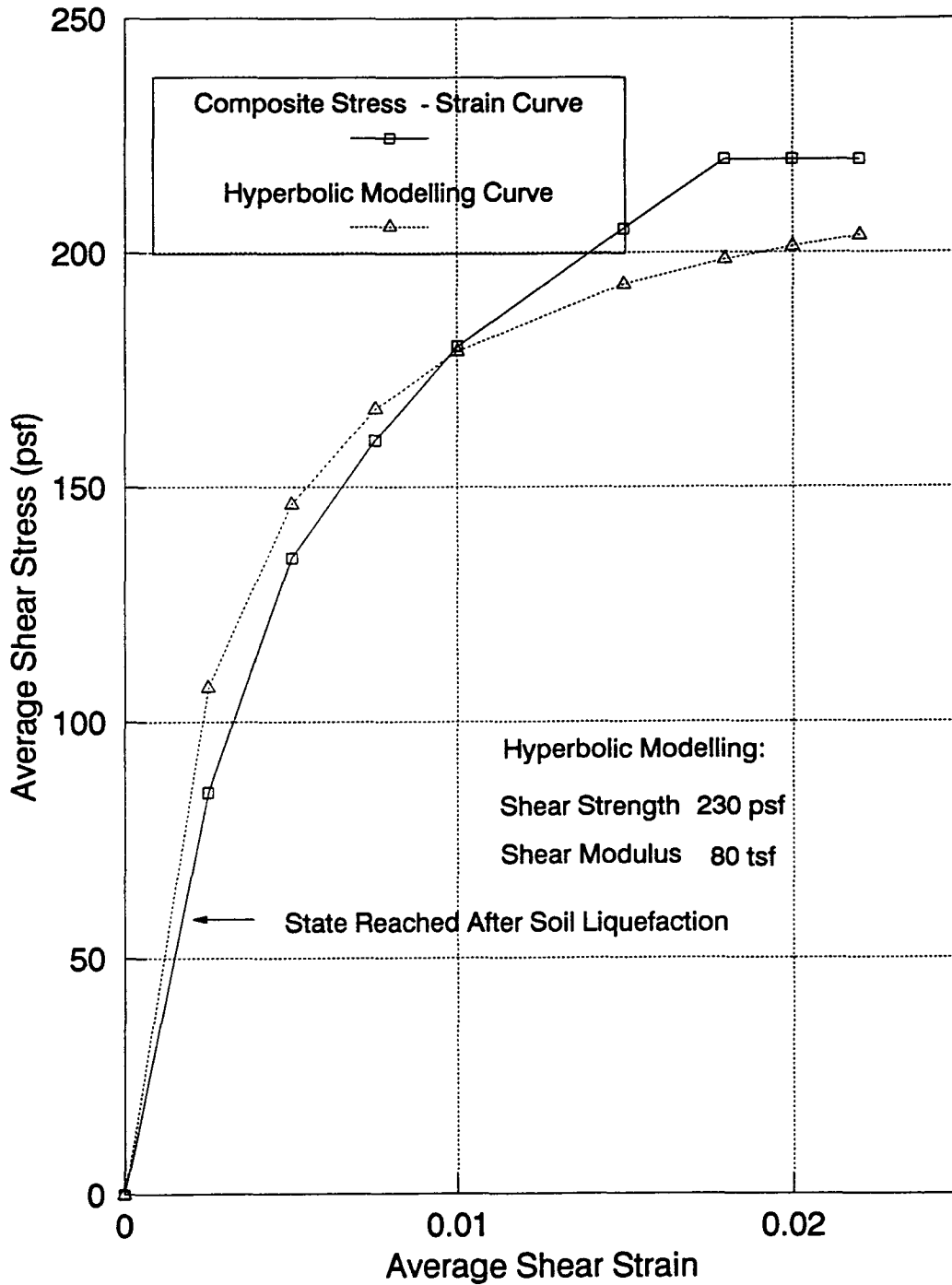


Figure 8.13: Shear Stress - Strain Relationship for the Pile-Reinforced Section, Elevation 240 to 250 ft

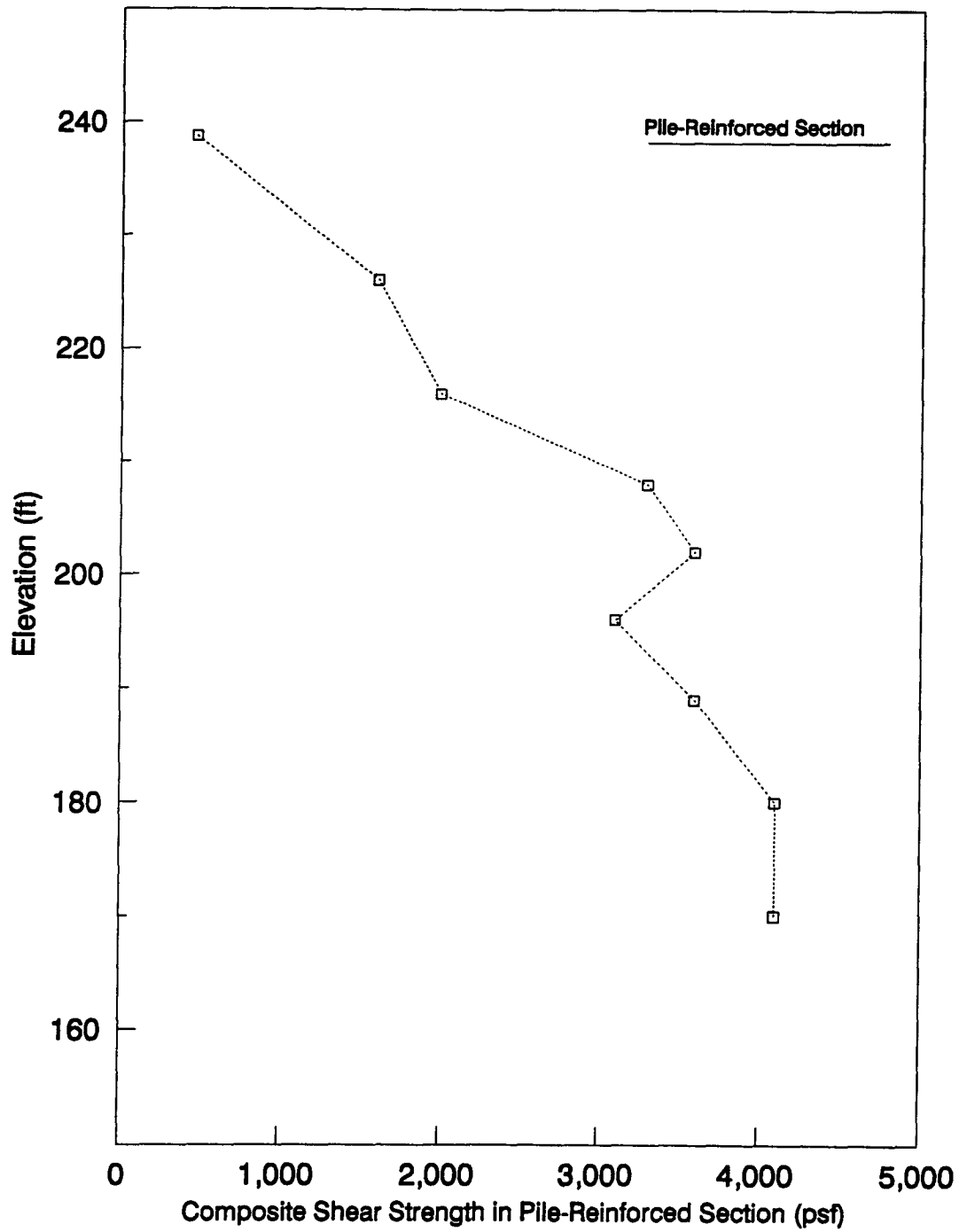


Figure 8.14: Variation of Shear Strength in Pile - Reinforced Section Versus Elevation

Table 8.1: Composite Strengths and Moduli of the Pile-Reinforced Section

<i>Elevation (ft)</i>	<i>Composite Strength (psf)</i>	<i>Composite Modulus (psf)</i>
240-250	230	80,000
230-240	700	168,000
220-230	1600	176,000
215-220	2000	240,000
205-215	3300	396,000
200-205	3600	180,000
191-200	3100	1240,000
185-191	3600	540,000
173-185	4100	443,000

230 psf at elevation 245 ft to 4100 psf at elevation 180ft, with an average value of 2900psf.

8.2 Comparison of Results Between the Pile-Reinforced Section And the Plug

As the composite shear strengths and moduli of the pile-reinforced section have been determined, the post-liquefaction behaviour of Sardis Dam was reassessed with the pile-reinforced remediation in place in the upstream slope as shown in Fig. 8.1. In the analysis, 50% of pore water pressure is assumed to be generated in the non-liquifiable sand shell.

8.2.1 Loss of freeboard

The results of the pile-reinforced section were compared with the results of the plug model which has a constant shear strength of 3000 psf and a width of 120ft. When minimum residual strength in the weak clayey silt layer drops to its minimum value of 100

psf, the loss of freeboard is 4.50 ft for the plug, and it is 4.74 ft for the pile-reinforced section. Since the composite shear strengths of the upper part of the pile-reinforced section, between the elevations of 215 ft and 240 feet, are less than those of the plug model. Therefore, the pile-reinforced section has a little less resistance than plug model to displacement in the upper section of the zone.

8.2.2 Horizontal pressures against the remediated zone

Fig. 8.15 presents the post-liquefaction pressure distribution against the downstream face of the remediated section (side A). The maximum horizontal pressure against the pile-reinforced section is about 10000 psf, compared with a horizontal pressure of 12000 psf against the uniform plug. But apart from the peak value near the weak layer, the pressure distributions are very similar.

8.2.3 Ratio of shear stress to strength of the remediated zone

The ratio of the shear stress to the composite shear strength of the pile-reinforced section is used to examine the shear resistance of the pile-reinforced section. Fig. 8.16 shows the ratios of the shear stress to the shear strength in the remediated section versus elevations when the minimum residual strength in the weak clayey silt is 100 psf. For the pile-reinforced section, these ratios are high at elevations between 215 ft and 240 ft because of the relatively low shear strengths there, and they are low at elevations below 215 ft because of relatively high shear strengths. The maximum ratio of the shear stress to the shear strength of the remediated zone occurs at the level of the weak clayey silt layer with a value of 0.49. This relatively low ratio indicates a relatively high factor of safety

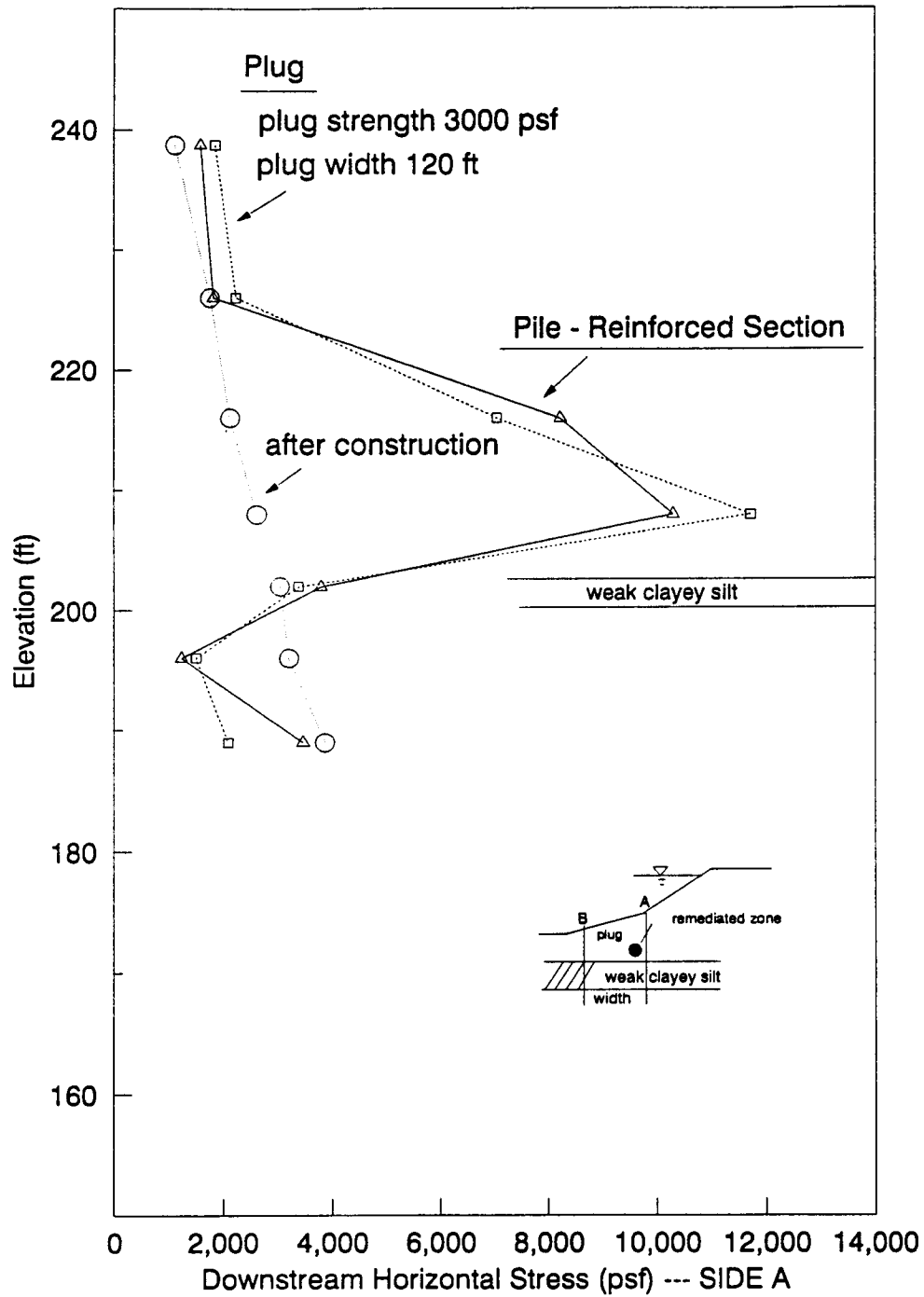


Figure 8.15: Pressure Distribution on Downstream Face of Pile - Reinforced Section

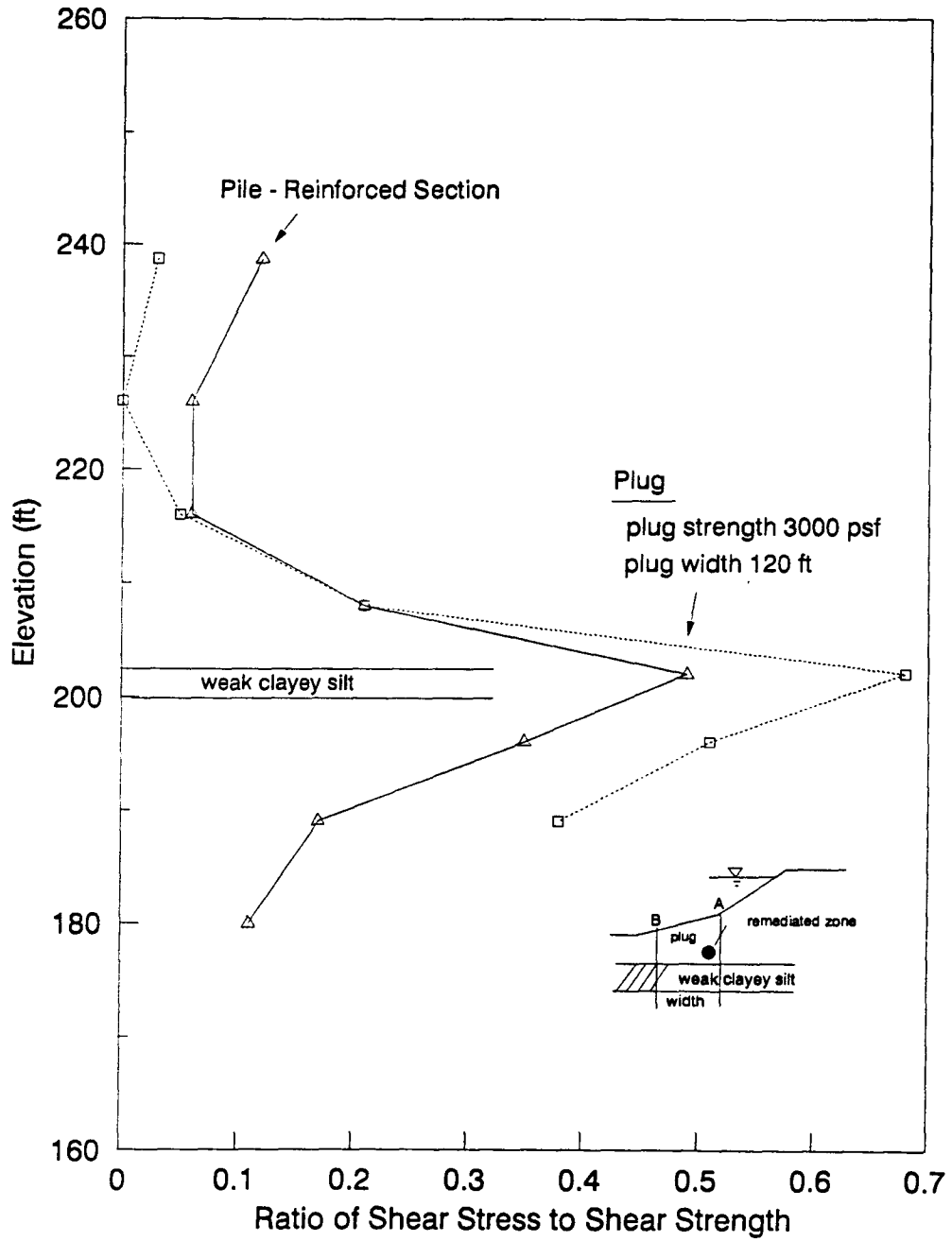


Figure 8.16: Distribution of Ratio of Shear Stress to Strength at Downstream Face of Pile - Reinforced Section

against a shear failure of the remediated zone.

8.2.4 Horizontal movement of the remediated zone

Fig. 8.17 illustrates the downstream horizontal movements of the remediated zone after liquefaction. The pile-reinforced section shows a larger displacement at the top of the remediated section because of the lower composite shear strengths and moduli in the upper regions. The maximum horizontal movement of the pile-reinforced section is about 0.49 ft, compared with the plug model of 0.24 ft. These values are within tolerable limits

It is clear that 24-inch square prestressed concrete piles at 12 ft centres arranged in the remediated zone can provide sufficient strength and stiffness to control the deformations of Sardis Dam within tolerable limits provided they can be designed structurally to carry individually the required moments and shears. This is the next stage in the design process and will be carried out by structural engineers.

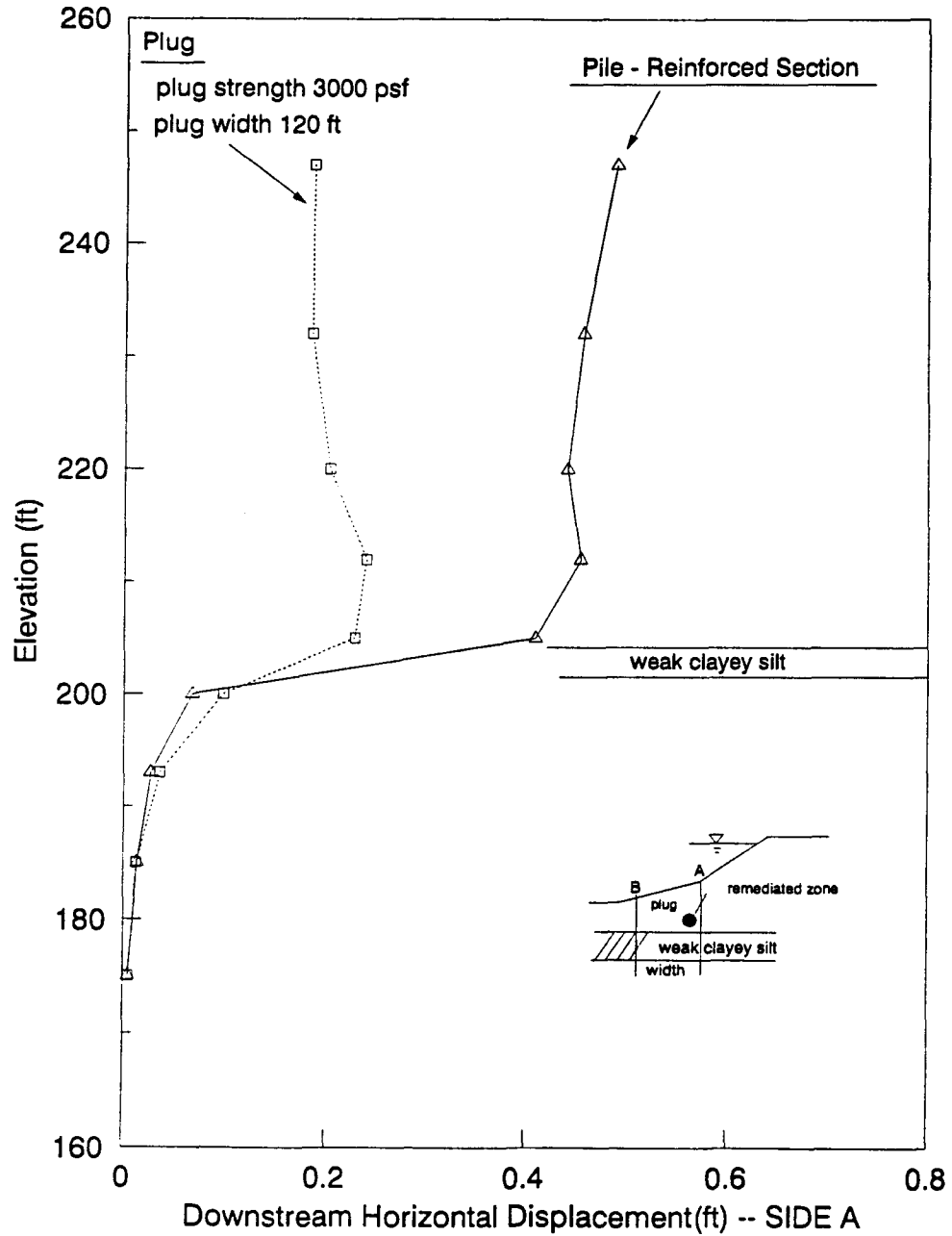


Figure 8.17: Distribution of Downstream Horizontal Movement of Pile - Reinforced Section

Chapter 9

SUMMARY AND CONCLUSIONS

Sardis Dam is expected to suffer a great loss of shear strengths in the liquefied soils during the design earthquake shaking. Studies have been made to examine the post-liquefaction performance of the dam. First, post-liquefaction deformation analyses were conducted on the initial configuration of the dam without remediation. Results of this analysis show that a significant loss of freeboard and large horizontal displacements of the dam will occur after liquefaction. Furthermore, necessary remedial measures were proposed, and studies have been made to determine the general requirements of both the extent of the remediation and the average properties of the proposed remediated section. Finally, the studies show that remediation requirements can be met by driving 24-inch square piles into the remediated section. The research performed for Sardis Dam leads to the conclusions below:

1. For Sardis Dam without remediation, the overall performance of the dam is very poor after liquefaction. The loss of freeboard of the dam is 45.5 ft after soil liquefaction. The dam will fail along the weak clayey silt layer under the upstream slope.

2. The dam is to be stabilized by a 120ft wide remediated zone that crosses the weak foundation layer and provides an adequate resistance to sliding or bending.
3. Parametric studies show that an average shear strength of 3000 psf and a shear modulus of 900,000 psf are needed to supply the necessary resistance to shearing and bending.
4. The remediation zone is to be located with its downstream face at the slope break in the upstream slope near the conservation level of the pool.
5. Porewater pressures up to 50% of effective overburden pressures can be developed in the sand shell without deformations exceeding tolerable levels.
6. The preferred method of meeting the strength and stiffness requirements of the remediated section is to drive prestressed concrete piles across the weak clayey silt layer. Preliminary studies show that 24-inch square prestressed concrete piles at 12 ft spacing would be adequate.

The above studies have indicated that the remediation requirements for the strength and stiffness can be met by driving piles into the dam. Research piles have been driven in a section in order to test the feasibility of driving piles into the foundation sands. The studies have indicated that it is feasible to drive the 24-inch piles. In-situ tests were performed to evaluate densification of the sand shell by the pile driving. Increasing densification increases the ability of load transfer between the piles. These data are now being analyzed. Studies have begun to determine the shear and moment both statically and dynamically for which the individual piles must be designed structurely. The reliable

determination of the shear and moment is a difficult problem in analysis, and various methods for analyzing the dynamic response of the piles are being evaluated to determine which method of analysis may be best.

Bibliography

- [1] Bathe, K-J, Wilson, E.L., Iding, R.H., (1974), " NONSAP, A Structural Analysis Program for Static and Dynamic Response of Nonlinear Systems", Report No. VC SESM 74-3, College of Engineering, University of California, Berkeley, California, February.
- [2] Casagrande, A. 1936. "Characteristics of Cohesionless Soils Affecting the Stability of Slopes and Earth Fills, " Journal of the Boston Society of Civil Engineers, reprinted in: Contribution to Soil Mechanics, 1925 to 1940, Boston Society of Civil Engineers, 1940, pp257-276.
- [3] Castro, G., T.O. Keller and S.S. Boynton.(1989). Re-evaluation of the Lower San Fernando Dam. Report No. 1, USACE, Waterways Experimental Station, Vicksburg, Mississippi, September.
- [4] Castro, G., Poulos, S. J. , and Leather F.D. 1985. " A Re-examination of the Slide of the Lower San Fernando Dam," Journal of Geotechnical Engineering Division, ASCE, Vol. 111, GT9.
- [5] De Alba, P., H.B., Seed, E. Retamal, and R.B., Seed. 1987. Residual Strength of Sand from Dam Failures in the Chilean Earthquake of March 3, 1985. Earthquake Engineering Research Center, Report No. UCB/EERC-87-11, University of California , Berkeley, September.
- [6] Duncan, J.M., and Chang, C.Y., 1970, "Non-linear Analysis of Stress and Strain in Soils", Proceedings, ASCE, Vol. 96, No. SM5, pp.1629-1653.
- [7] Finn, W.D. Liam, 1981. Liquefaction Potential Development since 1976. International Conference on Recent Advances in Geotechnical Engineering and Soil Dynamics, St. Louis, MO, Vol. 2, pp. 655-681.
- [8] Finn, W.D.L., Ledbetter, R.H., Fleming JR, R.L., Templeton, E.T., Forrest, T.W., Stacy, S.T., (1990a). " Dam on Liquefiable Foundation : Safety Assessment and Remediation"
- [9] Finn, W.D. Liam, and Byrne, P.M., (1976), Estimating Settlements in Dry Sands During Earthquakes, Canadian Geotechnical Journal, Vol. 13, No. 4, pp. 355-363.

- [10] Finn, W.D. Liam, M. Yogendrakumar, N. Yoshida, and H. Yoshida. (1986). TARA-3: A Program for Nonlinear Static and Dynamic Effective Stress Analysis, Soil Dynamic Group, University of British Columbia, Vancouver, B.C., Canada.
- [11] Finn, W.D. Liam and Yogendrakumar (1989). TARA-3FL - Program for Analysis of Liquefaction Induced Flow Deformations, Dept. of Civil Engineering, University of British Columbia, Vancouver, B.C., Canada.
- [12] Finn, W.D. Liam, M. Yogendrakumar, R. C. Lo, and R.H. Ledbetter. (1990b). Seismic Response of Tailings Dams, State of the Art Paper, Proc., Int. Symposium on Safety and Rehabilitation of Tailings Dams, Internation Commission on Large Dams, Sydney, Australia, May.
- [13] Finn, W.D. Liam. (1985) Dynamic Effective Stress Response of Soil Structures; Theory and Centrifugal Model Studies, Proc. 5th Int. Conf. on Num. Methods in Geomechanics, Nogoya, Japan, Vol. 1, 35-46.
- [14] Idriss, I.M., J. Lysmer, R.N. Hwang, and H.B. Seed. (1973) QUAD4: A Computer Program for Evaluating the Seismic Response of Soil Structure By Variable Damping Finite Element Procedures, Rept. No. UCB/ERRC-73-16, University of California, Berkeley.
- [15] Klohn, E.J., Maartman, C.H., Lo, R.C.Y., Finn, W.D.L., 1978. Simplified Seismic Analysis for Tailings Dams, Proc. ASCE Geotech. Engng. Div., Specialty Conf. on Earthquake Engineering and Soil Dynamics, Pasadena, California, June, Vol. 1, pp. 540-556.
- [16] Koester, J.P. (1990). Letter Report to Vicksburg District, U.S. Army Corps of Engineers.
- [17] Lee, K.W., and Finn, W.D.L., 1978, DESRA-2: Dynamic Effective Stress Response Analysis of Soil Deposits with Energy Transmitting Boundary Including Assessment of Liquefaction Potential, Soil Mechanics Series Report No. 38, Dept. of Civil Engineering, University of British Columbia, Vancouver, B.C.
- [18] Lysmer, J., Udaka, T., Tsai, C.F., and Seed, H.B., (1975). FLUSH: A Computer Program for Approximate 3-D Analysis of Soil Structure Interaction Problems, Report No. EERC75-30, Earthquake Engineering Research Center, University of California, Berkeley.
- [19] Martin, G.R., Finn, W.D.Liam, and Seed, H.B., 1975. Fundamentals of Liquefaction Under Cyclic Loading, Journal of the Geotechnical Engineering Division, ASCE, Vol. 101, GT5, May, 423-438.

- [20] Newmark, N.M. (1965). Effects of Earthquakes on Dams and Embankments, 5th Rankine Lecture, Geotechnique, Vol. 15, No. 2, June, pp139-160.
- [21] Poulos, S. J., Castro, G., and France, J. W. 1985. "liquefaction Evaluation Procedure," Journal of the Geotechnical Engineering Division, ASCE, pp772- 792.
- [22] Pyles, M. (1981). The Undrained Shearing Resistance of Cohesive Soils at Large Deformation, Ph.D. Dissertation, University of California, Berkeley.
- [23] Robertson, P.K. and R.G., Campanella, 1983. "Interpretation of Cone Penetration Tests," Part II (clay), Canadian Geotechnical Journal, Vol. 20, No. 4.
- [24] Seed, H.B., and Idriss, I.M., 1970. Soil Moduli and Damping Factors for Dynamic Response Analysis, Report No. EERC 70-10, Earthquake Engineering Research Center, University of California, Berkeley.
- [25] Seed, H. B., R.B., Seed, L.F. Harder and H.-L. Jong, 1988. Re-Evaluation of the Slide in the Lower San Fernando Dam in the Earthquake of February 9, 1971. Report No. UCB/ERRC-88/04, University of California, Berkeley, April.
- [26] Seed, H.B., Tokimatsu, K., Harder, L.F. and Chung, R.M. 1985 "Influence of SPT Procedures in Soil Liquefaction Resistance Evaluations," Journal of Geotechnical Engineering, ASCE, Vol. 3, No. 12.
- [27] Seed, H. B. 1987, Design Problem in Soil Liquefaction, Journal of Geotechnical Engineering, ASCE, Vol. 113, No. 7, pp. 827-845.
- [28] Seed, H.B., and Martin, G.R., The Seismic Coefficients in Earth Dam Design, Jnl. Soil Mech. Fdn. Div. ASCE Vol. 92, No. SM3, May, 1966, pp. 25-28.
- [29] Seed, R.B., and L.F., Harder Jr. (1990). SPT-Based Analysis of Cyclic Pore Pressure Generation and Undrained Residual Strength. Proceedings, H. Bolton Seed Memorial Symposium, J. Michael Duncan (ed.), Vol. 2, May, pp. 351-376.
- [30] Seed, H.B. (1979). Consideration in the Earthquake Resistance Design of Earth and Rockfill Dams, 19th Rankine Lecture, Geotechnique 29, No. 3, pp. 215-263.
- [31] Spencer, E., (1973). Thrust Line Criterion in Embankment Stability Analysis, Geotechnique, Vol. 23, No. 1, pp. 85-167.
- [32] USACE (1989). User's Guide: UTEXAS2 Slope Stability Package, Vol. II. Theory by Task Group on Slope Stability , Instruction Report GL-87-1, Final Report, U.S. Army Corps of Engineers, Washington, D.C.

- [33] Vaid, Y.P., and J.C. Chern. (1985). Cyclic and Monotonic Undrained Response of Saturated Sands. ASCE National Convention, Session Advances in the Art of Testing Soils Under Cyclic Loading, Detroit, October 21-25, pp. 12-0 147.
- [34] Vaid, Y.P., and Finn, W.D.Liam, 1979. Effect of Static Shear on Liquefaction Potential, Journal of the Geotechnical Engineering Division, ASCE, Vol. 105, GT10, OCT., pp. 1233-1246.
- [35] Vaid, Y.P., E.K.F. Chung, and R.H. Kuerbis, 1990. "Stress Path and Steady State," Canadian Geotechnical Journal, Vol. 27, No. 1.
- [36] Wang, W. 1979, "Some Findings in Soil Liquefaction," Water Conservancy and Hydroelectric Power Research Institute, Beijing, China, August.
- [37] Woodward Clyde Consultants 1989, Private Communication
- [38] Woodward Clyde Consultants 1991, Private Communication